



**HAL**  
open science

## A few aspects of topological waves

Pierre Delplace

► **To cite this version:**

Pierre Delplace. A few aspects of topological waves: Chiral modes in Unitary Dynamics and Continuous Media. Physics [physics]. Ecole Normal Supérieure de Lyon, 2019. tel-03402162

**HAL Id: tel-03402162**

**<https://hal.science/tel-03402162>**

Submitted on 25 Oct 2021

**HAL** is a multi-disciplinary open access archive for the deposit and dissemination of scientific research documents, whether they are published or not. The documents may come from teaching and research institutions in France or abroad, or from public or private research centers.

L'archive ouverte pluridisciplinaire **HAL**, est destinée au dépôt et à la diffusion de documents scientifiques de niveau recherche, publiés ou non, émanant des établissements d'enseignement et de recherche français ou étrangers, des laboratoires publics ou privés.

**A FEW ASPECTS  
OF  
TOPOLOGICAL WAVES**

**Chiral modes  
in Unitary Dynamics and Continuous Media**

Thèse d'Habilitation à Diriger des Recherches  
École Normale Supérieure de Lyon

Pierre DELPLACE

Defense date : November 25, 2019

**Composition of the Jury**

Mme. Jacqueline BLOCH : Présidente du jury  
M. Benoît DOUÇOT : rapporteur  
M. Nathan GOLDMAN : rapporteur  
M. Yasuhiro HATSUGAI : rapporteur  
M. Denis BARTOLO : examinateur  
M. Peter HOLDSWORTH : examinateur



## Acknowledgements/Remerciements

I am sincerely grateful to the members of the committee : Denis Bartolo, Jacqueline Bloch, Benoît Douçot, Nathan Goldman, Yasuhiro Hatsugai and Peter Holdsworth, who had the kindness to spontaneously accept to evaluate my work. I truly thank them for their abnegation and hope they could have found a few lines interesting enough in compensation for the time they spent reading these pages. I would like to especially thank the three referees : Benoît Douçot, Nathan Goldman and Yasuhiro Hatsugai, who had to spend a non negligible amount of time reading this manuscript in detail and comment it in rather a short notice. Their constructive and stimulating feedbacks were highly appreciated.

Cette thèse d'habilitation à diriger des recherches a été rédigée et porte sur des travaux effectués au laboratoire de physique à l'ENS de Lyon (LPENSL) depuis mon arrivée en 2014 et plus particulièrement mon recrutement au CNRS en 2015. J'y ai trouvé le cadre idéal pour y développer la recherche qui me plaît, tant pour l'excellente ambiance qui y règne, que pour son environnement scientifique exceptionnel, et bien sûr aussi, pour son efficacité administrative. Je tiens à ce titre à remercier la direction du laboratoire de physique (LPENSL) en la personne de Thierry Dauxois, pour son accueil il y a quelques années ainsi que pour m'avoir poussé à déposer un dossier ANR@raction quelques jours avant la date butoir et dont j'ai finalement été lauréat. Cela m'a permis de commencer ma carrière au CNRS avec un confort financier hélas inhabituel pour un chercheur fraîchement recruté. Je souhaiterais remercier Laurence Mauduit et Nadine Clervaux, pour leur gentillesse, leur efficacité et leur patience à mon égard, ainsi que Fatiha Bouchneb pour sa merveilleuse gestion du workshop interdisciplinaire sur les phénomènes topologiques que nous avons organisé en 2017.

J'aimerais également remercier chaleureusement les membres du groupe théorie (équipe 4) dans lequel j'évolue, et en particulier Jean-Michel Maillet qui le dirige, pour son accueil, ses encouragements et ses conseils avisés. Depuis mon arrivée dans l'équipe, j'ai eu la chance de pouvoir y interagir de façon fructueuse avec plusieurs chercheurs permanents et non-permanents, en particulier Krzysztof Gawedzki, Andrei Fedorenko, Michel Fruchart, Thibaud Louvet, Marco Marciani et Lavi Kumar Upreti que je tiens à saluer chaleureusement. Je souhaite également remercier tout particulièrement Clément Dutreix et Clément Tauber pour leurs collaborations dynamiques et enrichissantes sur les propriétés topologiques des ondes que nous avons su maintenir après leurs passages au LPENSL.

Ma trajectoire scientifique de ces dernières années eût été toute différente, et à n'en pas douter beaucoup moins stimulante, pertinente et productive, sans la rencontre de deux chercheurs du

## Acknowledgements

---

laboratoire à qui je réserve des remerciements particuliers, mes plus proches collaborateurs, David Carpentier et Antoine Venaille. Je leur suis extrêmement reconnaissant de tout ce que j'ai pu apprendre et comprendre à leurs côtés. Notamment, je dois l'essentiel de ma compréhension de la topologie en physique à David Carpentier qui m'a également accordé sa confiance en me recrutant comme postdoc avant que je n'obtienne un poste, c'est-à-dire quand l'avenir était incertain. Ses conseils et avis scientifiques constituent mes premières références. Et je dois mon initiation aux fluides géophysiques à Antoine Venaille qui m'a fait découvrir un domaine passionnant et insoupçonné et qui occupe aujourd'hui, grâce à lui, une place centrale dans ma recherche et en constitue sans aucun doute à ce jour la direction la plus novatrice. Je suis enchanté par notre collaboration originale et stimulante, qui, je pense, ne fait que commencer. Il va sans dire que ce manuscrit leur doit beaucoup.

Enfin, je tenais à remercier ma famille pour son soutien indéfectible, à commencer par ma mère qui s'était promis de me pousser au moins jusqu'au Baccalauréat. J'ai également une pensée émue pour mon oncle Claude qui m'a fait découvrir le pendule de Foucault lorsque j'étais enfant, et que j'ai redécouvert bien plus tard à travers le langage des phases géométriques. Enfin, je voulais exprimer ici toute ma gratitude envers ma compagne, Mirja, pour ses encouragements et son soutien quotidien sans faille, en dépit des trop nombreux week-ends, soirées, et vacances que j'ai passés à travailler au détriment du reste. Je n'aurais notamment jamais trouvé le temps et l'énergie nécessaires pour écrire ce mémoire sans son aide, sa compréhension et sa patience.

*Lyon, November/Novembre 2019*

Pierre. A. L. Delplace



## Foreword

The writing of an Habilitation à Diriger des Recherches (HDR) thesis is not formatted and therefore varies from a candidate to another. It leaves the author a free hand to adapt his/her message and target specific readers. As far as I am concerned, I tried to provide a viewpoint on the recent craze for topology in physics and to describe how abstract but powerful concepts, mainly developed in (quantum) condensed matter physics, fruitfully spreads into various communities that deal with classical waves. This manuscript is thus dedicated to non-specialists, and a special effort has been made to ensure that the presentation of the main ideas is not clogged up with technical details.

The present manuscript is constituted of two parts, each of them being composed of three chapters. Part I is the heart of the HDR. Chapter 1 is a general introduction to the subject far beyond the scope of my personal contributions and specifies also what I mean by *topological waves*. Chapter 2 proposes a consistent overview of a selection of my recent works, roughly over the last two years. Results that are summarized in that chapter concern unitary dynamics (periodically driven (Floquet) systems, scattering networks (including random graphs)) and classical continuous media (including electromagnetic waves and fluid waves). Finally, chapter 3 addresses a few perspectives for future works which I intend to tackle in the next coming years. Derivations, calculations and other complementary informations are intentionally missing. They can be found if necessary in the related published papers attached.

The risk when presenting works on topology in physics with almost no technical content, is that the very topological aspects may remain too elusive and mysterious for non-specialists, who may find the key ideas appealing but still would be unable to apply or even reproduce them in the examples that are presented in this thesis. As a consequence, I added as a Part II, a pedagogical introduction to a few basic (but not necessary simple) topological tools that were used in Part I. This part can be read as an introduction course independently of Part I, with explicit detailed derivations, and inversely, readers familiar with Chern numbers, winding numbers and degrees of maps can skip Part II and only focus on its application to physical waves discussed in Part I.





## Abstract

This manuscript of Habilitation à Diriger des Recherches thesis addresses works in theoretical physics that deal with topological aspects of propagating waves.

The investigation of the topological properties of waves have mainly consisted in the study of waves singularities in their intensity, phase or polarization. Inspired by the discovery of topological phases of matter, whose quantum Hall effect discovered in 1980 and topological insulators discovered in 2005 are some manifestations, new topological properties of waves have been identified these last years. A few topological tools used and developed to describe these quantum materials revealed the key cornerstone concept of bulk-edge correspondence, that relates the topological characterization of electronic wavefunctions in a quantum material to the existence of confined states at its boundaries, that make for instance possible the transport of information without dissipation. This correspondence being applicable to classical waves, it turned out to be a powerful tool to describe and predict the existence of guided waves, from specifically designed metamaterials to natural systems.

This thesis, comprised of two parts, first presents this evolution by illustrating it with recent results dealing with the existence of unidirectional confined waves (so-called "chiral waves") in driven systems, random graphs, and continuous media such as gyrotropic optical systems and geophysical fluids. The second part is an introduction of mathematical tools in topology that are necessary to capture more technical aspects that underlie this common phenomenology shared by plentiful waves physical systems.





## Résumé

Ce mémoire de thèse d'Habilitation à Diriger des Recherches présente des travaux en physique théorique traitant d'aspects topologiques de la propagation d'ondes.

L'étude des propriétés topologiques des ondes s'est longtemps déclinée comme l'étude des singularités d'intensité, de phase ou de polarisation d'un champ. Ces dernières années, de nouvelles propriétés topologiques des ondes ont été identifiées, en s'inspirant de la découverte des phases topologiques de la matière, dont l'effet Hall quantique entier découvert en 1980, et les isolants topologiques découverts en 2005 en sont des manifestations. Certains des outils de topologie utilisés et développés pour décrire ces matériaux quantiques ont permis de mettre en évidence le concept fédérateur clé de correspondance bord-volume, qui relie la caractérisation topologique des fonctions d'onde électroniques d'un matériau quantique à l'existence d'états confinés sur ces bords, ces derniers pouvant par exemple propager de l'information sans dissipation. Cette correspondance pouvant être appliquée aux ondes classiques, elle s'est avérée être un outil puissant pour décrire et prédire l'existence d'ondes guidées, que ce soient dans des méta-matériaux conçus sur mesure ou dans des milieux naturels.

Cette thèse, composée en deux parties, présente d'abord cette évolution en l'illustrant de résultats récents portant sur l'existence d'ondes confinées unidirectionnelles (dites « chirales ») dans des systèmes dynamiques forcés, des graphes aléatoires, et des milieux continus tels que des systèmes optiques gyrotropiques et des fluides géophysiques. La deuxième partie propose une introduction des outils mathématiques de topologie permettant d'appréhender les aspects plus techniques qui sous-tendent cette phénoménologie commune à de nombreux systèmes physiques ondulatoires.





# Contents

<b>Acknowledgements/Remerciements</b>	<b>iii</b>
<b>Foreword</b>	<b>v</b>
<b>Abstract (English/Français)</b>	<b>vii</b>
<b>I THE RISE OF TOPOLOGY IN PHYSICS</b>	<b>1</b>
<b>1 Chern numbers in physics : a matter of waves</b>	<b>3</b>
1.1 Why topology in physics ? An apology of topology . . . . .	3
1.2 From the quantum Hall effect to Chern insulators . . . . .	8
1.2.1 The quantum Hall effect . . . . .	8
1.2.2 Chiral edge states . . . . .	11
1.2.3 The bulk-edge correspondence . . . . .	12
1.3 Chern numbers beyond Chern insulating phases . . . . .	14
1.3.1 Fractional topological phases . . . . .	14
1.3.2 Symmetry-protected topological insulating phases . . . . .	14
1.3.3 Topological semi-metals . . . . .	15
1.3.4 Topological physics beyond condensed matter . . . . .	15
<b>2 Topological chiral waves</b>	<b>19</b>
2.1 Summary of the main results from the perspective of the bulk-edge correspon- dence . . . . .	19
2.2 Floquet systems and topological dynamics . . . . .	21
2.2.1 Dynamically-induced gauge fields . . . . .	21
2.2.2 Anomalous chiral edge states . . . . .	23
2.2.3 Oriented scattering networks . . . . .	27
2.3 Topological (classical) waves in continuous media . . . . .	30
2.3.1 Topological interface waves . . . . .	32
2.3.2 Missing chiral edge states . . . . .	45

## Contents

---

<b>3 Perspectives</b>	<b>51</b>
3.1 Scattering networks . . . . .	51
3.1.1 Floquet "metals" in photonics . . . . .	51
3.1.2 Random oriented scattering networks . . . . .	52
3.2 Continuous media . . . . .	52
3.2.1 Geophysical and astrophysical fluids . . . . .	52
3.2.2 Spectral flows and bulk-edge correspondences in continuous media . . . . .	54
<b>II METHODOLOGY</b>	
<b>A few topological tools for physicists</b>	<b>55</b>
<b>4 Basic concepts</b>	<b>57</b>
4.1 Homotopy, winding and degree . . . . .	57
4.1.1 An heuristic introduction to homotopy . . . . .	57
4.1.2 Winding and degree . . . . .	60
4.1.3 Winding of an Eulerian graph . . . . .	62
4.2 Topological aspects of degeneracy points . . . . .	62
4.2.1 Energy degeneracies as defects . . . . .	62
4.2.2 Phase singularity of the eigenstates . . . . .	63
4.2.3 Some insights on fiber bundles . . . . .	64
4.2.4 Degree of the Hamiltonian map . . . . .	65
4.3 Berry curvature and first Chern number . . . . .	68
4.3.1 Topology from the eigenstates . . . . .	68
4.3.2 Topological charge of a two-fold degeneracy point . . . . .	70
4.4 Berry monopoles . . . . .	74
<b>5 Spectral Flow and degeneracy points</b>	<b>79</b>
5.1 An anisotropic 2D Dirac Hamiltonian . . . . .	79
5.2 A generalized "spin-oscillator" model . . . . .	83
<b>6 Winding numbers in unitary dynamics : from Floquet systems to scattering networks</b>	<b>89</b>
6.1 Winding numbers in the unitary dynamics . . . . .	89
6.1.1 Winding of the Floquet operator . . . . .	89
6.1.2 Winding of the time-evolution operator and anomalous chiral states . . . . .	90
6.1.3 Gap invariants <i>u.s.</i> band invariants . . . . .	93
6.1.4 Phase rotation symmetry . . . . .	94
6.2 Discrete-time dynamics as scattering networks . . . . .	96
6.2.1 Graph representation of a periodically driven model . . . . .	96
6.2.2 Phase rotation symmetry of a cyclic graph . . . . .	98
6.2.3 Topological chiral states in random scattering networks . . . . .	102
<b>Bibliography</b>	<b>116</b>

# THE RISE OF TOPOLOGY **Part I** IN PHYSICS



# 1 Chern numbers in physics : a matter of waves

Le troisième exemple va nous montrer comment nous pouvons apercevoir des analogies mathématiques entre des phénomènes qui n'ont physiquement aucun rapport ni apparent, ni réel, de telle sorte que les lois de l'un de ces phénomènes nous aident à deviner celles de l'autre. [...] En résumé le but de la physique mathématique n'est pas seulement de faciliter au physicien le calcul numérique [...]. Il est encore, il est surtout de lui faire connaître l'harmonie cachée des choses en les lui faisant voir d'un nouveau biais.

---

Henri Poincaré  
*La valeur de la science* (1905)

## 1.1 Why topology in physics ? An apology of topology

The craze of physicists for topology has considerably increased since the discovery of new electronic phases of matter around 2005, called topological insulators [42]. This growing interest for topology is visible in the number of manuscripts submitted on the arXiv platform over the years ; while almost 4 physics manuscripts were in average daily submitted during the year 2000 with "topological" in their title or their abstract, there are about 13 papers that appeared each day during the last year (2018-19). Among those, almost 9 of them deal with condensed matter, against only 1 in 2000. In the meantime, the Nobel prize in physics awarded in 2016 David Thouless, Duncan Haldane and Michael Kosterlitz for "*theoretical discoveries of topological phase transitions and topological phases of matter*", that cover different topological properties of matter. This fast and continuing expansion reveals the successful input of topology in physics whose applications diversified and spread over many areas beyond quantum condensed matter. It has become such a staple and transversal tool for many physicists that the appellation *topological physics* is sometimes employed to refer to this multi-faced community, where a common theoretical tool federates fields that differ by their specific underlying processes and mechanisms as well as by their typical energy, time or length scales.

## Chapter 1. Chern numbers in physics : a matter of waves

---

It is worth mentioning the historical interconnection between the early stages of topology and physics, long before the rise of topological insulators, that can be traced back to the nineteenth century, from the description of vortices in fluids (that are phase singularities of the velocity field) to the attempt of describing the hypothetical atoms by knots [15]. Around the turn of the nineteenth century, Henri Poincaré's work embodies this intertwining of physics and topology. For instance, stimulated by the three-body problem encountered in celestial dynamics, he pioneered the investigation of singular points appearing in differential equations of motion on different surfaces and showed that these singularities could be classified according to the topology of these surfaces only, namely their genus  $g$ , that is roughly speaking the number of "holes" in the surface ( $g = 0$  for the sphere,  $g = 1$  for the torus ...) [15].

If topology did not quickly become a natural mathematical tool for most physicists, as usual as differential calculus, linear algebra, symmetry groups or probabilities, it nonetheless impregnated physics throughout the twentieth century by manifesting itself through numerous phenomena. The description of stable defects in materials and superfluids, sparkles of a wavy sea, boundary modes in quasi-crystals, helicity in hydrodynamics, instantons in quantum chromodynamics, quantization of the electrical transverse conductance, quantum computation *etc...*, use various topological tools such as homotopy theory, catastrophe theory, knots theory, homology, cohomology, K-theory,  $C^*$  algebra *etc...*

In the meantime, topology developed as an influential branch of mathematics. It can be basically thought as *geometry* without *metrics*, i.e. without the notion of distances, shapes and other local details (even though it is actually deeply connected to differential geometry, for instance). Topology deals with refined notions of continuity and equivalence between various objects under continuous deformations, such as functions, operators or spaces. It relates local properties, such as singularities or geometrical properties of a space, such as its curvature, to global properties, such as the genus of a surface. It is an active field of mathematics that diversified through years in various branches such as differential topology, combinatorial topology, algebraic topology, and established several fruitful connections with other branches such as geometry, knots theory, graph theory and partial differential equations theory, that are widely used in physics. The interested readers could immerse themselves into more dedicated books, such as *History of Topology* [15], to get a clearer overview on that point.

As often in mathematics, these developments were motivated by very concrete problems (such as Poincaré's three body problem) and reached highly abstract and technical considerations, often too obscure for most physicists, and far too removed from physical or practical concerns. Indeed, after Poincaré's works, topology was essentially developed by mathematicians and for mathematicians. It was not aimed to be of any use for physicists. And when the cream of the crop of topologists and physicists gathered together in a shared room, like a common lounge at the Princeton graduate school in the early forties, where "*people would sit around playing Go, or discussing theorems. In those days topology was the big thing*" as Richard Feynman experienced [28], topological physics did not spontaneously emerge as an obvious and fruitful combination. Actually topology and physics were so disconnected from each other that they

## 1.1. Why topology in physics ? An apology of topology

---

seemed to be irreconcilable, according to George Gamow, who noticed in the early sixties that [31] "*only the number theory and topology still remain purely mathematical disciplines without any application to physics. Could it be that they will be called to help in our further understanding of the riddles of nature?*"

As a matter of fact, at that time, topology had already subtly and implicitly interfered in physics : The famous example of the magnetic monopole introduced by Paul Dirac in 1931 [23] as an attempt to justify the quantization of electric charges, and later the prediction of the Ehrenberg-Siday-Aharonov-Bohm effect (1949-1959) [1] that accounts for the phase accumulated by charge particles that surround a magnetic flux line without being coupled to the magnetic field, are both re-interpreted nowadays through the prism of topology. Remarkably, these very examples have also strongly influenced the rise of topological physics in condensed matter these last decades.

For topology to become a natural tool for physicists, it required the breakthrough initiatives of few creative minds who unexpectedly shown how physical systems could be naturally described with topological concepts, sometimes simply because other approaches did not work. This was the case, to cite a few, of Lars Onsager who predicted the existence of quantized flux circulation in superfluid Helium, of Vadim Berezinski, John Kozterlitz and David Thouless who understood the key role of pairs of topological defects (namely vortices) to explain the transition to a superfluid state in two dimensions, of Michael Berry who revealed both the generic emergence of wave front dislocations in the large wavelength limit and the classification of stable shapes of caustics in the other limit, of Thouless, Kohmoto, Nightingale and den Nijs when they recognized a topological invariant of complex fiber bundles, called the first Chern number, in the transverse electric conductivity of a quantum Hall sample, thus explaining its quantization. Inversely, physics also keeps stimulating topologists, for instance when Charles Kane and Eugene Mele proposed a novel topological index in 2005 to characterize the quantum spin Hall effect that they predicted [54, 55]. This dialog between topology and physics has become more natural (even though not always easy) with time as it has been greatly facilitated by these successful pioneering works.

The reasons for the success of topology in physics are manifold. First it is useful because it can turn a complicated problem into a simpler one, by "topological equivalence", whose precise meaning depends on the object one considers (a function, a surface or a more complex structure), but typically deals with the notion of continuity between these two objects. Doing so, it somehow erases "unessential differences" and therefore reveals similarities between what may look different at first sight. Objects that are then "topologically equivalent" may be ranked into the same "box", usually labelled with a number, called *topological invariant*. Topology only makes distinction between boxes labelled differently, and confuses elements in the same box. Thus, topology is also useful in physics, not because it provides a fine and detailed information on the system, but on the contrary because this information is *coarse*. This is in strong contrast, for instance, with universal fluctuations of conductance that gives a fingerprint of a disorder configuration through the coherent propagation of electrons in

## Chapter 1. Chern numbers in physics : a matter of waves

---

diffusive metals. This coarse information allows *classifications*, that offer *intelligibility* to a wide class of phenomena. Topology was thus used in physics to classify defects in ordered phases, caustics of propagating waves and more recently phases of matter such as topological insulators.

Classifications account for the insensibility to interchanges between elements in a box, to follow the analogy. Topology is thus inherently related to a notion of *robustness* or *stability* against any transformation that leaves an element in its box. The system or the physical property of interest then inherits a *topological protection* which for instance helps explaining robust transport properties, from quantum electrons to oceanic waves, and is envisioned to be used in quantum computing.

Finally, topology also allows a *common phenomenology* between fields. This is in particular the case of what one could call *topological waves*, that are the classical analogues of topological phases. These are the main topic of this manuscript. All along the 19<sup>th</sup> century, the concept of wave allowed a unified understanding of various phenomena such as sound, tides, light, seisms and radio communications. It is thus not surprising that concepts of topology concern all these waves, as soon as it applies to one of them.

Actually, topology of waves has a long history, almost as ancient as waves themselves, through the study of their singularities. As recalled by Michael Berry in a limpid and synthetic article [12], three distinct wave singularities were already known back to the "miraculous 1830s" : the singularity of the intensity discovered by George Airy in 1838 when studying rainbows (and later revisited by Michael Berry within the broader concept of caustics and the formalism of catastrophe theory developed by René Thom), the singularity of the phase, revealed by William Whewell between 1833 and 1836 when discovering amphidromic points in the North sea, which are phase singularity points of tide waves, where tide must vanish, and finally the singularity of the polarization discovered by William Hamilton in 1832 that led to the prediction of the conical refraction. The more modern field of *singular optics* is inherited from these considerations. Topology of waves were also enriched in the late seventies, in particular through several works of Michael Berry and his collaborators, for instance with the highlight of wavefront dislocations of water waves that emerge when scattered by a vortex, thus providing a classical analog of the aforementioned Aharonov-Bohm effect [80, 11]. This last example anticipates how topological properties of quantum wave functions may inspire the search of novel topological properties of waves. Indeed, during the last ten years, physicists realized that topological properties similar to that of the integer quantum Hall effect and of the recently discovered topological insulators could be engineered with classical waves of various kinds. These topological properties are related to phase singularities of the complex eigenstates of the system in a parameter (or reciprocal) space, and translate in real space as the existence of confined modes at the boundary of the system that can be used to guide information, through the celebrated *bulk-edge correspondence*. This burst started with electromagnetic waves in the optical and micro-wave regimes, and was later pursued and extended to mechanical, elastic, acoustic, plasma, oceanic and atmospheric waves. And the search is still on! Coincidentally,

## 1.1. Why topology in physics ? An apology of topology

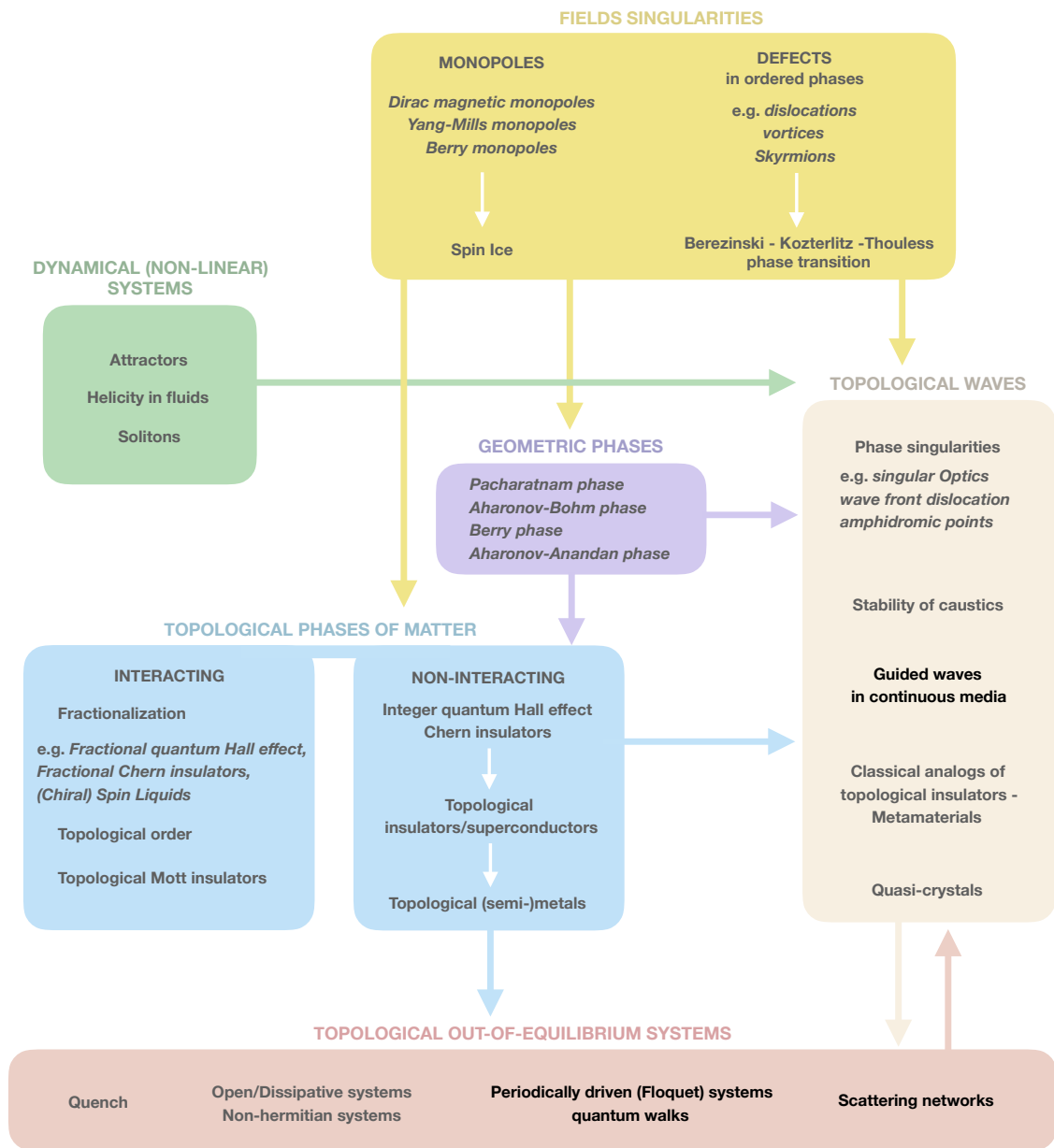


Figure 1.1 – Sketch of an overview of the spread of topology in physics. Keywords in bold are the subjects of chapter 2.

these topological properties, whose a few physical manifestations are illustrated in the rest of the part I of this manuscript and described more mathematically in part II, are closely related to the existence of degeneracies of eigenvalues of matrices (e.g. the Hamiltonian) precisely like the conical refraction driven by the polarization singularities mentioned above, that is certainly one of the very first manifestation of topology in physics.

Let us end this broad introduction with the figure 1.1 that sketches an attempt of summarizing this complex spreading of topology in physics (emphasized on low energy physics), and highlights different influences and articulations around the recent rise of topological phases and of topological waves. This is of course incomplete and subjective, but might help to have a first overview of the interconnections between different fields and concepts.

## 1.2 From the quantum Hall effect to Chern insulators

### 1.2.1 The quantum Hall effect

The quantized (or quantum) Hall effect emerges as a universal phenomena in two-dimensional electron gases subjected to a perpendicular magnetic field [61]. For a sufficiently large magnetic field, the longitudinal conductivity vanishes, as sketched in figure 1.2, meaning that a longitudinal current cannot be induced by an electric field applied in the same direction. The system thus becomes insulating. This insulating behavior can be understood easily from the energy spectrum of the simple Landau model of a quantum free electron gas coupled to a perpendicular magnetic field. Under the action of the magnetic field  $B$ , the quadratic dispersion relation of the electrons becomes that of the quantum harmonic oscillator : it consists in equally spaced non-dispersive (Landau) levels separated in energy by  $\hbar\omega_c$ , where  $\omega_c = eB/m_e$  is the cyclotron resonance frequency, with  $e$  is the elementary electric charge and  $m_e$  the electron mass. Generically, the Fermi energy lies between two successive Landau levels, and the system is thus insulating. This corresponds to the intuitive semiclassical picture where the electrons describe close cyclotron orbits. When, on the contrary, it coincides with a Landau level, for instance by sweeping the magnetic field, the system becomes suddenly conductor. Accordingly, the longitudinal conductivity exhibits a series of pics when increasing the magnetic field and vanishes everywhere else. This simple picture can be refined by introducing disorder : the Landau levels acquire some finite width and the sudden rise of conductivity can be interpreted as a quantum percolation transition, as understood by Chalker and Coddington [17].

The main surprise in the quantum Hall effect was the remarkable precise quantization of the transverse conductivity (or Hall conductivity)  $\sigma_H$  or equivalently of the Hall resistivity  $\rho_H$  as

$$\sigma_H = \rho_H^{-1} = \frac{e^2}{h} n \quad (1.1)$$

where  $n$  is an integer and  $\frac{h}{e^2} = 25812.807557\Omega$  is called the von Klitzing constant. When sweeping the magnetic field, the Hall conductivity thus exhibits a series of plateaus indexed by an integer  $n$ , reproduced in figure 1.2. These plateaus coincide with the vanishing longitudinal conductivity aforementioned and accordingly a jump between two plateaus is accompanied with a percolation transition. The quantum Hall effect reflects an unusual electronic phase of matter, as it cannot be naively ranked neither as an insulator nor as a metal.

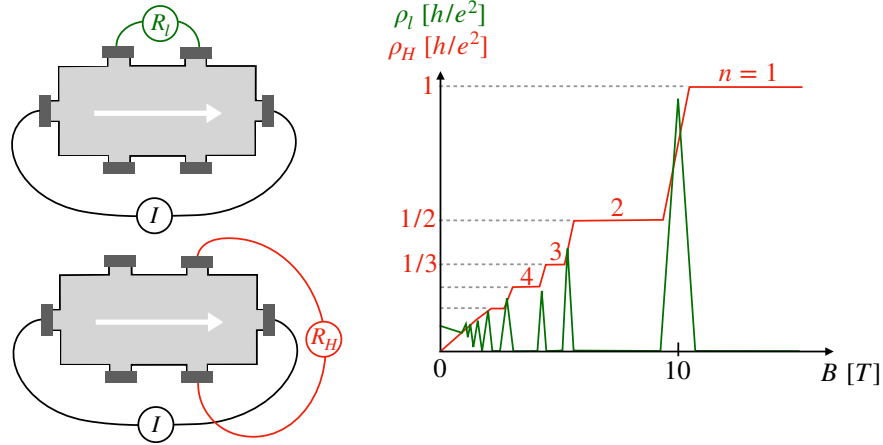


Figure 1.2 – Sketch of a typical measurement of the quantum Hall effect.

This effect was discovered by von Klitzing, Dorda and Pepper in 1980 in high mobility and low temperature GaAs/AlGaAs hetero-junctions for sufficiently high magnetic fields (typically at least a few Teslas) [61]. It was then reproduced in other two-dimensional electronic systems, and in particular at room temperature in graphene, that is a single sheet of graphite, where Carbon atoms organize according to a honeycomb lattice, as reviewed in [32].

The quantization of the Hall conductivity, and more specifically its high precision and reproducibility, irrespective of the imperfections of the samples, was unexpected and puzzling. The first step to its understanding was performed by Laughlin [65] who exploited the fact that the quantization did not seem to depend on the detailed geometry of the sample. He proposed to deform the Hall sample into an annulus, also called Corbino disk, so that the applied voltage is changed into an "angular" time-dependent flux through the disk  $V_\varphi = -\partial\phi/\partial t$ . In that geometry, Laughlin showed, thanks to gauge invariance of the electronic wave functions, that an adiabatic insertion of a quantum flux  $\phi_0 = h/e$  after a time  $t_0$ , shifts a state of radial quantum number  $m$  to the next  $m + 1$  toward the outer edge, which moves a charge  $-e$  in that direction, leading to the radial current  $I_r = -e/t_0$ . This shift of states is also referred to as *spectral flow*. It is accompanied with a bias voltage  $V_\varphi = h/e t_0$  and thus a transverse conductivity  $\sigma_{xy} = I_r/V_\varphi = -\frac{e^2}{h}$ .

The role of gauge invariance, both in quantum mechanics and classical electromagnetism, plays a central role in this argument. It was further exploited by David Thouless, Mahito Kohmoto and their collaborators in a series a papers [101, 62, 79, 78] where a more microscopic approach was used to compute the transverse conductivity both in the linear response theory (Kubo formula) and in the adiabatic regime, that both assume a weak bias voltage perturbation so that no transition to excited states occurs. These works reveal that the Hall conductivity (1.1) has a topological interpretation, as it relates the quantization number  $n$  to an integer-valued

topological invariant  $C_m$ , called first Chern number, as

$$\sigma_H = \frac{e^2}{h} \sum_{m < m_F} C_m \quad (1.2)$$

where the sum runs over all the occupied states  $m$  below the Fermi energy. This Chern number can be expressed as an integral of a *local* quantity  $F_n(k_x, k_y)$ , called Berry curvature, over the space of parameters, that is here the first Brillouin zone (or magnetic-Brillouin zone)

$$C_n = \frac{1}{2\pi} \int_{T^2} dk_x dk_y F_n \in \mathbb{Z}. \quad (1.3)$$

The first Brillouin zone is the smallest periodic area in reciprocal space. As such, it can be seen as a close two-dimensional torus  $T^2$  for the eigenstates  $|\psi_m(k_x, k_y)\rangle$ . This can be extended to "generalized boundary conditions" for a finite size (gapped) system without an underlying lattice structure and possibly weak interactions [79, 78]. In that case, the use of gauge invariance allows one to treat the Hall system as a torus whose two axes are fluxes  $\phi_x$  and  $\phi_y$  that substitute  $k_x$  and  $k_y$  in (1.3).

The mathematical formula (1.3) was obtained (in a more formal and general way) by Shiing-Shen Chern in 1945 [18] as a generalization of the Gauss-Bonnet formula that relates the gaussian curvature  $\kappa$  of a close surface  $S$  to its genus  $g$  as

$$2(1 - g) = \frac{1}{2\pi} \int_S \kappa dS \quad (1.4)$$

which emphasizes the relation between local and global properties.

The emergence of a Chern number in the expression of the transverse conductivity was unexpected. It revealed the topological nature of the quantum Hall effect. It has several benefits : First, it helps understanding the robustness and the precision of the measured Hall conductance, whose value cannot fluctuate. Second, it yields a new classification for the electronic phases of matter beyond Landau paradigmatic symmetry-based theory of phase transitions, that is based on topology. Instead of a local order parameter, *topological* phases are described by the value of a topological invariant, namely the first Chern number here, that encodes a global property of the system. Different plateaus of the Hall conductivity thus correspond to distinct topological phases.

Not to be confused with this Gauss-Bonnet result, the surface under consideration in equation (1.3), is fixed to be the torus. Still, the value of  $C_n$  may change because of a change of the Berry curvature, which is not the curvature of the torus. It rather characterizes the continuous family of complex eigenstates  $\psi_n(k_x, k_y)$  that are parametrized by  $k_x$  and  $k_y$ , and can be expressed as

$$F_n(k_x, k_y) = i(\partial_{k_x} \psi_n^*)(\partial_{k_y} \psi_n) - i(\partial_{k_y} \psi_n^*)(\partial_{k_x} \psi_n) \quad (1.5)$$

where the  $*$  stands for complex conjugation. Actually, time reversal symmetry, as an anti-

---

## 1.2. From the quantum Hall effect to Chern insulators

unitary symmetry that reverses momentum, acts on quantum states as  $\psi(k_x, k_y) \rightarrow \psi^*(-k_x, -k_y)$ . As a consequence, the Berry curvature  $F_n(k_x, k_y) = -F_n(-k_x, -k_y)$  is an odd function in the Brillouin zone, yielding vanishing Chern numbers. It is thus crucial to break time-reversal symmetry in order to obtain a topological phase characterized with Chern numbers. One way to break time-reversal symmetry is to insert a fixed magnetic field in the system. This corresponds to the quantum Hall effect. But this is not the only possibility, and one may break time-reversal by other means, e.g. with inserting magnetic impurities, by rotating the system or by applying a time-dependent electric field. Systems that exhibit the same phenomenology than that of the quantum Hall effect, but without a net magnetic flux through the sample, or in other words without Landau levels, are said to realize an *anomalous* quantum Hall effect. Furthermore, as their bands are labelled by Chern numbers, they are called *Chern insulators*. A celebrated model for Chern insulators was cooked up by Duncan Haldane in 1988 [40]. This is a toy model for spinless electrons on the honeycomb lattice. When electrons hop to second nearest neighbours sites, they pick-up a phase in such a way that the total flux through the unit cell vanishes. Even though this model may seem artificial, it captures the essential conditions to obtain a Chern insulator : breaking time-reversal symmetry by the additional phase which opens a gap in a different way from what an on-site potential does. It inspired many theoretical works (like the first model for the quantum spin-Hall effect [54]) as well as numerous experimental works from photonic crystals [109] to trapped cold atoms [53] to cite a few.

### 1.2.2 Chiral edge states

The existence of an extremely stable transverse conductivity means that the quantum Hall phase cannot really be considered as an insulator, or at least in the usual sense, since a transverse electric current can actually flow in the system. How is this possible since the energy spectrum is gapped? Actually, as shown by Halperin [41], the energy spectrum is not gapped anymore if one includes the boundary of the system, that adds a potential of confinement and thus bends the Landau levels. If an edge is added, say along the  $y$  direction, then the Landau levels acquire a dispersion along  $k_y$ . This dispersion have a simple semiclassical interpretation : At the Hamiltonian level, the presence of the magnetic field in the system enters through a vector potential via the Peirels substitution, for instance  $k_y \rightarrow k_y + eA_y = k_y - eBx$  in the Landau gauge, where  $x$  is the position variable perpendicular to the edge. This leads to the definition of the center of the cyclotron orbit as  $x_c = k_y/eB$  and allows an interpretation of the bending of the energy spectrum in real space via  $E_n(k_y) \rightarrow E_n(x_c)$ . It turns out that the bending occurs when approaching the edge, while the Landau levels remain flat in the bulk. The semiclassical interpretation is that for certain values of  $k_y$  the cyclotron orbit touches the edge and becomes open. The semi-classical electron "skips" along the edge and consistently have a finite group velocity. Thus, wherever the Fermi energy lies, it has to intersect the bending dispersion relation meaning that dispersive states are available *only* close to the edge, even in the presence of a small amount of disorder. These are more generally referred to as *chiral edge states*. The *chirality* here means that the sign of the group velocity is fixed, and

that there is no other accessible state at the same energy toward which they could couple by exchanging momentum, especially in the presence of disorder. Chiral edge states are thus expected to be immune against backscattering, meaning that they contribute to the electric conductance  $G$  as modes  $m$  with a perfect transmission  $T_m = 1$ , according to the Landauer formula  $G = e^2/h \sum_m T_m$  and are thus insensitive to Anderson localization. A more general approach of these transport properties, based on scattering matrices, and developed mostly by Markus Büttiker, can take into account an arbitrary multi-terminal geometry with different bias voltages between the terminals [14]. More sophisticated sample geometries (4 terminals, 6 terminals...) are useful to relate explicitly the (theoretical) conductivity with the (measured) conductance, and also to predict correctly the values of terminal-dependent non-local conductances by only assuming the existence of the chiral edge states, and thus corroborate their existence.

### 1.2.3 The bulk-edge correspondence

The simple semi-classical skipping orbits argument yields the uni-directional edge modes, whose existence allows correct predictions of the measured quantized Hall conductance and its multi-terminal generalizations [14]. It is remarkable that these edge modes are associated to some back-scattering immunity, or *robustness* against effects of disorder such as Anderson localization. This robustness must be put in parallel with the quantized bulk conductivity that has a topological origin. Actually, there is a deep connection between the existence of chiral edge states and the bulk topological invariant, called the *bulk-edge correspondence*, and pioneered by Yasuhiro Hatsugai in 1993 [44, 43]. Originally, this correspondence was derived for a Bloch electron on a square lattice subjected to a magnetic flux. It relates the number of chiral edge states, i.e. that bridge an energy gap, to the Chern numbers of the bands. More precisely, in a cylinder geometry (or infinite strip), a chiral edge state localized at one boundary is necessarily accompanied with a counter-propagative chiral edge state localized at the opposite boundary, by conservation of the current. This pair constitutes a loop in a spectral gap : one edge state flowing from a band  $n$  to a band  $n + 1$  while the other flows from the band  $n + 1$  to the band  $n$ , their group velocity necessarily having opposite signs, as sketched in figure 1.3 (a).

An elegant construction, based on transfer matrix theory allows the assignment of each energy gap to the genus of a Riemann surface of complex energies. The introduction of these complex energies makes possible a common analysis of the bulk propagative modes and of the evanescent edge states that live in these gaps. Within that picture, each pair of propagating and counter-propagating chiral edge states, that are localized on opposite boundaries and that bridge a gap in opposite directions, form a loop that winds around a hole of the Riemann surface. This winding  $I_j$  is a topological property of the (pair) of chiral edge state(s) that bridge the gap  $j$ . The bulk-edge correspondence then relates this winding number to the Chern

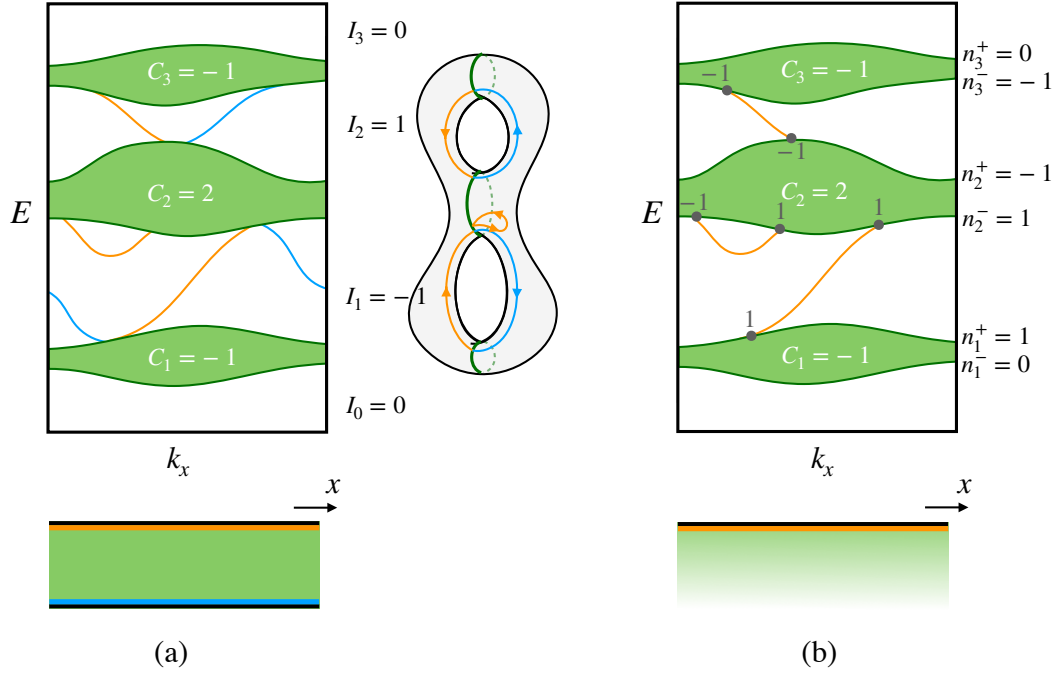


Figure 1.3 – Illustrations of the bulk-edge correspondence according to (a) Hatsugai in the case of an infinite strip geometry and (b) Graf and Porta in the case of a half infinite geometry.

numbers as

$$I_j - I_{j-1} = C_j \quad (1.6)$$

where the gap  $j$  lies just above the band  $j$ , thus establishing a simple relation between the spectral flow of the chiral edge states and a topological index of the bulk bands. It thus confers a topological nature to the chiral edge states : a Chern insulator is guaranteed to have chiral edge states whose spectral flow is determined by the relation (1.6).

Another point of view developed later by Gian Michele Graf and Marcelo Porta uses scattering states [37]. This approach, rooted by Levinson theorem, counts the number of evanescent states (i.e. edge states lying in the gap) that merge to a band, even though they do not cross the gap, via the winding number of the determinant of a scattering matrix. In particular, this approach applies to a semi-infinite system, as there is no need to form a loop made of two counter-propagating edge states. There, the Chern number of a band  $j$  is related to the sum  $n_j^-$  ( $n_j^+$ ) of the winding numbers associated to states that merge to the band from the gap below (above) as

$$n_j^- - n_j^+ = C_j \quad (1.7)$$

which amounts to count the number of states that merge to the band  $j$  when sweeping  $k_x$ . An example is shown in figure 1.3 (b).

There are many other works that deal with the bulk-edge correspondence, not only about Chern insulators, but also for other topological insulators in one and three dimensions and in different symmetry classes. The universality of the bulk-edge correspondence is remarkable, and it is also remarkable that this commonly accepted concept is still an active topic of research.

### 1.3 Chern numbers beyond Chern insulating phases

Chern insulators have become a cornerstone of topological physics. They stimulated different fruitful directions that are current active fields of research. Let us give a brief overview of the main ones.

#### 1.3.1 Fractional topological phases

Chern insulators constitute a building block to realize *fractional* topological phases without Landau levels, called fractional Chern insulators, for which the transverse conductivity is quantized by a rational number rather than by an integer, for instance  $\sigma_{xy} = \frac{1}{3} \frac{e^2}{h}$ . Such remarkable phases, first discovered in the fractional quantum Hall effect [102], can emerge for specific partial filling factors of the bands, when repulsive interactions between electrons become relevant and lead to a degenerate ground state separated from the other excited states by an energy gap. A good starting point to implement such an exotic phase is then to consider a Chern insulator whose bands are (almost) flat so that the kinetic energy becomes negligible in comparison to the interaction [90, 97].

#### 1.3.2 Symmetry-protected topological insulating phases

Chern insulators are actually a particular case of *topological insulators*, that are essentially band insulators whose bulk wave functions own a topological property. Indeed, it turns out that other topological insulating phases may exist when an additional symmetry is imposed. In that case, bands of the gapped single-particle Hamiltonian are characterized by a topological invariant, that in general is not the first Chern number. Of main importance was the theoretical discovery in 2005 by C. Kane and E. Mele of a new insulating topological phase in two dimension protected by time-reversal symmetry [54]. Its physical manifestation, called quantum spin Hall effect, was first observed in group of L. Molenkamp in HgTe/CdTe quantum wells [63] following a theoretical prediction by Bernevig, Huh and Zhang [9]. This new phase can somehow be simply apprehend as a "superposition" of two time-reversal copies of a Chern insulator, so that the full system preserves time-reversal symmetry. In that simple limit, the Chern number remains a good topological invariant to describe the phase. Actually, when the two copies are coupled, by any term that preserves time-reversal symmetry, this simple picture does not hold anymore and a new topological invariant, not referenced in the mathematics literature, had to be introduced to correctly characterize the Kane and Mele phase [55].

### 1.3. Chern numbers beyond Chern insulating phases

---

Unlike Chern numbers, this new invariant can only take two distinct values. It is said to be a  $\mathbb{Z}_2$ -valued topological number. Soon after these theoretical and experimental discoveries, other topological insulating phases were proposed and some of them were quickly observed, such as three-dimensional topological insulators, also characterized by  $\mathbb{Z}_2$ -valued topological numbers. This demonstrated the possibility to achieve new topological phases by exploring different symmetry classes and dimensions. Single-particle gapped Hamiltonians were then classified according to their symmetry classes, (unitary, anti-unitary such as time-reversal symmetry, crystallographic ...), together with the space dimension, leading to classifications of topological insulators and superconductors [94]. In this unexpected new world, where boring insulators revealed their hidden beautiful diversity, Chern insulators constitute a single example (but not the least) of topological insulating phases among many others.

#### 1.3.3 Topological semi-metals

By definition, Chern insulators deal with gapped Hamiltonians. However, it was realized [106, 75, 107, 7] and later observed in TaAs [113], that peculiar kinds of three-dimensional semi-metals own a topological property characterized by the first Chern number. The band structure of these materials is gapped everywhere, except at a few points in the Brillouin zone where two bands touch linearly. In the vicinity of these two-fold degeneracy points, the linearized Hamiltonian has the typical form of a Weyl Hamiltonian  $H \sim v_F \mathbf{k} \cdot \boldsymbol{\sigma}$  with  $\boldsymbol{\sigma}$  the vector of Pauli matrices and where the celerity of light is substituted by the Fermi velocity  $v_F$  when the Fermi energy lies near by such points. For this reason, these semi-metals are called *Weyl semi-metals*. Remarkably, the band touching points, or Weyl points, have a topological property, often associated to the fact that a small perturbation cannot remove them by lifting the degeneracy. Actually, Weyl points can be seen as hedgehog point defects in reciprocal space, in respect of the spin (or pseudo-spin) structure  $\langle \boldsymbol{\sigma} \rangle$  that surrounds it. The orientations of this hedgehog structure are opposite for each of the two eigenstates involved in the band crossing. Furthermore, these two eigenstates, parametrized in reciprocal space around a closed surface that surrounds the Weyl point, carry an opposite (non-vanishing) first Chern number, called *topological charge* in this context.

#### 1.3.4 Topological physics beyond condensed matter

An important fruitful development, that we will be concerned with for the rest of this review, is the possibility to realize Chern insulators beyond electronic quantum systems, where atoms, photons, or classical waves play the role of electrons.

In the absence of a Fermi energy, the condensed matter notion of a band insulator is ill-defined. However, the dispersion relation is a meaningful concept. By engineering an "artificial lattice", in order to mimic a solid, energy (or frequency) band structures can be defined in the Brillouin zone. These bands are typically separated by gaps, in the absence of accidental degeneracies. The existence of these gaps, implying that states at certain energies/frequencies cannot propa-

gate through the system, is sufficient to generalize the concept of band insulator. The novelty inherited from topological insulators, is that the bands (or should we say their corresponding eigenstates parametrized over the Brillouin zone) can have a topological property, for instance characterized by a Chern number.

In insulating phases, the physical content of Chern numbers lies both in the quantized Hall conductivity and in the existence of chiral edge states. However, even though these two properties are related to the same measurable transport property, they are not equivalent. In particular, the expression of the conductivity as a Chern number lies on several hypothesis such as the existence of a Fermi energy, but also the equivalence of gauge invariances of electromagnetism (the applied electric field) and quantum mechanics (the electrons wave-function in the material). These properties are specific to condensed matter systems, and cannot be easily generalized to any other classical insulator (optical, acoustic ...). However, the existence of chiral edge states, that is guaranteed by the bulk-edge correspondence, is a spectral property that does not require these peculiar physical properties. As a consequence, chiral edge states can be implemented in generalized band insulators beyond the electronic ones, while the quantized transverse conductivity cannot. The bulk-edge correspondence is the universal concept that allows the generalization of Chern insulators (and more generally topological insulators) beyond quantum electronic systems. It offers new opportunities in the manipulation of robust guided transport, in particular with classical waves.

This led to an impressive prominent diversification of platforms, from quantum to classical *artificial* lattices (by contrast with quantum electronic materials) in order to engineer and to probe topological properties, often (but not always) through the observation and the manipulation of the boundary modes. This includes cold atoms trapped in optical lattices, gyromagnetic photonic crystals, optical coupled waveguides arrays, circuits of quantum-electro-dynamical systems, silicon ring resonator arrays, microwave resonator arrays, radio-frequency circuits, electrical circuits, circuits quantum electrodynamics, bianisotropic metamaterials, exciton-polariton lattices, optomechanical arrays, photonic mesh lattices, circulating airflow acoustic lattices, gyroscope lattices, pendula lattices, geared metamaterials, origami metamaterials, acoustic resonator lattices, structured plates, granular crystals, Helmholtz resonators lattices, active liquid metamaterials, among others... Detailed descriptions of most of these setups can be found in specific reviews dedicated to topological physics in different platforms in photonics [82], acoustics [116] and ultra cold atoms [35].

The versatility of these platforms allows an experimental control of relevant physical parameters, different from those that can be usually tuned in condensed matter, such as hopping amplitudes between neighbours sites, landscape of disorder, amplitude of the interactions, shape of the system's boundaries, and so on. Some of these platforms give also access to physical observables that are usually out of reach in solids, such that the direct probe of boundary modes or their dispersion relation.

The main conceptual difficulty to conceive "artificial" topological insulators is to engineer

### 1.3. Chern numbers beyond Chern insulating phases

---

”artificial” gauge fields, analogous to the electromagnetic vector potential in the quantum Hall effect or in the Haldane model. In the case of Chern insulators, time-reversal symmetry must be broken. This steers the search for appropriate mechanisms, in particular when the particles or waves under consideration do not couple to a magnetic field. Many clever solutions were found, as reviewed in [2]. For instance, time-reversal symmetry breaking gauge fields can be created for trapped (neutral) cold atoms from Raman transitions between internal degrees of freedom [98, 34], for photons from a coupling with acoustic phonons [84], and for acoustic waves from the irreversibility of a spontaneous active liquid flow confined in a lattice composed of annular channels [96]. A fruitful general strategy consists in imposing a chirality in the system, by means of a rotation. This idea can translate as : circularly shaking/irradiating the system [81, 53, 33], including rotating elements (gyroscopes, rotors acoustics, circulators) or changing in time the hopping parameters [58, 89]. These different processes all imply (periodic) time-dependent couplings, and are referred to as Floquet engineering, whose certain aspects are discussed in section 2.2.



## 2 Topological chiral waves

Vous savez, les idées, elles sont dans l'air. Il suffit que quelqu'un vous parle de trop près pour que vous les attrapiez!

---

Raymond Devos

### 2.1 Summary of the main results from the perspective of the bulk-edge correspondence

This chapter reviews some of the main results obtained during the last two years that are hinged around the search for chiral waves beyond Chern insulating phases. Two main directions have been followed, that compose the two sections of this chapter : *Floquet systems and topological dynamics* in section 2.2 and *Topological waves in continuous media* in section 2.3. Each in their own way, these two directions show how the concept of bulk-edge correspondence can be extended beyond electronic phases in crystals, to characterize the existence of topological uni-directional guided waves in various systems from optics to geo-fluids.

In *Floquet* systems, that are periodically-driven systems, *anomalous* regimes can be found where topological chiral edge states exist despite the vanishing of the Chern numbers  $C$ . Instead, a *dynamical* topological invariant, quoted  $W \in \mathbb{Z}$ , can be defined from the evolution operator rather than from the Hamiltonian. This index takes into account the full (unitary) dynamics that turns out to enrich the topological properties of the system, with in particular the existence of these *anomalous* chiral edge states. The bulk-edge correspondence can then be rephrased in terms of this new index that correctly predicts the existence of chiral *edge* states and therefore of chiral *interface* states between two Floquet systems of different indices  $W$ . Unlike the Chern number, the  $W$  index is assigned to a spectral gap rather than to a band.

There is a close connection between Floquet systems and **scattering networks**, that model the propagation of confined waves as a succession of free propagations and scattering events. In particular, their evolution operator has topological properties similar to that of Floquet

systems, encoded into a topological invariant  $\tilde{W} \in \mathbb{Z}$ . Actually certain discrete-time dynamics (or discrete-time drivings) can be mapped onto oriented scattering lattices. But scattering networks are also interesting in themselves. First, because the topological invariant  $\tilde{W}$  is ill-defined as it depends on the choice of unit-cell (unlike  $W$  in periodically driven systems), and thus does not predict correctly the existence of edge states, but only of interface states. Second, because they exhibit anomalous chiral interface states in the total absence of periodicity; in particular they show that these exotic topological uni-directional modes are not specific to *periodically* driven systems and are actually quite generic in random scattering networks even when the  $\tilde{W}$  index cannot be defined at all.

Classical waves such as light and sound are commonly described in **continuous media**. In the absence of a Brillouin zone, the characterization of their topological properties is more involved, and requires a special care. When the Chern numbers  $\tilde{C}$  can be properly defined for the wave bands, it turns out that they do *not* guaranty the existence of chiral edge modes whose existence and the number actually depend on the boundary conditions. However, it is observed that the Chern number still enters a generalized *anomalous* bulk-edge correspondence that also accounts for non-chiral edge states as well as for additional hidden bulk modes. In contrast, the number of interface chiral modes is well described by the difference of Chern numbers.

It is remarkable that the concept of bulk-edge correspondence survives these different extensions beyond its original formulation, and applies for spectra other than energy spectra (e.g. quasi-energy or frequency) and for parameter spaces other than the Brillouin zone (e.g. wave numbers). It is also remarkable that edges and interfaces do not play an identical role. In particular, edges somehow make more troubles than interfaces, and for different reasons, whether it is in scattering networks or in continuous media. In contrast, chiral interface states can always be described by a "local" approach, around the band touching point that separates the two distinct gapped media. Such a band touching point is actually the source of a Berry curvature  $\mathcal{F}$ , whose flux is a Chern number  $\mathcal{C}$  that directly accounts for the existence of interface states through a *spectral flow*, irrespective of the possible ill-definition of the bulk Chern numbers of the gapped systems from each side of the interface. In that sense, this Chern number  $\mathcal{C}$  is somehow more "fundamental" than that of the gapped phases  $C$ . It also allows the prediction of chiral modes in anisotropic media, along a line in space where a "mass" parameter  $m$  changes sign, and by doing so generates the band touching at the origin of the topological property. In this case, there is no actual edge in the system. The figure 2.1 summarizes this viewpoint.

This following presentation is aimed to be accessible to non specialists and is thus deprived of calculations and technical details. These could be found in the related publications or preprint attached in appendix. The basic technical aspects of topological properties that are discussed in this chapter are introduced in detail in Part II.

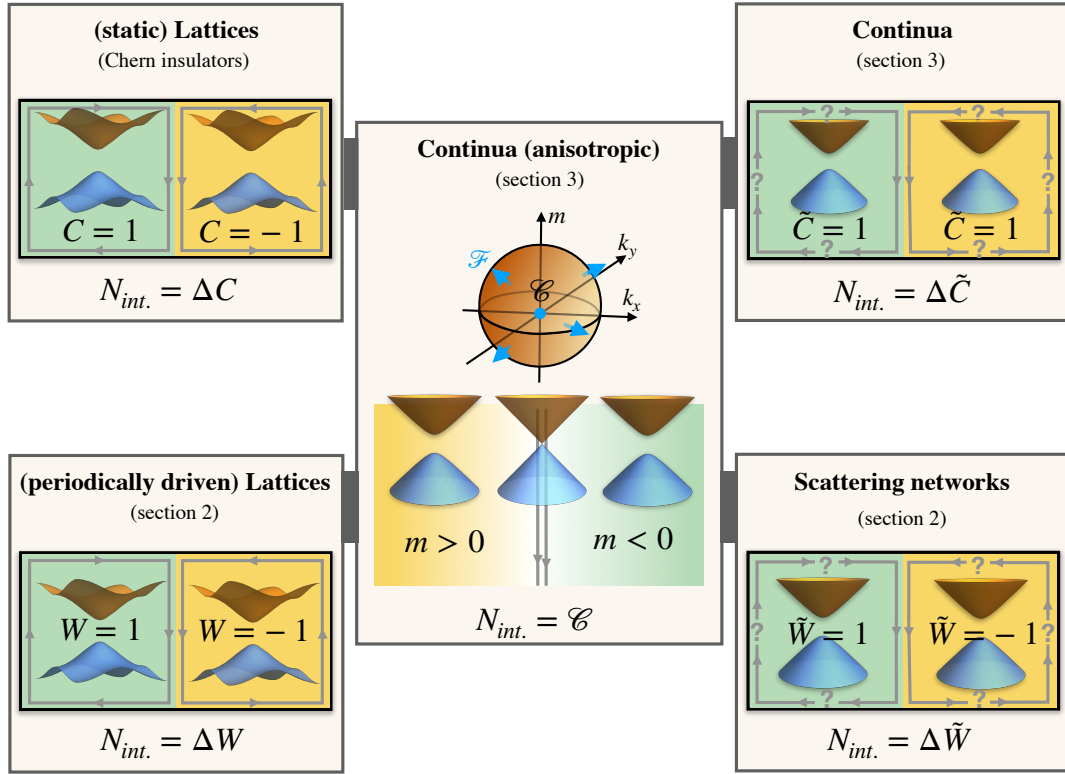


Figure 2.1 – Perspective of the concept of bulk-edge correspondence, from Chern insulators to Floquet systems, scattering networks and continuous media.

## 2.2 Floquet systems and topological dynamics

### 2.2.1 Dynamically-induced gauge fields

Geometrical or topological effects are inherently related to a gauge field (see [2] for a review in various systems). This is explicit in the quantized Hall effect or in the Haldane model for Chern insulators, that both require the existence of magnetic fluxes, either due to an external magnetic field that acts globally over the scale of the sample in the former case, or that is imposed locally in a staggered way in the later one. It follows that in both cases, the quantum particle experiences a *static* vector potential  $A(r)$  that enters for instance the Aharonov-Bohm phase that dresses the hopping energy coupling  $J$  between sites  $R$  and  $R'$  on the two-dimensional lattice as  $J \rightarrow J e^{i \frac{e}{\hbar} \int_R^{R'} A dr}$  and thus breaks time-reversal symmetry by making this coupling complex. Engineering a phase entering as  $J e^{i\phi}$  in the coupling terms is thus the goal to reach to make topological properties appear.

In 2009, Takashi Oka and Hideo Aoki proposed to induce a Hall-like state by replacing the external magnetic field by an in-plane *circularly polarized light* [81]. Non linear polarization breaks the time-reversal symmetry of the Schrödinger equation, and one should expect that the resulting effect is reversed when switching the polarization from clockwise to anti-clockwise,

in the same way that one can reverse the orientation of the magnetic field in the quantized Hall effect. The polarized light is considered through a classical time-periodic electric field  $\mathbf{E}(t) = \mathbf{E}(t + T)$ , and it follows that the gauge field, namely the vector potential that satisfies  $\mathbf{E}(t) = -\partial_t \mathbf{A}(t)$ , is also periodic in time. Applying this idea to the low energy massless Dirac fermions of graphene, Oka and Aoki shown that this ac driving opens a gap and generates a Berry curvature with the same sign in the two valleys, so that the net effect does not vanish. Applying an additional bias voltage, they shown numerically that a transverse conductivity emerges giving rise to a *photovoltaic Hall effect*.

There is a deep connection between this approach and the Haldane model since in both cases time-reversal symmetry is broken without adding a net magnetic flux through each unit cell, and thus without changing the effective size of the Brillouin zone, unlike with an actual magnetic field. This equivalence can be established more rigorously in the regime of high frequency and low amplitude of driving. Beyond this regime, Floquet systems exhibit a much richer topological phase diagram than that of the Haldane model, as we shown in [21, 36]. In particular, as shown in figure 2.2, a topological transition that flips the sign of the Chern number can be induced by increasing the amplitude  $E$  of the driving electric field, while keeping the polarization fixed. This results from an interplay between gaps opening mechanisms and the motion of the Dirac points, that are both controlled by the external driving. It follows that the chirality of the edge states is reversed while the polarization of the driving is not. This is where the similitude with the Haldane model and with the quantized Hall effect breaks down. Our prediction was later confirmed in a photonics experiment by the group of Mikael Rechtsman, where a fictitious in-plane circularly polarized electric field is engineered in helical coupled waveguides arrays [39], an experimental platform that allowed the first observation of chiral edge states in the Floquet systems in 2013 [89].

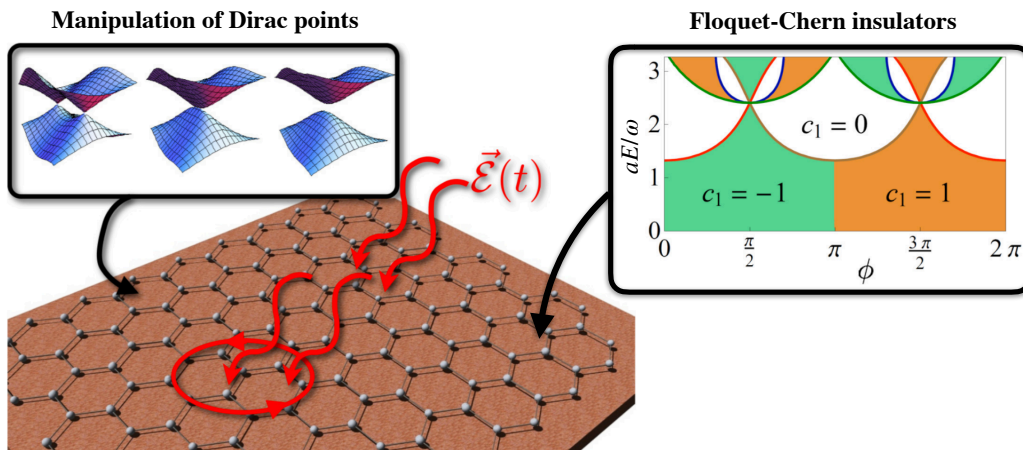


Figure 2.2 – The tight-binding model of a honeycomb lattice subjected to an in-plane rotating electric field shows various topological phenomena such as the merging of Dirac points in the Floquet spectrum and Chern phases that can be manipulated with the amplitude, the frequency and the polarization  $\phi$  of the driving field.

The idea of Oka and Aoki was shortly followed by Inoue and Tanaka [50] and then by Lindner,

Refael and Galitski [68] who proposed the idea of a "Floquet topological insulator" where a quantum spin Hall effect could be triggered in a semiconductor by shining light on it. Similar ideas of 'artificial gauge fields' were already developed in the beginning of the 2000s in cold atom systems; the state of the field in 2007 is reviewed in [70]. In any cases, this idea essentially consists in creating an artificial gauge field by periodically driving the system. This driving could have different physical origins such as a circularly polarized electric field in electronic systems, a circular shaking of the optical trap for cold atoms or a helical change of optical index in photonics waveguides arrays. In 2010, Kitagawa et al. also revisited the adiabatic limit of Thouless pumping in one-dimensional insulators, and reinterpreted the quantization of the pumped current over a period of drive as the winding of the quasi-energy in the one-dimensional Brillouin zone, thus establishing an elegant equivalence between a first Chern number of the instantaneous eigenstates in  $(k, t)$  space and the winding of a spectral quantity in  $k$  space [58]. At this stage, the use of Floquet physics essentially consisted in providing a new way to engineer already known topological states. But it turned out that there was more to be discovered.

### 2.2.2 Anomalous chiral edge states

#### Chiral edge states with vanishing Chern numbers

There is a key difference between usual Chern insulators as a static equilibrium phase and Floquet Chern insulators. Without even addressing the physical problems of heating and dissipation that must be considered to discuss the existence of steady states in electronic and cold atoms driven systems, the spectral properties (and thus the topological properties) are distinct to those of equilibrium systems. Indeed, the Hamiltonian  $H(t)$  is not invariant by arbitrary translation in time, but only by multiples of the driving period  $T$ , that is  $H(t + T) = H(t)$ . A direct consequence is that energy is only conserved up to  $2\pi/T$ . A Floquet system is somehow the time analog of a crystal : The momentum of a particle in a periodic spatial potential of lattice spacing  $a$  is only conserved up to  $2\pi/a$ . In that case, Bloch theorem states that the wave function of this particle is parametrized by a quasi-momentum  $k$  as  $\Psi_k(r) = e^{ikr} u_k(r)$  where  $u_k(r) = u_k(r + a)$  has the spatial periodicity of the lattice, such that two states  $\Psi_k$  and  $\Psi_{k+G}$  that differ from a vector  $G$  of the reciprocal lattice describe the same physical state. Similarly, for Floquet systems, a quasi-energy  $\epsilon$  is introduced, that follows from the periodicity in time of the Hamiltonian. The Floquet theorem then states that the solutions of the Schrödinger equation  $i\hbar\partial_t\Psi(t) = H(t)\Psi(t)$  read  $\Psi_\epsilon(t) = e^{i\epsilon t}\Phi_\epsilon(t)$  where  $\Phi_\epsilon(t) = \Phi_\epsilon(t + T)$  and where  $\Psi_\epsilon(t)$  and  $\Psi_{\epsilon+2\pi/T}(t)$  describe the same physical state. Such dynamical systems are equivalently described by their unitary evolution operator  $U(t, t_0)$  that satisfy  $i\hbar\partial_t U(t, t_0) = H(t)U(t, t_0)$  where  $t_0$  is an arbitrary initial time. In particular, the Floquet operator<sup>1</sup>  $U_F = U(T + t_0, t_0)$  that is the evolution operator over one time period, plays a key role in the analysis of periodically driven systems, as it describes the stroboscopic evolution

<sup>1</sup>The Floquet operator is not unique, as it depends on the choice of origin of times  $t_0$ . Its eigenvectors depend on this choice, not its eigenvalues. We shall ignore this depend in all the manuscript

## Chapter 2. Topological chiral waves

---

$U(t_0 + nT, t_0) = U_F^n$ . Moreover its eigenvalue spectrum  $\{\lambda\}$ , that lies on the unit circle in the complex plane, is directly related to the quasi-energy defined above as  $\lambda = e^{-i\epsilon T}$ .

In 2013, Mark Rudner, Netanel Lindner, Erez Berg and Michael Levin showed in an inspiring paper that Floquet systems may possess specific topological properties without any equivalence in usual static insulators [91]. In particular, they proposed a simple time-periodic tight-binding model to illustrate the possible existence of chiral edge states that are not captured by the first Chern number, as it is usually the case in the static situation by virtue of the bulk-edge correspondence. These edge states, dubbed as *anomalous*, appear in the spectral gap of the Floquet operator. The key point to understand the failure of the bulk-edge correspondence is that the eigenvalue spectrum  $e^{-i\epsilon T}$  of  $U_F$  is unbounded in sharp contrast with Hermitian tight-binding Hamiltonians whose eigen-energy spectra are bounded. Indeed, the bulk-edge correspondence states that the first Chern number of a bulk band  $n$  counts the difference of the number of edge states that merge to the bulk states from the gap above the band with those that merge to the bulk states from the gap below the band, when varying  $k_x$  (for a boundary that lies along the  $x$  direction). The periodicity of the Floquet phase spectrum allows situations where each gap hosts the same number of chiral edge states so that the Chern number of each band remains zero. The Chern numbers of the Floquet bands therefore cannot reveal the number of chiral modes in that case. Illustrations of different scenarios of Floquet chiral edge states are shown in figure 2.3.

A Floquet chiral edge state cannot be removed by a continuous deformation as long as the quasi-energy gap does not close. This is the hallmark of a spectral flow which is the typical signature of a topological property. How to figure out the topological invariant that accounts for this property? The Chern number we mentioned concerns the eigenstates of the Floquet operator  $U_F$ , that only gives a "snapshot" of the dynamical system after a time period. This information is of course incomplete as it ignores the full "movie", namely the path in time followed by the system during its evolution. The full evolution over a period is given by the evolution operator  $U(t + t_0, t_0)$  that is unitary. Here one must remember that the group of unitary operators is not simply connected, which means that two paths that connect two unitaries are not necessarily homotopic. As a consequence, there can exist different paths, i.e. different evolution operators, that connect  $U(t_0, t_0) = \mathbb{1}$  to the Floquet operator  $U_F = U(T + t_0, t_0)$ . This is how different time-evolutions can be topologically inequivalent, whereas the bulk Floquet eigenstates (and thus the Chern numbers) remain the same. As shown by Rudner, Lindner, Berg and Levin, this *dynamical* topological property is captured by a winding number  $W \in \mathbb{Z}$ . More precisely, this topological index is defined with respect to a spectral gap of the Floquet operator  $U_F$ . Two spectral gaps may be associated with different topological indices  $W$ . An important relation with Chern number of a band is that the  $W$  indices evaluated in the gaps "above" the band and "below" the band are related as

$$W_{\text{above}} - W_{\text{below}} = C. \quad (2.1)$$

The winding numbers  $W$  thus provide a finer topological description than the first Chern

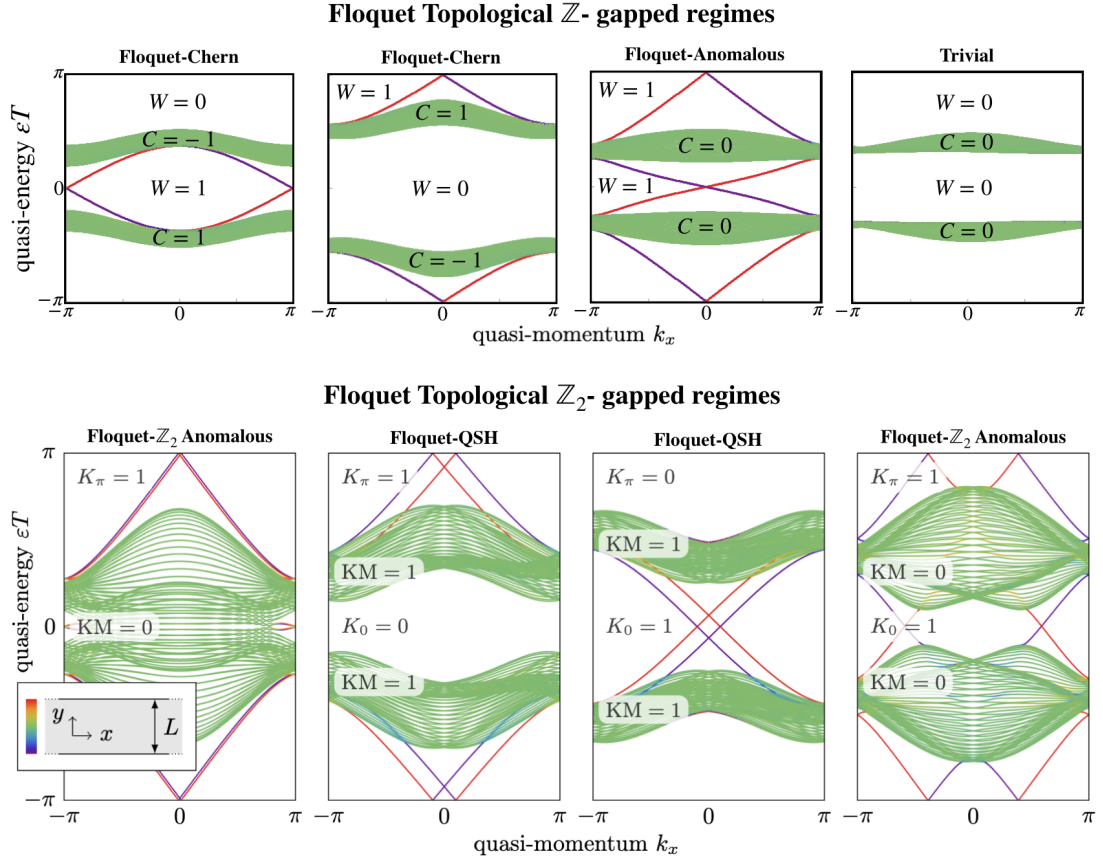


Figure 2.3 – Quasi-energy spectral that show the different topological regimes in an infinite strip geometry, (top) with time-reversal symmetry broken and (bottom) with time-reversal symmetry. The two models used are the one by Rudner-Lindner-Berg-Levin in [91] and its time-reversal symmetric situation that we proposed in [16]

numbers  $C$  of the bands since the set of all Chern numbers can be inferred from the set of  $W$  invariants, and not the other way around. The relation (2.1) is analogous to the one derived by Hatsugai in the context of the quantized Hall effect [44, 43], which is consistent with the fact that the index  $W_j$  gives the number  $N_j$  of chiral modes in the gap  $j$ .

A conceptual difference between the original bulk-edge correspondence and this *anomalous* bulk-edge correspondence for Floquet systems is that  $W_j$  is a *bulk* topological invariant while  $N_j$  is an *edge* topological invariant. Establishing the bulk-edge correspondence for Floquet systems thus consists in proving the equality  $W_j = N_j$  between these two kinds of invariants. This was performed by Tauber and Graf in 2018, by using a switch-function formalism that enables a connection between the unbounded bulk infinite system and the bounded semi-infinite one [38]. Besides, we showed with Clément Tauber that the geometrical interpretation of the spectral flow of chiral edge states that bridge gaps, in terms of a winding number in a complex energy Riemann surface [44, 43], can be generalized to unitary systems such as Floquet systems : the existence of an additional gap that makes the spectrum periodic yields an essential singularity in the Riemann surface around which edge states can wind. This

winding corresponds to a spectral flow in the quasi-energy gap around  $\pi/T$  [99].

### Phase rotation symmetry

From a topological perspective, the anomalous chiral edge states are certainly the most intriguing novelty brought by the Floquet dynamics. The existence of these states is related to an extra symmetry of the unitary dynamics that we have introduced in [22] and developed in [19], called *phase rotation symmetry*, that acts on the Floquet operator as

$$\mathcal{Z}U_F\mathcal{Z}^{-1} = e^{i2\pi/N} U_F . \quad (2.2)$$

where  $N$  is the number of bands. This symmetry rotates the eigenvalues of  $U_F$  on the unit circle and thus permutes the associated eigenvectors. It is specific to unitary systems, and does not have any counterpart in a static Hamiltonian description. Importantly, it follows from phase rotation symmetry that the Chern number of each band vanishes. Actually, the symmetry (2.2) is a very strong constraint, and is in general never satisfied except at some special points in parameter space where the spectrum is gapped. However, away from these symmetric points, the value of the Chern numbers cannot change until a gap closes, owing to its topological nature, ensuring the stability of the result. This property alone does not guarantee that the system is in an anomalous regime rather than in a trivial one. However, anomalous chiral states are guaranteed to exist at the *interface* between two Floquet systems that can be continuously deformed to different phase rotation symmetric points : In that case, the two subsystems have vanishing Chern numbers but cannot be continuously deformed into each other unless the gap closes. An example of such interface states is shown in figure 2.4.

### A few generalizations of anomalous boundary states

Experimental efforts have been made to engineer and observe anomalous edge states, in particular in photonics [74, 71]. Generalizations to other dimensions and or symmetry classes have been investigated. Along this line, an experimental collaboration with Matthieu Bellec (LPMC Nice) led to the observation of chiral-symmetric-protected anomalous boundary states of a one-dimensionnal Floquet system realized in optical coupled waveguides [8], a study motivated by a former collaboration with Janos Asbóth [3] (Wigner Research Center, Budapest) and by a theoretical work of Michel Fruchart [30] (former PhD student at the ENS-Lyon). Besides, with Michel Fruchart, David Carpentier and Krzysztof Gawedzki, we also proposed a new  $\mathbb{Z}_2$ -valued topological index to characterize time-reversal invariant Floquet systems in two dimensions [16]. This index, named  $K$ , is a time-reversal symmetric version of the  $W$  index : it is related to the Kane-Mele index of the quasi-energy bands of the Floquet operator [55], and correctly predicts the existence of a robust helical edge state in the spectral gaps of the Floquet operator, even in the anomalous regime where the Kane-Mele index of each band vanishes, as shown in figure 2.3. Similarly to the seminal work of Kane and Mele for

the quantum spin Hall effect [54], a minimal model was obtained by considering two time-reversed (coupled) copies of the toy model for anomalous chiral edge states by Rudner and collaborators. Our model was recently implemented in an array of coupled optical waveguides in the group of Alexander Szameit (University of Rostock) to engineer and observe analogous helical edge states protected by time-reversal symmetry in photonic [72].

### 2.2.3 Oriented scattering networks

#### Discrete-time periodic dynamics and oriented scattering networks

An interesting development of Floquet systems is the discovery of topological properties of oriented scattering networks. As first pointed out by Ydong Chong and his collaborators [67, 83], coherent waves that propagate in an oriented lattice whose nodes represent (unitary) scattering events and the links can be span by the waves in only one direction, may have topological properties such as chiral boundary modes. In particular, anomalous chiral boundary modes have been found experimentally both in microwaves and acoustic networks [47, 86]. This close similarity with Floquet systems originates from the fact that eigenmodes of the scattering lattices are described by a unitary scattering matrix that is formally equivalent to a Floquet evolution operator. In particular, we have shown that discrete-time periodically driven tight-binding models can be mapped onto particular oriented scattering networks, called *cyclic* oriented lattices [19]. Such networks are peculiar oriented graphs in which any path followed by a propagating signal necessarily consists in an *ordered* and *periodic* sequence of nodes representing the scattering processes [22]. This is for instance the case of the archetypal toy model proposed by Rudner, Lindner, Berg and Levin to illustrate the existence of anomalous chiral edge states, that can be explicitly mapped onto the Chalker-Coddington model [17, 19] (or rather its disorder-free version [45]), originally introduced to explain the transition between plateaus of conductivity in the quantum Hall effect. This Chalker-Coddington network, represented in figure 2.4, is the simplest case of a cyclic oriented lattice.

Several differentiations must be done, however, between periodically driven systems and scattering networks. The first one being that there is no external driving in scattering networks; a wave is sent through the system and propagates freely according to the different transmission/reflection coefficients at the nodes and by following the orientation of the links. Thus, time does not enter explicitly as it usually does in periodically driven systems. Instead, an effective discrete- (artificial) time approach is used that accounts for the cyclic sequence of nodes (scattering events) the wave must follow during its spreading through the network, as it does e.g. in the Chalker-Coddington lattice. The evolution operator of a cyclic oriented scattering network is formally equivalent, up to a transformation [22], to that of a Floquet discrete-time quantum walk that can be realized with cold atoms or photons (see e.g. [59, 60, 4, 93]), except that it applies to classical waves as well here. A topological index  $W$  can then be defined for cyclic oriented lattices, by re-introducing a fictitious time that interpolates the different instantaneous scattering events and thus redefines a time-ordered evolution operator [22].

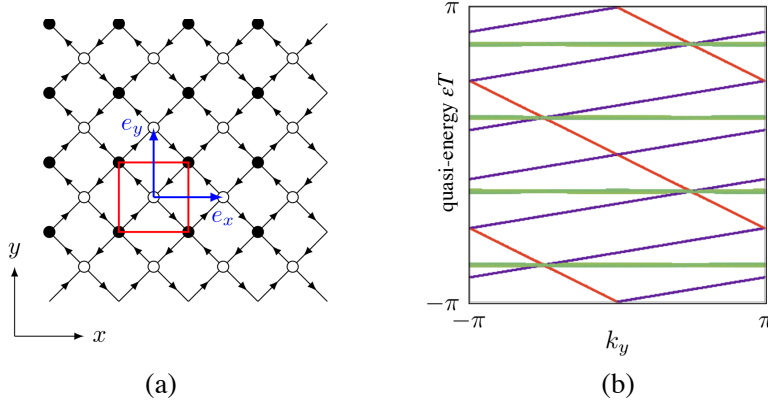


Figure 2.4 – (a) Chalker-Coddington network (also called L-lattice). Each node represents a scattering process encoded into a unitary matrix. This network is a cyclic oriented lattice since any path on it has to follow a staggered sequence of dark and white nodes. (b) Phase spectrum of the evolution operator for an interface between two Chalker-Coddington lattices close to different phase rotation symmetric points. For numerical convenience, the system was periodized so that two interfaces are considered instead of one, giving rise to two anomalous chiral interface states, each localized at an interface.

However, if this procedure seems to be safe in usual quantum walks, it turns out to be more subtle in scattering networks : There, the value of the  $W$  index depends on the choice of the unit cell and is thus ill-defined as a bulk invariant [22]. This is very analogous to the Zak phase, a winding number that accounts for the existence of zero-dimensional boundary modes of the one-dimensional Peierls (or so-called SSH) chain, *once a correct prescription is made to choose the unit cell that accommodates the boundary of the lattice* [92, 20]. This ambiguity is due to the separation in space of the two degrees of freedom, namely the two pseudospins that originate from the existence of two sublattices, and is indeed absent when these two degrees of freedom occupy the same sites in real space, like for actual spins. Indeed, in the former case, different boundary conditions can apply to each sublattice, while in the latter case, the same boundary condition applies for both spins. Scattering lattices show that the existence of anomalous chiral *edge* states is not guaranteed by the value of the bulk  $W$  index.

Of course, for the Peierls chain as well as for scattering networks, the existence of topological *interface* modes is still guaranteed by the non-zero difference of indices from each side, even though ill-defined. Actually, the existence of chiral anomalous interface modes turns out to be quite simple to predict, and does not require any calculation. Their existence is guaranteed in any oriented scattering network, even fully random, as a consequence of the the phase rotation symmetry (or its generalization to disordered cases), that emerges for specific values of the scattering parameters, that correspond to the *classical configurations* where the nodes of the network allow a transmission 1 in one direction and 0 in every other directions [19]. It follows that the waves are confined along close loops. Such decomposition of any (unitary) scattering network into a union of disconnected closed loops is guaranteed by Veblen theorem. Interestingly, the interface between two domains of distinct loops support a chiral mode, as illustrated in figure 2.5. When the networks are cyclic oriented lattices, the phase rotation

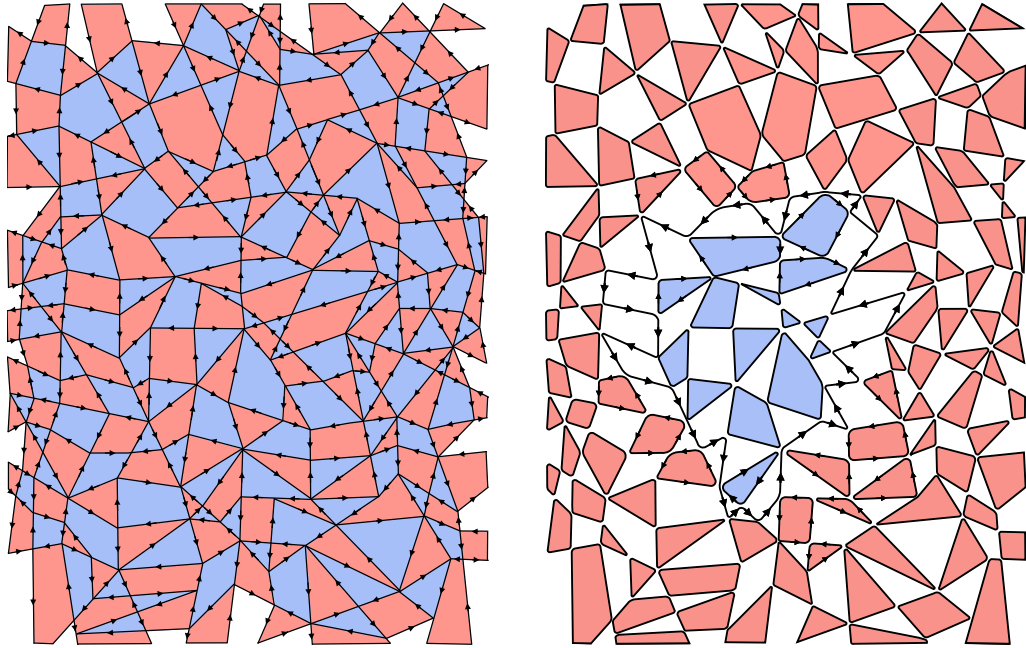


Figure 2.5 – (Left) Random scattering network. (Right) Interface between two distinct Veblen decompositions that generalize the phase rotation symmetry to arbitrary Eulerian graphs. A chiral mode necessarily exist at the interface between the two domains, and generalizes the anomalous chiral state of Floquet systems. The colors of the faces encode the circulation of the oriented links that surround them.

symmetry operator can be found explicitly and the Chern numbers of the eigenmodes of the (Floquet) evolution operator computed and found to vanish, as expected. Since the Chern numbers vanish in the two adjacent domains, these modes correspond to the anomalous chiral interface states of oriented scattering networks. In random networks, these chiral interface modes generalize the notion of anomalous chiral interface states beyond cyclic oriented lattices, and thus beyond Floquet systems, since no periodicity (in space or time) is actually required to guarantee their existence.

### Floquet winding metals

In Floquet systems, anomalous chiral edge states are made possible because the spectrum of interest is the one of a phase, that is unbounded, unlike the energy. Another similar property of phase spectra is that they can wind. In the adiabatic regime, and for one-dimensional gapped systems, such a winding in the Brillouin zone was shown to be equivalent to the first Chern number that enters the quantized pumped current found by Thouless [100, 58].<sup>2</sup> An interesting situation is the one, in two dimensions, that mixes both the winding of the bulk bands in one direction and the existence of chiral anomalous edge states. Scattering networks offer a simple realization of this double topological property that have no counter part in static

<sup>2</sup>In that case, the integral over  $dk_y$  in the expression (1.3) of the Chern number is replaced by an integral in  $dt$  over a period of adiabatic driving.

systems.

The idea is to start with an oriented scattering lattice with a preferential direction followed by the wave during its propagation, as depicted in 2.6. This scattering network is very similar to the one studied with Matthieu Bellec in 2017 in the search for chiral symmetry protected anomalous boundary modes [8], except that dynamical phases  $\phi_j$  are added along certain paths. When these phases are taken as multiples of a common phase  $\phi$ , then this  $\phi$  plays the role of an extra synthetic dimension. The introduction of such a phase allowed the first measurement in photonics of the Berry curvature of the bands via a semi-classical correction to the group velocity of a wavepacket [111]. Combining the control in time of the scattering parameters as in [8] together with the additional dynamical phase from [111] allows the realization of a two-dimensional Floquet photonic crystal that possess a phase rotation symmetry and thus that may exhibit anomalous chiral states [103].

More original situations are obtained when breaking the generalized inversion symmetry  $PU_F(k_x, \phi)P^{-1} = U_F(-k_x, -\phi)$  (where  $U_F$  is the Floquet operator and  $\phi$  is considered on the same footing as a quasi-momentum) by choosing the phases as  $\phi_1 \equiv m_1/n_1\phi$  and  $\phi_2 \equiv m_2/n_2\phi$  where  $n_i$  and  $m_i$  are integers. In this case, all the bulk bands wind  $\nu$  times along the  $\phi$  direction where  $\nu$  is fully determined by a combination of  $(m_i, n_i)$ . Examples of such Floquet *winding metals*, with and without anomalous edge states, are shown in figure 2.6.

A first important consequence of the winding of the bulk bands is that the generalized group velocity  $\partial_\phi \varepsilon$  has the same sign for every states *but one*, that is a chiral edge state, since the two chiral edge states localized on opposite edges have to have group velocities with opposite signs. It worth noticing that in the absence of a direct gap, the winding number  $W$  that characterizes the topology of chiral edge states in Floquet systems is not defined. However, chiral interface states can still be described locally as the spectral flow emanating from the degeneracy point (band touching point) that separates a trivial winding metal from an anomalous one.

A second remarkable consequence of this winding is the unconventional dynamics of wavepackets in position space when adiabatically increasing the phase  $\phi$ , that periodically oscillate while keeping the quasi-momentum  $k_x$  constant. These oscillations are very different in nature to Bloch oscillations, reported in photonics and cold atoms where the oscillation of the wavepackets in the spatial direction is accompanied with a periodic oscillation in the Brillouin zone.

### 2.3 Topological (classical) waves in continuous media

Most of the studies about topological insulating states use the framework of lattice models, and thus take advantage of the existence of a Brillouin zone to define rather easily the topological invariants, such as Chern numbers. The introduction of a periodic drive (Floquet systems) or of an extra dynamical phase, extends the size of the effective Brillouin zone without changing its nature of a compact close manifold, namely a torus, over which a differential form can be

### 2.3. Topological (classical) waves in continuous media

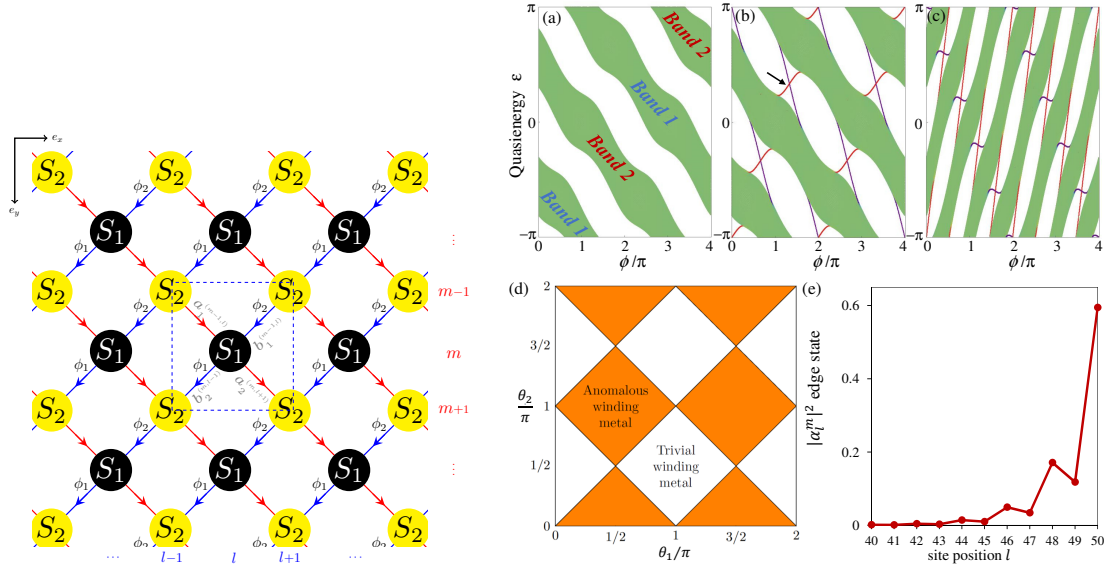


Figure 2.6 – (Left) Scattering network model. The scattering matrices  $S_1$  and  $S_2$  have different scattering parameters to separate the bands and  $\phi_1$  and  $\phi_2$  have different amplitudes to wind the bands. (Right) (a), (b) and (c) three examples of Floquet winding metals with  $\nu = -2$  for (a) and (b) and  $\nu = 6$  for (c). (d) shows the phase diagram of a Floquet winding metal with  $\nu = -2$  in terms of the scattering parameters that enter the scattering matrices  $S_1$  and  $S_2$  at the nodes of the network. (e) shows the localization of the edge state pointed out with an arrow in (b).

integrated, such as the Berry curvature.

The absence of a Brillouin zone is therefore a source of theoretical difficulties when investigating the topological properties. This is particularly true for disordered systems where more sophisticated mathematics are required to address the problem, such as non-commutative geometry [87]. This is also the case of continuum media, which are a natural framework to investigate classical waves.

The study of topological properties in the continuum is not new. Actually, a few milestone results were derived in the continuum, such as the quantization of electric charges by the magnetic monopole from Dirac in 1931 [23], the existence of a zero-energy state in the Dirac equation by Jackiw and Rebbi in 1976 [51], or the existence of a spectral flow and the related chiral anomaly in  $^3\text{He-A}$  superfluid Helium as described in details by Volovik [106]. Continuum models are also used in condensed matter as effective low energy approximations, and similar effects (zero energy states, spectral flow, chiral anomaly ...) are then found, as for instance in the seminal work by Raghu and Haldane where they pioneered topological photonics by proposing the first classical analogue of the quantum Hall effect [88]. However, when the physicists community started massively investigating topological properties of classical waves these last few years, they mostly focussed on artificial lattices in order to mimic condensed matter systems. While macroscopic classical waves are naturally described in continuum media, their topological properties have been overlooked.

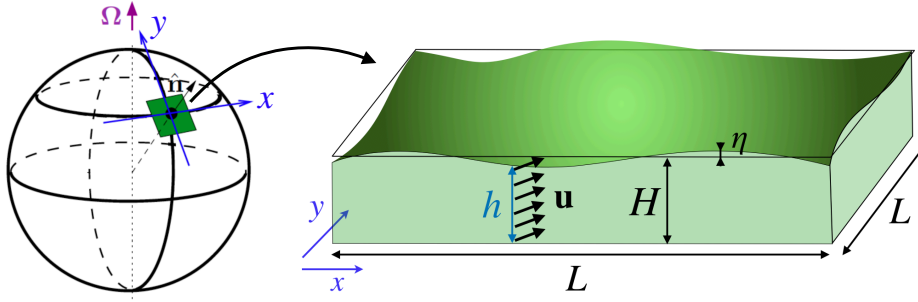


Figure 2.7 – Shallow water fluid describing ocean or atmosphere over large distances.

The following paragraphs summarize recent contributions in the search for topological chiral modes in continuum models describing classical fluid waves and electromagnetic waves.

### 2.3.1 Topological interface waves

#### Oceanic and atmospheric equatorial waves

Over large distances, the oceans and the atmosphere essentially consist in a thin layer of fluid, as sketched in figure 2.7. Assuming a homogeneous density and incompressibility, the momentum conservation and the mass conservation reduce to a two-dimensional model, called *shallow water model*, that describes the fluid dynamics through a coupling between the fluid's thickness  $h(x, y, t)$  and the horizontal velocity field  $\mathbf{u}(x, y, t)$ , the vertical dependence of the velocity being neglected. In Earth rotating frame, the shallow water model reads [104]

$$\text{mass conservation} \quad \partial_t h + \nabla \cdot (h\mathbf{u}) = 0 \quad (2.3)$$

$$\text{momentum conservation} \quad \partial_t \mathbf{u} + (\mathbf{u} \cdot \nabla) \mathbf{u} = -g \nabla h - f \hat{\mathbf{n}} \times \mathbf{u} \quad (2.4)$$

where  $g$  is standard gravity, and  $f \hat{\mathbf{n}} \times \mathbf{u}$  is the Coriolis force. Importantly, the Coriolis parameter  $f$  breaks time-reversal symmetry, that acts as  $t \rightarrow -t$ ,  $\mathbf{u} \rightarrow -\mathbf{u}$  and leaves  $h$  invariant. The shallow water model thus essentially describes a two-dimensional system that breaks time-reversal symmetry, and as such already bears some similarities with Hall systems to guide our intuition.

Let us focus on the linear regime around a state of rest ( $u_x = 0, u_y = 0, h = H$ ), so that one can neglect the advection term  $(\mathbf{u} \cdot \nabla) \mathbf{u}$ . Note that when  $f = 0$ , the system (2.4) then implies that the fields  $\mathbf{u}(x, y, t)$  and  $h(x, y, t)$  are solutions of the d'Alembert equation with celerity  $c = \sqrt{gH}$ . We are interested in the role of the Coriolis force on these shallow water waves. After Fourier transforms in space and time, that introduce wave numbers  $k_x$  and  $k_y$  and the frequency  $\omega$ , and a suitable change of variables, the linearized shallow water model reduces to

### 2.3. Topological (classical) waves in continuous media

the following eigenvalues problem

$$\begin{pmatrix} 0 & -if & k_x \\ if & 0 & k_y \\ k_x & k_y & 0 \end{pmatrix} \begin{pmatrix} u_x \\ u_y \\ \eta \end{pmatrix} = \omega(k_x, k_y, f) \begin{pmatrix} u_x \\ u_y \\ \eta \end{pmatrix} \quad (2.5)$$

with a slight abuse of notation for the velocity field components and where  $\eta$  denotes the Fourier component of the small variation of  $h(x, y, t) - H$ . It worth noticing that this equation is formally analogous to a Schrödinger eigenvalue equation for stationary modes, the  $3 \times 3$  matrix being Hermitian, making explicit the parallel with topological quantum systems.

The dispersion relation, shown in figure 2.8, is made of three bands : a flat one at  $\omega_0 = 0$  frequency and two symmetric ones at  $\omega_{\pm} = \pm \sqrt{k_x^2 + k_y^2 + f^2}$ . Frequency gaps open for  $f \neq 0$ , that is when time-reversal symmetry is broken. For  $f = 0$ , the three bands touch. In other words, there is a three-fold degeneracy point at  $(k_x, k_y, f) = (0, 0, 0)$ . This degeneracy point carries a topological information, similarly to that of a Weyl point encountered in condensed matter : for each eigenstate  $\psi_n(k_x, k_y, f)$  of (2.5), it is the source of a Berry curvature  $\mathcal{F}_n$  whose flux through the unit sphere that encloses it, is the first Chern number  $\mathcal{C}_n$ . For the shallow water model, one finds the triplet

$$(\mathcal{C}_-, \mathcal{C}_0, \mathcal{C}_+) = (2, 0, -2) \quad (2.6)$$

The Chern numbers  $\mathcal{C}_n$  must be distinguished from those of a Chern insulator  $C_n$ . They do not correspond to the number of chiral *edge* states; in particular there is no edge in the system. In the language of Chern insulators, they could be understood as "transition Chern numbers", that coincide with the differences of Chern numbers  $C$  of the two gapped phases separated by the gap closure at  $f = 0$ . This difference of Chern numbers  $C$  gives the net number of chiral *interface* states between the two phases, that generalizes the edge states when one of the two systems is the vacuum. Following this analogy, the two distinct "insulators" would correspond for the shallow water model to the north and the south hemispheres. Indeed, the Coriolis parameter  $f = 2\mathbf{\Omega} \cdot \hat{\mathbf{n}}$  being twice the projection of Earth rotation  $\mathbf{\Omega}$  on the local vertical, it is therefore positive in the north hemisphere, negative in the south hemisphere and vanishes at the equator that defines the interface. However, we will see in section 2.3.2 that each hemisphere cannot be rigorously considered as a Chern insulator. The topological description of the equatorial waves in terms of  $\mathcal{C}$  is thus sufficient and consistent.

The information content of the Chern numbers  $\mathcal{C}_n$  is related to the original and more complicated problem where the Coriolis parameter is actually a function of latitude  $f(y)$  rather than a parameter. In equation (2.5), this dependence was neglected. Actually, we used the so-called *f*-plane approximation, introduced by Kelvin to simplify the problem of the shallow water model on the sphere. This approximation consists in considering that the fluid evolves locally in a plane tangent to Earth where  $f$  is assumed to be constant. Then, to compute the Chern numbers, one needs to consider a close surface in  $(k_x, k_y, f)$  parameter space. This implicitly allows  $f$  to vary as an external parameter, as if the actual shallow water waves experienced

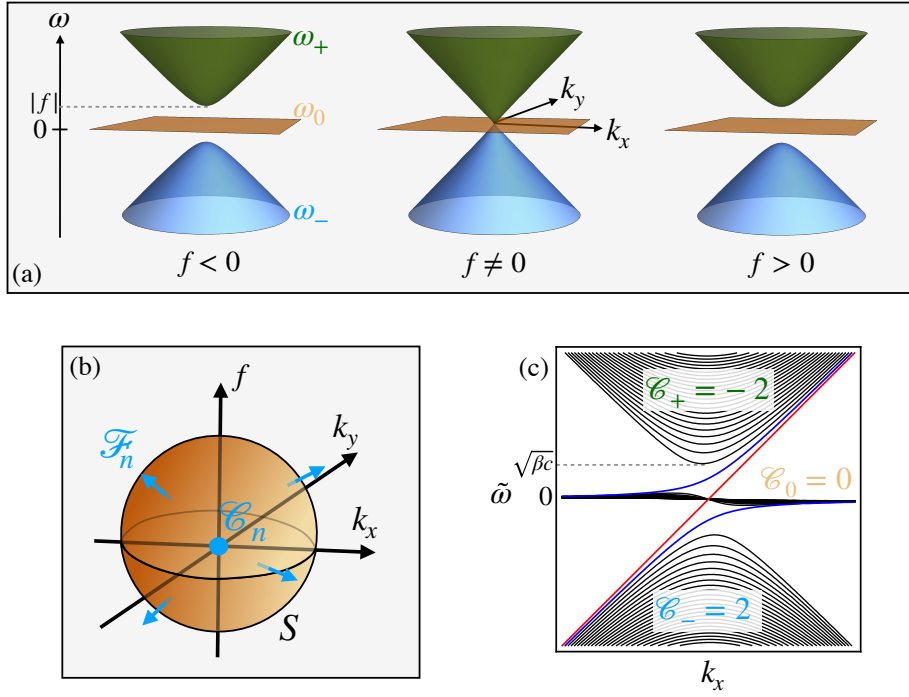


Figure 2.8 – (a) Dispersion relation  $\omega(k_x, k_y, f)$  of the shallow water model for fixed values of the Coriolis parameter  $f$ . At  $(k_x, k_y, f) = (0, 0, 0)$  the three bands touch. This threefold degeneracy point, represented in (b), is the source of a Berry curvature  $\mathcal{F}_n$  for each eigenstate  $n$  of the parametrized problem (2.5), whose flux through the unit sphere is the quantized first Chern number  $\mathcal{C}_n$ . (c) Eigen-frequency spectrum  $\tilde{\omega}(k_x)$  of the matrix of operators (2.7) obtained for  $f(y) = \beta y$ . It shows a spectral flow with a non-dispersive Kelvin wave (in red) and a dispersive Yanai wave (in blue). The number of modes  $N_n$  gained by each band  $n$  when sweeping  $k_x$  is fixed by the Chern number as  $N_n = -\mathcal{C}_n$ .

a weak variation of  $f$  when propagating towards the equator.<sup>3</sup> The Earth sphericity is thus partially re-introduced in the problem, simply by considering that  $f$  can change sign.

If one considers now the latitude dependence of  $f$  explicitly, then the problem becomes much harder to solve, since one has to diagonalize a matrix of operators that do not commute

$$\begin{pmatrix} 0 & -if(y) & k_x \\ if(y) & 0 & i\partial_y \\ k_x & i\partial_y & 0 \end{pmatrix} \begin{pmatrix} \tilde{u}_x \\ \tilde{u}_y \\ \tilde{\eta} \end{pmatrix} = \tilde{\omega}(k_x) \begin{pmatrix} \tilde{u}_x \\ \tilde{u}_y \\ \tilde{\eta} \end{pmatrix}. \quad (2.7)$$

However, a remarkable property of the frequency spectrum  $\tilde{\omega}(k_x)$  can be directly inferred from the Chern numbers  $\mathcal{C}_n$  computed above : Generically, this spectrum also consists in bands  $\tilde{\omega}_n(k_x)$ . A Chern number  $\mathcal{C}_n$  then imposes that the band  $\tilde{\omega}_n(k_x)$  gains  $\mathcal{C}_n$  states when sweeping  $k_x$ . This is a spectral flow, whose topological property is related to that of the degeneracy point. These extra flowing states are missing in the dispersion relation of figure 2.8 (a). Their number is thus guaranteed by topology, irrespectively of the precise latitude

<sup>3</sup>This point can be formalized more quantitatively though semi-classical WKB approximation that we shall not discuss here.

### 2.3. Topological (classical) waves in continuous media

---

dependence of the Coriolis parameter  $f(y)$ , provided it changes sign somewhere. As it relates bands of different frequencies, the spectral flow imposes the sign for the group velocity  $\partial_{k_x} \tilde{\omega}$ . It thus corresponds to unidirectional propagating waves. This result thus applies to any rotating shallow water fluids on curved surfaces. For instance, it applies to a catenoid whose curvature is opposite to that of the sphere, leading to an inverted equator; the unidirectional modes would thus propagate in the opposite direction, the south ( $f < 0$ ) and north ( $f > 0$ ) hemispheres being reversed.

Coming back to the geophysical context, the topological content of the shallow water model guarantees that there exists 2 eastward propagating modes whose dispersion relation  $\tilde{\omega}(k_x)$  "flows" toward the high frequency (Poincaré) band. The existence of these two unidirectional modes are known as the Kelvin equatorial wave and the mixed Rossby-gravity (or Yanai) wave. They constitute a remarkable and rare example in geophysics of waves that were theoretically predicted before being observed [73, 57]. The role of these two waves was identified in several important geophysical phenomena, such as the celebrated *El Niño southern oscillations* that impact global climate [104]. These oscillations consist in a repeating increasing/decreasing of the water temperature on the coasts of Peru (and near by) every 3 to 7 years. The El Niño phenomenon corresponds to the increasing temperature part of these oscillations, that considerably increases the rains in South America. The El Niño southern oscillations are a complex non predictable phenomenon that results from a non linear coupling between the Pacific ocean and the atmosphere [115, 108]. Its mechanisms implies an inflow of heat through the Pacific ocean towards America. This energy is carried by a Kelvin equatorial wave that brings the accumulation of heat from Indonesia and crosses the Pacific ocean in about two months.<sup>4</sup>

To predict the existence of the Kelvin and the Yanai waves without the topological argument, one needs to solve the shallow water model (2.7). In 1966, Taroh Matsuno had the fruitful idea to linearize the Coriolis parameter in the vicinity of the equator,  $f \sim \beta y$  [73]. This approximation, known as the  $\beta$ -plane approximation, yields solutions that decompose as Hermite polynomials, which gives rise to a discretization of the three bands in an infinite numbers of sub-levels. Actually, Matsuno showed that the transverse velocity field  $u_y(y)$  is solution to an equation analogous to that of the quantum harmonic oscillator. This is a striking coincidence that the same structure precisely also appears in the Landau levels of the quantum Hall effect. The spectrum found by Matsuno is reproduced in figure 2.8 (c), except that the negative frequencies are also represented. These are usually missing in the geophysics literature for good physical reasons. However, they turn out to be quite useful to reveal the complete spectral flow as a gain and loss of modes between the bands, in agreement with the

---

<sup>4</sup>The Kelvin wave that carries the heat anomaly through the Pacific ocean is not a surface Kelvin wave, whose amplitude is typically a few centimeters high, but an *internal* Kelvin wave that propagates at the interface between the top hot layer of the ocean, called thermocline, and the much thicker, stable and colder layer that lies below, the abyss. A propagation of the increase of thickness of the thermocline at the expense of the abyss thus goes along with a propagation of a heat *anomaly*, that translates a change of the average temperature integrated over the thickness of the ocean. The amplitude of these internal Kelvin waves is about 100m, and its celerity is about  $2m.s^{-1}$ .

Chern numbers. The solutions with the correct Coriolis term  $f(y) \sim \sin(y)$  were computed more recently. The general aspect of the spectrum is preserved, and in particular the spectral flow, as expected from its topological nature.

Equatorial Kelvin and Yanai waves were discovered in the sixties, but their topological origin was only revealed recently. This is pretty surprising in view of the relative simplicity of the linearized shallow water model in the  $\beta$ -plane approximation, in comparison to that of the quantum Hall effect. We could speculate about how would have been the recent fruitful history of topological condensed matter, but also of geophysics, if this discovery had been made at the time of Matsuno, about 15 years before that of the quantum Hall effect. Anyhow, this analysis shows how topology can reveal fundamental and concrete properties of waves in nature, despite its high complexity, rather than in an artificial lattice that was engineered on purpose. It provides a new interpretation for the existence of these waves. In the next example, we show that the exact same approach may also lead to predictions in geo/astro-physics.

### A polariton-like toy model as a guide to guided waves

The equatorial waves are associated to a three-fold degeneracy point. These are not the more common degeneracies, and moreover, in general, the eigenstates of three-fold degeneracy points do not necessarily have a Chern number. In the case of equatorial waves, it turns out that the matrix in the system (2.5) decomposes into three matrices that satisfy a spin-1 algebra, so that this problem is formally analogous to the celebrated example of a spin-1 particle coupled to a slowly varying magnetic field in space that yields non-zero Chern numbers.<sup>5</sup> In the absence of this spin algebra,  $n$ -fold degeneracy points do not necessarily lead to a spectral flow neither, and the Chern numbers must be computed accordingly. However, there is an exception for 2-fold degeneracy points, which are fortunately the more likely. In particular, when the dispersion relation around the 2-fold crossing point is linear (which is also the more likely) the Chern numbers of the two bands is  $\pm 1$ .

A generic physical situation where such band crossings happen in wave physics is when a non-dispersive propagating wave meets a resonator (or a resonant medium). Consider first this situation in one-dimension, where the dispersion relation of the wave is  $\omega = ck_x$ , and the mode of the resonator has an eigenfrequency  $\Omega$ . The resulting superposition of these two dispersion relations obviously gives a linear band-crossing, but in 1d parameter space (span by  $k_x$ ). To get topologically guided modes out of this simple situation, one needs to embed this two-fold degeneracy point in the larger three-dimensional parameter space  $(k_x, k_y, m)$ . One thus needs to implement a dependence in  $k_y$  and  $m$  through coupling  $\gamma(k_y, m)$  between the wave and the resonator. This coupling is necessary complex in order to embed the degeneracy point in the three-dimensional space span by the three Pauli matrices. One ends up with the

---

<sup>5</sup>See part II for more details.

### 2.3. Topological (classical) waves in continuous media

following heuristic Hermitian model

$$\begin{pmatrix} ck_x & \gamma^*(k_y, m) \\ \gamma(k_y, m) & \Omega \end{pmatrix} \begin{pmatrix} \varphi_1 \\ \varphi_2 \end{pmatrix} = \omega \begin{pmatrix} \varphi_1 \\ \varphi_2 \end{pmatrix} \quad (2.8)$$

whose eigenvalues  $\omega_{\pm} = \frac{ck_x + \Omega}{2} \pm \sqrt{\left(\frac{ck_x - \Omega}{2}\right)^2 + |2\gamma(k_y, m)|^2}$ , plotted in figure 2.9, are degenerated at  $(k_x^0 = \frac{\Omega}{c}, k_y^0, m^0)$  with  $\gamma(k_y^0, m^0) = 0$  by construction. The fact that  $\gamma(k_y, m)$  is required to be a complex number ensures that this Hamiltonian decomposes onto the three Pauli matrices which guarantees that the degeneracy point carries a non-vanishing topological charge. If, moreover,  $\gamma(k_y, m)$  varies linearly with  $k_y$  and  $m$  around the degeneracy point, then the two normalized eigenstates carry opposite Chern numbers whose value is  $\pm 1$ . A simple choice is e.g.  $\gamma = k_y + im$ . It may take higher values if this dependence is non linear.<sup>6</sup> Then, the existence of unidirectional guided modes that propagate along the direction  $x$ , is guaranteed by the value of  $\mathcal{C}_+$  provided that  $m$  changes sign in the direction  $y$ . The guided modes are then localized around in the  $y$  direction where  $m$  changes sign. An example where  $m \sim y$  is shown in figure 2.9.

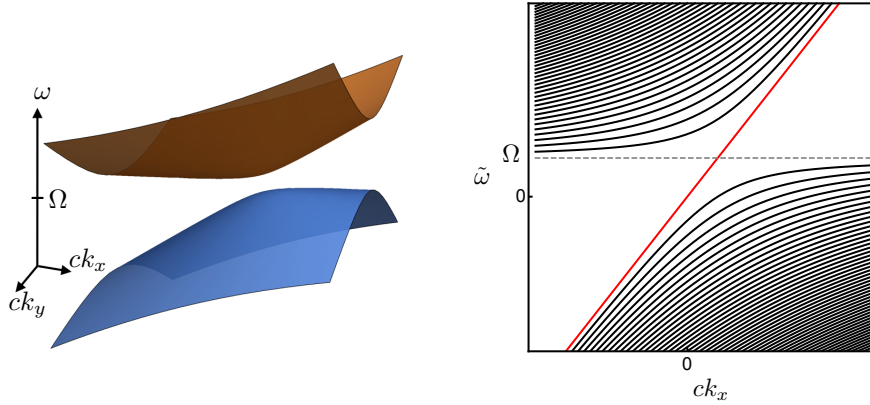


Figure 2.9 – Spectra of the polariton-like toy model for (left)  $\gamma = k_y + im$  and (right)  $\gamma = i\partial_y + iy$

This heuristic approach, based on a tricky coupling between a wave and a resonator, suggests a direction to obtain topological guided waves. In spirit, the modes resulting from this coupling could be called *polaritons*. Polaritons are hybrid subwavelength states resulting from the interaction between an ensemble of resonators and a propagating wave [85]. It is a broad concept that applies in quantum mechanics [26, 46], where photons could be strongly coupled to mechanical oscillators (e.g. phonons, plasmons) or to excitons (i.e. electron-hole pairs) in semiconductors, as well as in classical mechanics for instance when an acoustic wave couples to Helmholtz resonators whose size is smaller than the wavelength [66]. These different platforms are used to engineer and investigate topological waves, most of the time when the resonators are arranged on a lattice (periodic or quasi-periodic) as in [114, 6, 56].

<sup>6</sup>See Part II for more a detailed justification of this result, and concrete examples.

## Chapter 2. Topological chiral waves

---

Finally, it worth noticing that in this toy model, a coupling  $\gamma(k_y, m)$  cannot open a direct gap. However, this does not preclude the existence of a spectral flow. Nevertheless, a situation where a direct gap opens would allow a selective excitation of the guided waves in a certain range of frequency, like for the equatorial waves. The next paragraph is dedicated to a manifestation of this effect in fluid waves.

### Acoustic-gravity waves in stratified compressible fluids

The main difficulty to make more realistic the polariton-like toy model (2.8) resides in the implementation of the complex coupling  $\gamma(k_y, m)$ . The following example shows how this physics arises in fluids.

For the non-dispersive wave, let us consider an acoustic one. The continuum media must therefore be compressible. Then, the resonator must be replaced here by an intrinsic frequency of this media. This role will be played by the buoyancy frequency  $\Omega \equiv N$  of a stratified fluid in density. Therefore, a natural starting point is a compressible three-dimensional fluid with a gradient of the density  $\rho_0(z)$  along the vertical  $z$ . Such stratification in density is actually commonly taken into account in the description of atmospheres or oceans. Because of gravity, the flow isotropy is broken, leading to two intrinsic frequencies :  $g/c_s$  where  $c_s$  is sound velocity in the absence of stratification and the aforementioned buoyancy frequency  $N = \sqrt{-g(\partial_z \rho_0)/\rho_0 - g^2/c_s^2}$  that characterizes the vertical oscillation of a fluid particle that results from a competition between gravity and the Archimedes force in the stratified media. It is typically about 10mHz in the Earth atmosphere. The equations of motion of the fluid follow from from the following conservation laws

$$\text{mass conservation} \quad \partial_t \rho + \nabla \cdot (\rho \mathbf{u}) = 0 \quad (2.9)$$

$$\text{momentum conservation} \quad \partial_t \mathbf{u} + (\mathbf{u} \cdot \nabla) \mathbf{u} = -\rho g \hat{\mathbf{e}}_z - \nabla p \quad (2.10)$$

$$\text{entropy conservation} \quad ds = 0 \quad (2.11)$$

where the last line, that corresponds to the hypothesis of an adiabatic displacement of a fluid particle, is added to close the system. Indeed, in the limit of a weak perturbation around a state ( $\rho = \rho_0, \mathbf{u} = 0, p = p_0$ ), and after a suitable change of variables and a Fourier transform with respect to  $t$  and  $x$ , the linearized system reads

$$\begin{pmatrix} 0 & 0 & 0 & c_s k_x \\ 0 & 0 & iN & -iS + ic_s \partial_z \\ 0 & -iN & 0 & 0 \\ c_s k_x & iS + ic_s \partial_z & 0 & 0 \end{pmatrix} \begin{pmatrix} \tilde{u}_x \\ \tilde{u}_z \\ \tilde{\rho} \\ \tilde{p} \end{pmatrix} = \tilde{\omega}(k_x) \begin{pmatrix} \tilde{u}_x \\ \tilde{u}_z \\ \tilde{\rho} \\ \tilde{p} \end{pmatrix} \quad (2.12)$$

which is again analogous to the Schrödinger equation.<sup>7</sup> In equation (2.12), the *stratification*

---

<sup>7</sup>To obtain equation (2.12), the sound velocity was assumed to be constant for simplification.

parameter

$$S = \frac{c_s}{2g} \left( N^2 - \left( \frac{g}{c_s} \right)^2 \right) \quad (2.13)$$

compares the two intrinsic frequencies introduced above. It is crucial in the description of the problem, since it will play a role analogous to that of the Coriolis force in the shallow water model. We shall thus use  $S$  instead of  $N$  to describe the stratification, the two variables being related. In particular the condition  $N > 0$  of a stable stratification imposes  $S > -\frac{g}{2c_s}$ .

In general, the stratification parameter  $S$  depends on the altitude  $z$ , and the equation (2.12) is difficult to solve analytically. Instead, one can follow another strategy, and use the topological approach to investigate under which conditions guided waves may emerge. For that purpose, one considers the much simpler problem where  $S$  is a parameter (not a function of  $z$ ) and then Fourier transform the equation (2.12) with respect to time and space. Its eigenfrequencies give the dispersion relation shown in figure 2.10 (a) that consists in four bands, called acoustic and gravity. Its eigenvectors possibly encode a topological information related to a spectral flow of (2.12). Searching for such a topological property actually simply reduces to looking for degeneracy points in  $(k_x, k_z, S)$  parameter space.

Two such points actually exist and are located at  $(k_x, k_z, S) = (\pm g/c_s^2, 0, 0)$ . Remarkably, the existence of these two-fold degeneracy points is accompanied with a restoration of the vertical mirror symmetry, that occurs when  $S = 0$  and  $k_z = 0$  despite the presence of gravity. Besides, the dispersion relation around these points corresponds to the superposition of an acoustic wave (associated with a horizontal oscillatory motion in the  $x$  direction) and the intrinsic buoyancy frequency of the stratified fluid (associated with a vertical oscillatory motion). This corresponds to the polariton-like toy model presented in section 2.3.1. To emphasize this point, one can obtain the coupling Hamiltonian that describes the two-band touching by squaring the Fourier transform of (2.12) and then linearizing around each touching point  $(\pm g/c_s^2, 0, 0)$ . It reads

$$\begin{pmatrix} 1 \pm 2k_x & k_z + iS \\ k_z - iS & N^2 \end{pmatrix} \quad (2.14)$$

in terms of dimensionless parameters, which is essentially (2.8). The Chern numbers of the eigenstates of the bands that touch are thus  $\pm 1$ , which guarantees a spectral flow along the  $x$  (horizontal) direction *if*  $S(z)$  changes sign at a given  $z = z_0$ .

There is however one interesting difference with the polariton-like toy model, which is that a direct gap opens in the full spectrum between the acoustic and the gravity waves when  $S \neq 0$ , which is missed by the linearization to derive (2.14). As a consequence, the modes of the spectral flow are the only one to be excited in a specific range of frequency around the buoyancy frequency.

The prediction for the existence of a spectral flow can be checked numerically, by comparing

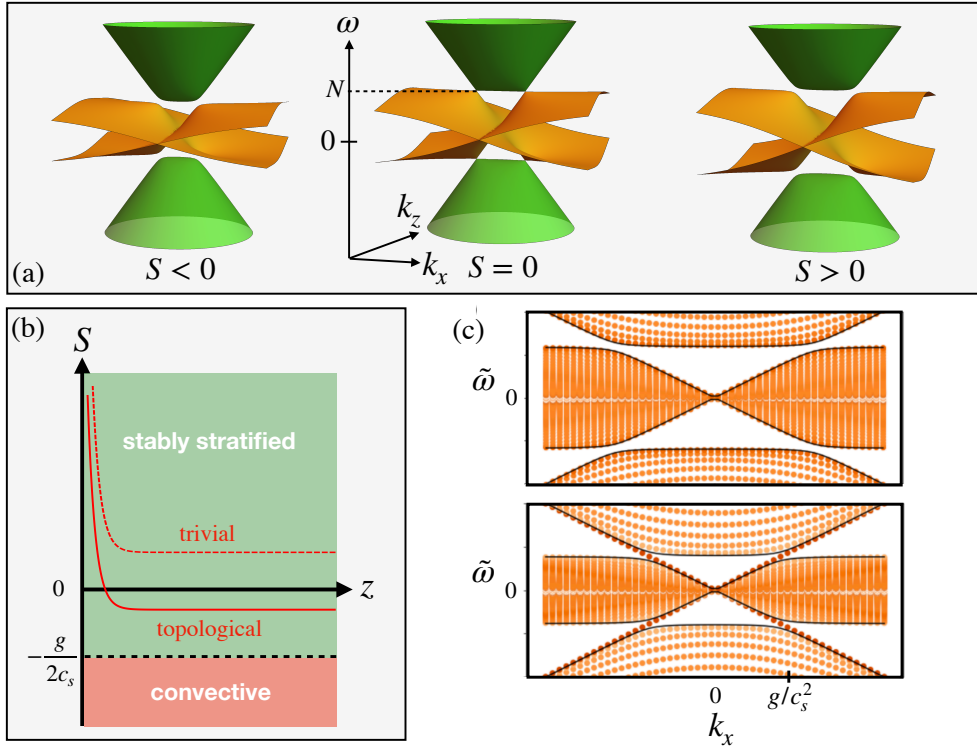


Figure 2.10 – (a) Dispersion relation of the stratified compressible fluid in the linearized regime for different values of the stratification parameter  $S$ . When  $S = 0$ , acoustic bands (in green) and internal-gravity bands (in orange) touch linearly. This gives rise to two-fold degeneracies in  $(k_x, k_z, S)$  parameter space that carry topological charges of  $\pm 1$ . (b) and (c) This guarantees a spectral flow if  $S(z)$  is a function that changes sign, which is in principle possible without entering the convective regime. If  $S(z)$  does not change sign with  $z$ , no spectral flow is obtained.

the spectra obtained with two stratification profiles of the form  $S(z) = S_0 e^{-z/z_0} + S_\infty$  that only differ by the sign of  $S_\infty$ , keeping in mind that  $S(z) > -\frac{g}{2c_s^2}$  must always be satisfied, otherwise the fluid enters the convective regime. The results, shown in figure 2.10, clearly shows the existence of a spectral flow around  $k_x = \pm g/c_s^2$  when  $S_\infty < 0$  and no spectral flow when  $S_\infty > 0$ , in agreement with the topological approach. It is worth noticing that, inversely, the observation of such confined waves would give an information on the stratification profile of the fluid.

Remarkably, this spectral flow corresponds to acoustic waves that are insensitive to the stratification in density, and remain non-dispersive. Besides, they are the only modes that can be excited at a frequency around  $\omega \sim N$ . Such waves are analogous to the atmospheric Lamb waves discovered by Horace Lamb in 1911 [64], with the strong differences that Lamb waves require both a solid boundary (the ground) and a fixed stratification parameter  $S < 0$ . In contrast, the topological Lamb-like waves described here do not require any solid boundary, and the question of their possible existence in gaseous planets or stars is thus relevant. Moreover, their existence only depends on the zeroth of the stratification profile, and not on its specific shape, while Lamb waves are surface waves whose existence depend on the boundary conditions [49]. Fortunately, a solid ground constitutes a boundary condition for which Lamb waves exist,

### 2.3. Topological (classical) waves in continuous media

and those were observed in Earth atmosphere.

Finally, it is worth stressing that topological Lamb-like waves are not strictly speaking chiral, since they appear as a pair of modes with opposite group velocities at the same frequency. This is a consequence of the time-reversal symmetry that is preserved. In condensed matter, an analogous effect, known as the quantum valley Hall effect, arises when inversion symmetry is broken [112]. This effect is illustrated on the boron-nitride model in figure 2.11. In that case, a double spectral flow arises when the sign of the on-site staggered potential  $m$  changes sign. This spectral flow corresponds to two contra-propagative chiral states that are *valley polarized* i.e. that are excited around different points of the Brillouin zone where the gap is the smaller. Note that in contrast, Lamb-like waves propagate in two-dimensions inside a three dimensional fluid: they are *horizontally confined* topological interface waves.

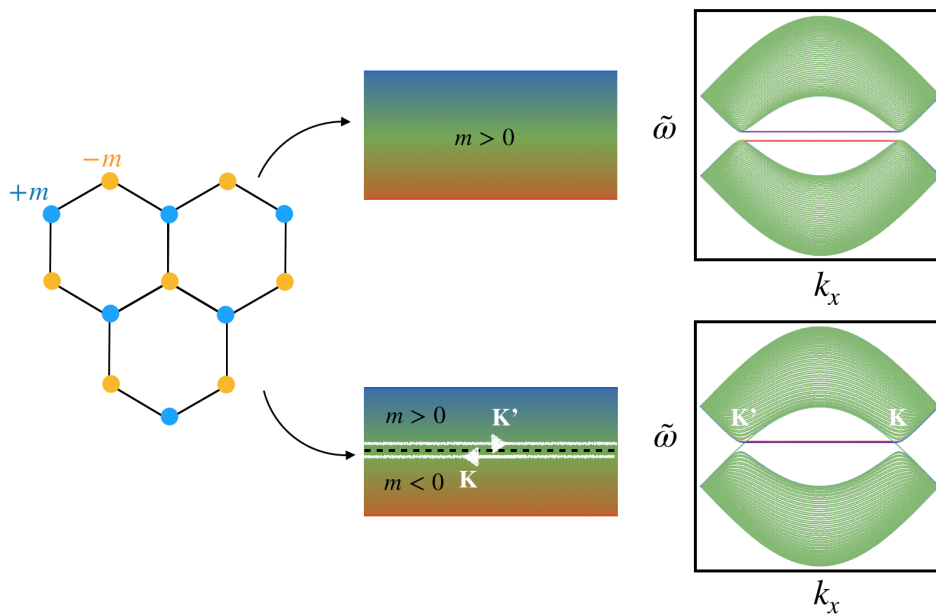


Figure 2.11 – Honeycomb lattice of Boron-Nitride. The two inequivalent sites carry opposite potential  $m$ . When  $m$  is constant, it opens a gap. When it changes sign along a direction, it constitutes an interface that hosts two counter-propagative chiral modes visible in the spectral flows that bridge the gap around the points  $K$  and  $K'$ .

#### Electromagnetic waves

The equatorial shallow water waves and the Lamb-like acoustic-gravity waves are two examples of guided modes in continuous fluids. Of course, the strategy to find other guided waves from degeneracy points in the dispersion relation is not restricted to fluid waves and can be used, for instance, for electromagnetic waves. Let us illustrate how guided Maxwell waves can be generated in gyrotropic media.

In continuous media, the electric field  $\mathbf{E}$  and the magnetic field  $\mathbf{B}$  are related to the magnetizing

field  $\mathbf{H}$  and the electric displacement field  $\mathbf{D}$  through the constitutive equations

$$\begin{pmatrix} \mathbf{D} \\ \mathbf{B} \end{pmatrix} = \begin{pmatrix} \epsilon & \xi \\ \zeta & \mu \end{pmatrix} \begin{pmatrix} \mathbf{E} \\ \mathbf{H} \end{pmatrix} \quad (2.15)$$

where  $\epsilon$  and  $\mu$  are the permittivity and permeability  $3 \times 3$  tensors respectively, and  $\chi$  and  $\zeta$  are the magneto-electric ones. In the absence of source terms (current or charge density), the dynamics of the fields  $\mathbf{B}$  and  $\mathbf{D}$  is given by the Maxwell equations

$$\partial_t \begin{pmatrix} \mathbf{D} \\ \mathbf{B} \end{pmatrix} = \begin{pmatrix} 0 & \nabla \times \\ -\nabla \times & 0 \end{pmatrix} \begin{pmatrix} \mathbf{E} \\ \mathbf{H} \end{pmatrix} \quad (2.16)$$

that automatically satisfy the two other Maxwell equations  $\nabla \cdot \mathbf{B} = 0$  and  $\nabla \cdot \mathbf{D} = 0$ . Injecting the constitutive equations (2.15) leads to a close system for the dynamics for the pair of fields  $(\mathbf{D}, \mathbf{B})$  or equivalently  $(\mathbf{E}, \mathbf{H})$ .

$$\begin{pmatrix} \epsilon & \xi \\ \zeta & \mu \end{pmatrix} \partial_t \begin{pmatrix} \mathbf{E} \\ \mathbf{H} \end{pmatrix} = \begin{pmatrix} 0 & \nabla \times \\ -\nabla \times & 0 \end{pmatrix} \begin{pmatrix} \mathbf{E} \\ \mathbf{H} \end{pmatrix} \quad (2.17)$$

The goal here is to consider two-dimensional systems, and see whether it is possible to implement chiral modes by varying in space one of the material parameters entering the permittivity or permeability tensors. For simplicity, these two tensors only are considered, the magneto-electric ones being assumed to vanish.

There are two usual ways to define a two-dimensional electromagnetic field : the first one is to physically confine the fields in the plane with two metallic plates [52], and the second one is to deal with a three-dimensional system but assuming invariance along the transverse  $z$  direction ( i.e. fixing  $k_z = 0$  after a Fourier transform of the Maxwell equations from real space to reciprocal space). For the sake of simplicity, we shall opt for the second one.

For the discussion of examples, later we shall consider uniaxial responses of the material concerning the permittivity tensor (gyro-electric effect) or the permeability tensor (gyro-magnetic effect) with  $\hat{z}$  as the principal axis. In these case, the  $6 \times 6$  set of Maxwell equations simplifies into two uncoupled sets of  $3 \times 3$  equations operating on  $(E_x, E_y, H_z)$  and  $(H_x, H_y, E_z)$  that are respectively referred to as transverse magnetic (TM) and transverse electric (TE) modes.

Then one introduces a parametrized constitutive matrix  $M(\xi)$  that continuously interpolates between two materials of constitutive matrices  $M_1$  and  $M_2$  as

$$M(\xi) = \frac{M_1 + M_2}{2} + \xi \frac{M_1 - M_2}{2} \quad (2.18)$$

that can represent, for instance, a metal ( $\epsilon \neq \mathbb{1}, \mu = \mathbb{1}$ ), a ferrite (gyro-magnetic media,  $\epsilon = \mathbb{1}, \mu \neq \mathbb{1}$ ) or a Drude cold plasma (gyro-electric media,  $\epsilon \neq \mathbb{1}, \mu = \mathbb{1}$ ).

### 2.3. Topological (classical) waves in continuous media

The first step in the search for chiral modes is to find degeneracy points in parameter space  $(k_x, k_y, \xi)$ . A quick inspection of the dispersion relation around these points already allows one to make a guess about the absolute value of the Chern numbers, which can anyway be computed numerically. Their values gives the spectral flow – say as a function of  $k_y$  – when the interpolation function  $\xi \rightarrow \xi(x)$  is now replaced by a function of the position, and thus accordingly  $k_x \rightarrow i\partial_x$ .

The case of the gyro-electric media is shown below. In that case the permittivity tensor reads

$$\epsilon_{\text{gyro-elec.}} = \begin{pmatrix} 1 - \frac{\omega_p^2}{\omega^2 - \omega_c^2} & i\omega_c \frac{\omega_p^2}{\omega(\omega^2 - \omega_c^2)} & 0 \\ -i\omega_c \frac{\omega_p^2}{\omega(\omega^2 - \omega_c^2)} & 1 - \frac{\omega_p^2}{\omega^2 - \omega_c^2} & 0 \\ 0 & 0 & 1 - \frac{\omega_p^2}{\omega^2} \end{pmatrix} \quad (2.19)$$

where  $\omega_p$  is the plasma frequency and  $\omega_c$  is the cyclotron frequency, that is proportional to the applied external magnetic field in the direction perpendicular to the plane  $B_{\text{ext}} = B_z$ . A possible parametrized matrix  $M_{\text{gyro-elec.}}(\xi)$  can consist in the interpolation between  $\epsilon^{(1)} = \epsilon_{\text{gyro-elec.}}(\omega_c > 0)$  and  $\epsilon^{(2)} = \epsilon_{\text{gyro-elec.}}(\omega_c < 0)$  that corresponds for instance to taking  $\xi = B_z$ .

Under these conditions, the frequency spectrum is computed numerically for the TM modes and shown in figure 2.12. It reveals three degeneracies (two of them being symmetric to each other by  $\omega \rightarrow -\omega$ ), a three-fold degeneracy at  $(k_x, k_y, \omega) = (0, 0, 0)$  and a two-fold degeneracy at  $(k_x, k_y, \omega) = (0, 0, \omega_0)$ . A guess of the absolute value of the Chern numbers associated to these degeneracy points can be made by inspecting the dispersion relation around these points. In the vicinity of the two-fold degeneracy point, the dispersion relation is quadratic rather than linear, which suggests Chern numbers  $C = \pm 2$  rather than  $C = \pm 1$ . The dispersion relation in the vicinity of the three-fold degeneracy point is linear, as in the shallow water model. This suggests also Chern numbers of value  $C = \pm 2$ . A numerical calculation of these Chern numbers confirms these guesses and also clarifies their signs.

These values of Chern numbers correctly predict the spectral flows when the parameter  $\xi = B_z \rightarrow B_z(x)$  is replaced by a function that changes sign with  $x$ , as shown in figure 2.13. The TM modes show two double spectral flows of opposite chirality appearing at different frequencies. The TE modes, that do not exhibit any topological property (because  $\mu = \mathbb{1}$ ) overlap with one of the two spectral flows, but leave the second one, at low frequency, untouched.

Other topological spectral flow for Maxwell waves have been found for different interfaces implying also metals and gyro-magnetic media (see attached paper).

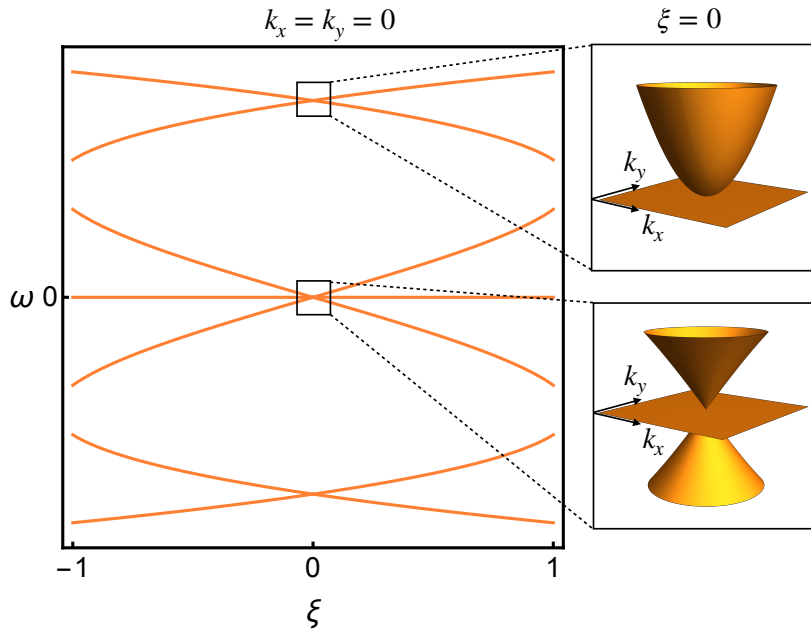


Figure 2.12 – Transverse magnetic modes for an anisotropic gyro-electric media whose permittivity matrix  $\tilde{\epsilon}(\xi)$  continuously interpolates between  $\tilde{\epsilon}(\xi = -1) = \epsilon(\omega_c > 0)$  and  $\tilde{\epsilon}(\xi = 1) = \epsilon(\omega_c < 0)$ . Insets show the dispersion relations in the vicinity of the degeneracy points.

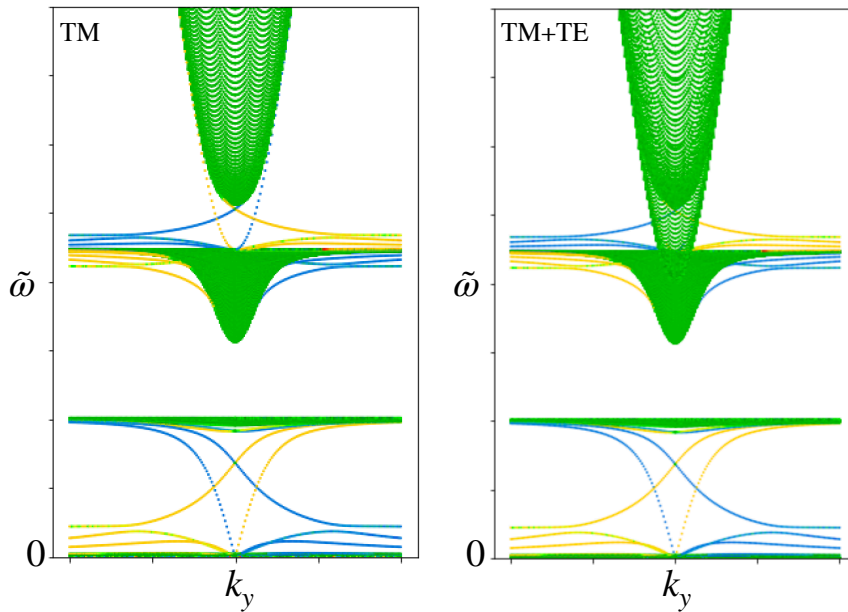


Figure 2.13 – Numerical frequency spectra of the TM modes and both TM and TE modes for the two-dimensional gyro-electric media with cyclotron frequency that changes sign along the  $x$  direction. For numerical convenience, two interfaces with a  $B_z \sim \tanh(x)$  profile have been considered to make the system periodic in the  $x$  direction. The resulting interface chiral modes are represented in different colors (red or blue) according to their localization around either interface.

### 2.3.2 Missing chiral edge states

#### A word about compactification

In the previous sections, we saw how the topological properties of degeneracy points in a three-dimensional parameter space regulate spectral flows in anisotropic continuous media with a "mass term" changing sign on a line in space. At first sight, these different situations could be interpreted as interface problems between two media with different topological properties, the interface being defined where the mass term vanishes. Indeed, from each side of the interface, where the sign of the mass term is fixed, the dispersion relation is gapped, which somehow defines an insulating state. This intuition would be correct if one dealt with lattices. There, Chern numbers could be defined from the bulk states in each side, as the integral of the Berry curvature over the Brillouin zone. In continuous media, there are issues that make this picture incorrect.

In the absence of a Brillouin zone, the Chern numbers are not systematically defined. It would be tempting to consider instead the integral of the Berry curvature over the plane  $(k_x, k_y)$

$$\tilde{C}_n = \frac{1}{2\pi} \int_{\mathbb{R}^2} dk_x dk_y F_n(k_x, k_y). \quad (2.20)$$

Obviously, the plane is not a closed manifold, and this quantity is not supposed to be a Chern number. To define a meaningful topological invariant, the problem must be *compactified*, i.e. a procedure must be found to map each parametrized eigenvector in the plane to a closed surface such that the fiber-bundle is well-defined. One can then argue that the infinite plane can be mapped onto a (Riemann) sphere by stereographic projection, but this does not guaranty that the eigenmodes defined on the plane can be smoothly mapped onto the sphere. In particular, it may happen that singularities that cannot be cured by a gauge transformation appear, thus preventing the compactification. For instance, the massive two-dimensional Dirac Hamiltonian, used as a cornerstone in topological physics, cannot be compactified, and the integral (2.20) gives  $\pm 1/2$  according to the sign of the mass. The same applies to the polariton-like model of section 2.3.1, or to the shallow water model for which the integral (2.20) gives the integer  $\pm 1$  according to the sign of the Coriolis parameter.

This result being an integer, it may lead to some confusion about its topological nature and therefore its role in the bulk-edge correspondence. Moreover, it turns out that the celebrated coastal Kelvin wave, that was first observed by Kelvin along the coasts of lakes, and that is solution of the shallow water model in the presence of the Coriolis force with impermeability conditions (fluid velocity normal to the boundary vanishes) is precisely a chiral mode. On this example, it turns out that the existence of one chiral mode coincides with the value of (2.20), and the fact that this integral is not the first Chern number does not seem to be a big deal after all. Actually, this coincidence is due to this peculiar choice of boundary conditions, even though naturally justified physically. Other boundary conditions may indeed lead to the disappearance of the chiral modes, as shown by Iga [48]. The bulk-edge correspondence is

therefore not satisfied, which is consistent with the fact that the integral (2.20) is not a Chern number for the non-compactified shallow water model.

The situation may seem disappointing, but is not desperate. The problem of the compactification essentially originates from the multi-valuation of the eigenvectors at  $\mathbf{k} \rightarrow \infty$  that cannot be identified to a single one (up to a phase) at the north pole of the Riemann sphere. This can be *regularized* at infinity if one substitutes the mass term with  $m \rightarrow m - \epsilon \mathbf{k}^2$ . Interestingly, the amplitude of the number  $\epsilon$  does not matter in the regularization, and can thus be as small as desired. Beyond this mathematical trick, it may also happen that this term has a physical significance. For instance, acoustic waves propagating in active fluid and transverse magnetic modes in a gyro-electric media can both be described by equations formally equivalent to that of the shallow water model with an additional regularization term  $\epsilon$  that is the *odd viscosity* in the first case and the non-local (classical) Hall conductivity in the second one. The same procedure on the Dirac Hamiltonian leads to the Hamiltonian analogous to that describing  $^3\text{He}$  films

$$H_{\text{Dirac}} = \begin{pmatrix} m & k_x - ik_y \\ k_x + ik_y & -m \end{pmatrix} \rightarrow H_{\text{regul.}} = \begin{pmatrix} m - \epsilon k^2 & k_x - ik_y \\ k_x + ik_y & -m + \epsilon k^2 \end{pmatrix} \quad (2.21)$$

$$\tilde{C}_{\pm} = \pm \frac{\text{sign}(m)}{2} \rightarrow C_{\pm} = \pm \frac{\text{sign}(m) + \text{sign}(\epsilon)}{2} \quad (2.22)$$

where  $\epsilon$  plays the role of the inverse of the mass of the atoms, and  $m$  is the chemical potential.

Thanks to the regularization term  $\epsilon$ , the integral (2.20) is a first Chern number  $C_n$ . In that case, one can interpret the interface chiral modes (like the equatorial waves) as resulting from the topological non equivalent topological properties of the eigenmodes from each side that nevertheless have to match at the interface, thus implying a gap closing. In the end of the day, the regularization procedure may seem unnecessary complicated to simply justify this statement, as it does not lead to original predictions for interface states that the spectral-flow approach based on degeneracy points could already tackle. The actual advantage of the regularization procedure is that it allows one to define Chern numbers for the bulk waves, as it is usually done for Bloch waves, and therefore to ask the question of chiral *edge* modes (not interface modes) at the boundary of a continuous media. Namely, does this Chern number correctly predict the number of chiral edge modes?

### Anomalous bulk-edge correspondence in continuous media

The introduction of the term  $\epsilon \Delta$ , where  $\Delta$  is the Laplacian operator, changes the order of the differential equations to be solved, and therefore, demands two boundary conditions instead of one when  $\epsilon = 0$ . A natural choice is the Dirichlet boundary condition for one of the fields, i.e. its vanishing at the boundary. In the shallow water model, this condition was imposed on the velocity field's component that is perpendicular to the boundary (impermeability condition) to get the coastal Kelvin waves. Similarly, one can also impose this condition on one of the two

### 2.3. Topological (classical) waves in continuous media

components of the eigenvectors of (2.21). What about the second boundary condition? There are an infinite number of possibilities, and among them, one focuses on those that do not violate hermiticity, that is, the solutions  $\phi$  and  $\psi$  that satisfy the condition  $\langle \phi, H\psi \rangle = \langle H\phi, \psi \rangle$ , for any  $\phi, \psi \in L^2(\mathbb{R} \times \mathbb{R}^+)$ . This leaves again many possibilities, but a few examples, displayed in figure 2.14, already show that the number of chiral edge modes that bridge the bulk gap is in general *not* fixed by the Chern number of the regularized problem.

To understand and solve this paradox, one needs to remind that the Chern number of a band counts the net number of states entering the band from the gap above and from the gap below the band. In the continuum, the bands are not bounded, and are free to expand to infinity. As a consequence, the notion of edge states entering a band of – say – positive frequency “from above”, is unclear. Moreover, in continuous media, a state entering a band from a gap at finite frequency does not have to bridge this gap to connect another band, but can lay at large  $k$  without crossing any other state. Therefore, an edge state entering a band is not necessarily a chiral edge state that bridges the gap.

The number of edge states entering a band can be calculated from a scattering approach [37] where one considers a incident bulk state that is reflected back to the bulk by the edge. The scattering state is defined as the superposition of these two contra propagating states together with evanescent states that are also solutions of the problem

$$\Psi_{scat}(y) = \alpha\psi(k_x, -\kappa)e^{i\kappa y} + \beta\psi(k_x, \kappa)e^{-i\kappa y} + \gamma\psi(k_x, f(k_x, \kappa))e^{-|f(k_x, \kappa)|y} \quad (2.23)$$

where  $\alpha$ ,  $\beta$  and  $\gamma$  are complex numbers,  $\psi$  is an eigenvector of the bulk problem ( i.e. in the absence of a boundary),  $f$  is a function that can be determined explicitly, and  $\kappa$  is a positive parameter that corresponds to  $k_y$  in the absence of boundary. This parameter  $\kappa$  is crucial in the analysis as it allows one to describe either the bottom of the projected band where chiral edge states may enter ( $\kappa \rightarrow 0$ ), as well as asymptotic top of the band ( $\kappa \rightarrow \infty$ ). A scattering matrix can be defined as

$$S(k_x, \kappa) = \frac{\beta}{\alpha} \in U(1) \quad (2.24)$$

that is simply a scalar here. Importantly, its expression is fully fixed by the boundary conditions (2 boundary conditions for 3 coefficients  $\alpha$ ,  $\beta$  and  $\gamma$  to determine). Following [37], a winding of the argument of  $S$  when sweeping  $k_x$  indicates the merging of an edge state into the bulk bands. The two regimes  $\kappa \rightarrow 0$  and  $\kappa \rightarrow \infty$  lead to winding numbers  $w^0$  and  $w^\infty$  that indicate the existence of modes entering a band, respectively from the gap and *from the bulk*. The figure 2.14 shows the winding of the argument of the scattering matrix  $S$  for different models and boundary conditions. When  $\kappa \rightarrow 0$ , the jump in the argument precisely corresponds to the merging of an edge mode coming from (or going to) the gap. Again, this mode is not necessarily chiral as it does not have to bridge the gap. Equivalently, the function  $\partial_{k_x} \text{Arg}(S)$  shows a series of peaks centered around the values  $k_x^i$ , whose width tends to zero as  $\kappa \rightarrow 0$ , and whose area (in units of  $2\pi$ ) gives the number of modes that enter the band at  $k_x = k_x^i$ . The

## Chapter 2. Topological chiral waves

---

existence of a winding  $w^\infty$  of  $\text{Arg}(S)$  in the limit  $\kappa \rightarrow \infty$  is surprising: it indicates the existence of an unexpected and different kind of modes at high frequency, dubbed *ghost modes* (as they are not directly visible in the gap). These modes have to be taken into account to rephrase the *anomalous bulk-edge correspondence* for continuous media as

$$C_n = N_{\text{chiral}} + N_{\text{non-chiral}} + N_{\text{ghost}} \quad (2.25)$$

This relation is satisfied on the five examples of figure 2.14.

### 2.3. Topological (classical) waves in continuous media

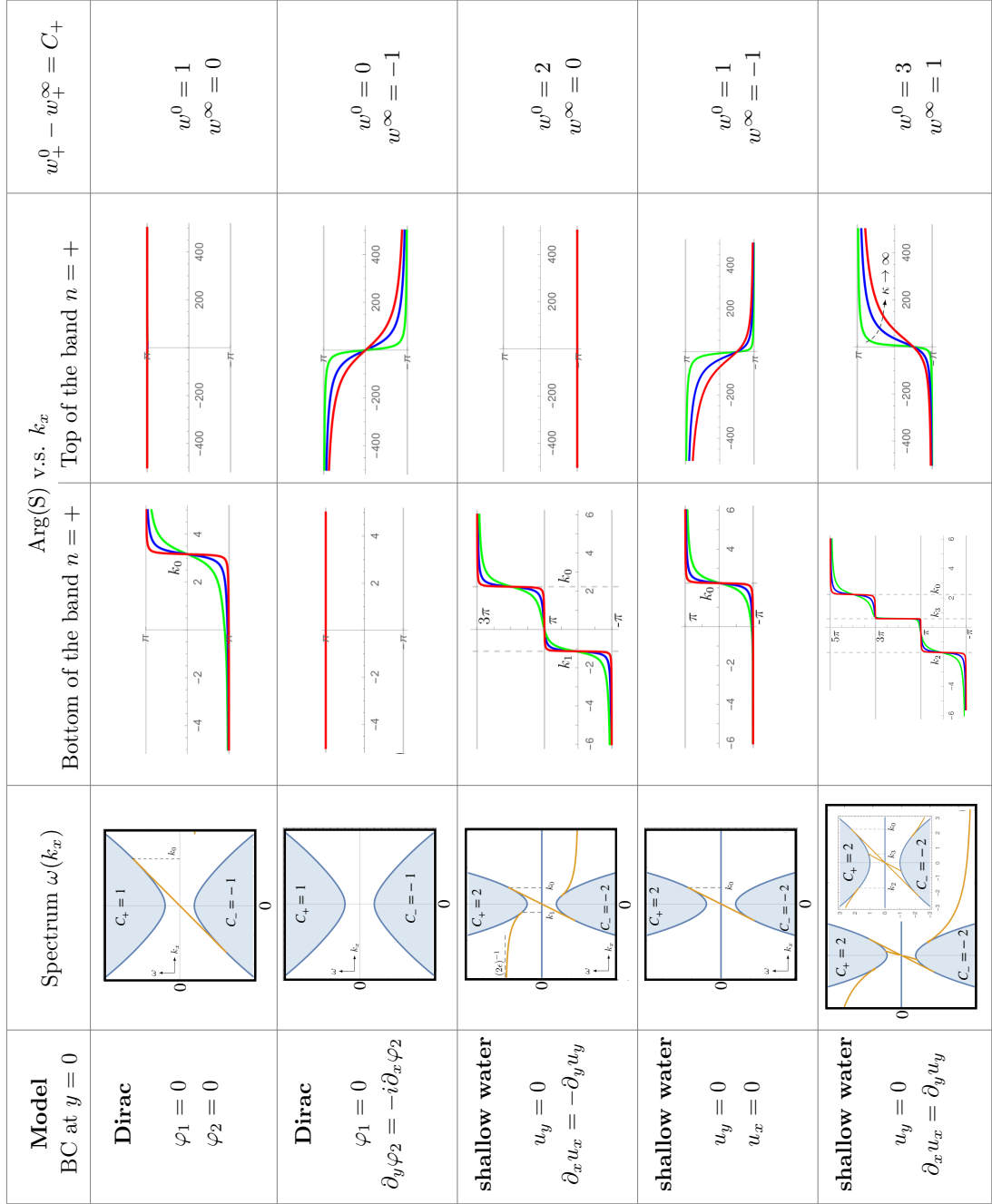


Figure 2.14 – Examples of the anomalous bulk-edge correspondence for continuous media. Two models are considered, the regularized Dirac model and the regularized shallow water model. Different boundary conditions (BC), that satisfy self-adjointness, are applied at  $y = 0$ . The phase of the scattering matrix exhibits a winding  $w_+^0$  at the bottom of the band  $n = +$  that is consistent with the number of edge states that enter this band from the gap. Another winding number  $w_+^\infty$  can be computed at higher frequency/energy that accounts for modes that enter the band from the bulk. The difference of these two winding numbers gives the Chern number of the band.



## 3 Perspectives

*La géométrie trompe, l'ouragan seul est vrai.*

---

Victor Hugo, *Les Misérables*

Here is presented a brief and non-exhaustive list of directions that I intend to follow in the next years. Some are natural follows-up of the works described in chapter 2. Others are more speculative and risky, but probably also more original.

### 3.1 Scattering networks

#### 3.1.1 Floquet "metals" in photonics

An experimental collaboration with Alberto Amo, Pierre Suret and Clément Evain and Stéphane Radoux from PhLAM laboratory (Lille, France) started a few months ago. One of the goals of this collaboration is to implement and probe, in a photonic device, the Floquet winding metals that were found and currently investigated by my PhD student Lavi K. Upreti. The idea is to realize a coherent discrete-time Floquet walk for optical wave packets propagating in coupled fibers, and whose time-evolution can be represented by an oriented graph with a preferential direction as the one in figure 2.6 (a). Other unusual kinds of topological Floquet metallic-like states with chiral edge-like modes and pumping effects, also recently found by Lavi K. Upreti, constitute the core of this experimental collaboration.

On a more theoretical aspect, the definition of a topological index that describes the anomalous chiral edge states in the metallic regime (i.e. in the absence of a spectral gap) is an interesting open question.

### 3.1.2 Random oriented scattering networks

Another experimental collaboration is starting with the group of Romain Fleury, at EPFL (Lausanne, Switzerland), whose goal is to investigate waves propagation in acoustic and photonic scattering networks. It would be interesting to observe the non persistence of anomalous chiral edge states under a change of boundary conditions that we predicted, and compare with the expected robustness chiral edge states protected by Chern numbers. This could be done for instance by engineering a Kagome oriented lattice rather than a square L-lattice (e.g. Chalker-Coddington network). The next direction could be to observe the chiral propagation of interface anomalous modes in random oriented networks, in particular in a finite size disordered (in scattering amplitudes) intermediate region that bridges two domains of opposite chirality, as suggested from the analysis with graph theory.

An important theoretical issue that is especially relevant for practical purposes, is the one of the synchronization of the dynamics : In the theoretical framework developed so far, it is implicitly assumed that the different wave packets that propagate along different links of the graph reach *simultaneously* the scattering nodes. In other words, all the "optical" paths between two nodes are equals. This is a restrictive framework, in particular in random graphs where the different links may have different lengths while their (say optical) indices remain the same. Do interface chiral modes survive beyond this approximation?

On the longer term, two more speculative directions are envisioned. One of them would be to investigate a continuous limit of random Eulerian oriented graphs beyond the original Chalker-Coddington model [45, 117], in order to explore the conditions for the existence of topological properties in non-periodic unitary dynamical coherent systems. The second line one would consist in evaluating the role of anomalous chiral interface modes of random scattering networks in the percolation transition, as these modes could also propagate energy through the bulk of the system. Moreover, it is known from the Chalker-Coddington model that a quantum percolation occurs at the transition between two plateaus of transverse conductivity in the quantum Hall effect, which, in the clean limit, is understood as a topological transition described by a Dirac Hamiltonian. It is thus natural to extend the description of this topological transition to the disordered case by trying to establish a link with the topological nature of the interface chiral states of random networks.

## 3.2 Continuous media

### 3.2.1 Geophysical and astrophysical fluids

The works dealing with fluid waves presented in this manuscript were obtained in close collaboration with Antoine Venaille from the laboratoire de Physique of the ENS de Lyon. This fruitful collaboration is continuing, in particular through the common supervising of a PhD student, Nicolas Perrez, and the coming hiring of a postdoc on this topic in the next few months. Different directions will be considered.

Geo-physical fluids are a wonderful playground to study waves and offer a rare occasion to apply topological concepts to natural phenomena. In particular, our two works on equatorial waves and Lamb-like waves have a straightforward follow-up in the study of rotating stratified fluids, which are common to describe oceans, atmospheres but also stars whose stratification in density could in principle be strong enough to host the topological Lamb-like waves we have proposed.

Other interesting directions are not only relevant for geophysical fluids, but also motivated by condensed matter considerations.

For instance, the effect of a non homogeneous topography was neglected in our studies. It could however play very important roles. For example, the effect of a disorder in topography onto the shallow water waves and their possible localization have been overlooked. It could be fruitful to revisit this problem, which is especially relevant for oceanic waves for instance, through the spectrum of the expected topological robustness of the Kelvin and Yanai waves against Anderson localization, in contrast to the other Rossby and Poincaré equatorial waves. This might give an interpretation on the observational data that turn out to be much more convincing for the two topological chiral modes than for the other waves. Smooth variations of topography could also be considered to realize different kind of boundary conditions, in view of questioning the topological nature of coastal waves beyond coastal Kelvin waves.

External periodic forcing due to the gravitational influence of the moon onto earth atmosphere and oceans, could also be considered. This is particularly relevant as tides are known to be related to coastal Kelvin modes. This would naturally lead us to consider the existence of topological modes through the framework of Floquet theory in the context of geo-fluids.

Considering the wave dynamics around a mean flow rather than a state of rest is relevant in geophysical fluids. This mean flow arises by linearizing the advection term. If the resulting "Hamiltonian" is still linear, it becomes non-Hermitian and satisfies a  $PT$ -symmetry, ensuring a real eigenvalue spectrum up to a threshold that is reached for a critical mean flow. Such systems are currently intensively studied for their topological properties, in particular in photonics where this symmetry can be engineered through a wise balance between gain and loss.

An ambitious longer term perspective would be to revisit the El niño phenomena, as it constitutes a physically relevant framework to address the interplay between non-linearities and topology. Indeed, it is established that the equatorial Kelvin wave plays a key role in the mechanism as a precursor of this phenomena. However, the role of the Yanai wave seems to be much less discussed. Moreover, El niño models require a non-linear ocean-atmosphere coupling, so basically a bi-layer of shallow water models. This gymnastic of stacking layers to implement novel properties is standard in mesoscopic physics, from bilayer graphene whose properties are distinct from that of monolayers, to three-dimensional Weyl semi-metals that can be obtained by stacking two-dimensional Chern insulators on top of each others in a subtle way. In those two examples, the resulting multi-layers systems host (topological)

properties that are distinct from those of the single layer.

### 3.2.2 Spectral flows and bulk-edge correspondences in continuous media

Finally, further investigations will be led around the emergence of a spectral flow in continuous media and the related bulk-edge correspondence.

For instance, it is remarkable that coastal Kelvin waves are chiral modes that appear as a spectral flow despite the ill-defined Chern number. This ill-definition suggests a direction to understand the non-robustness of this chiral mode to a change of boundary conditions. Atmospheric Lamb waves share this same particularity of appearing as a spectral flow but being at the same time boundary conditions dependent. As a chiral mode that bridges a spectral gap, the coastal Kelvin wave is the only accessible state in a certain range of frequency, and is thus expected to be insensible to backscattering in the presence of disorder. It is thus tempting to propose a definition of *marginal* topological waves, that would be immune against back-scattering but whose existence would be boundary dependent.

Another important direction will be to improve the understanding of the "ghost modes" that we have introduced with Clément Tauber (ETH Zurich, Switzerland) and Antoine Venaille, of their physical reality and possible observation. Along this line, I would like to bridge this finding with the existence of a wavefront dislocation emerging in the wave functions around an impurity in a topological material, as we recently found with Clément Dutreix (LOMA Bordeaux, France, and former postdoc of mine) [25]. The idea that the bulk states carry a topological information in their wavefront pattern in the presence of an impurity in one-dimension should be generalizable in two dimensions where the impurity is replaced by an edge. This would help characterizing the topological properties of waves by bridging two topological aspects of waves : wavefront dislocations and the bulk-edge correspondence.

## METHODOLOGY Part II

### A few topological tools for physicists



## 4 Basic concepts

Les leçons ne servent généralement qu'à ceux qui les donnent.

---

Pierre Dac,  
*Y'a du mou dans la corde à noeuds*

### 4.1 Homotopy, winding and degree

References for this section are the books of Nakahara [76], Frankel [29] and Dubrovin, Fomenko and Navikov [24].

#### 4.1.1 An heuristic introduction to homotopy

Homotopy is an intuitive key concept in topology that deals with continuous deformations of objects. More specifically, one speaks about homotopy to characterize continuous interpolations between two applications

$$A \xrightarrow{f_1} B \quad \text{and} \quad A \xrightarrow{f_2} B. \quad (4.1)$$

The maps  $f_1$  and  $f_2$  are said to be *homotopic* when there exists a continuous application  $h$

$$(t, s) : A \times [0, 1] \xrightarrow{h} B \quad (4.2)$$

called *homotopy*, such that

$$h(t, s = 0) = f_1(t) \quad \text{and} \quad h(t, s = 1) = f_2(t). \quad (4.3)$$

When an homotopy exists, the functions  $f_1$  and  $f_2$  are somehow "equivalent", in the sense that they are undistinguishable under continuous deformations. They thus belong to the same *class*. Another function  $f_3$  that is not homotopic to  $f_1$ , cannot be homotopic to  $f_2$  neither,

or to any function that is homotopic to  $f_1$  and  $f_2$ , and will therefore belong to a different class. One can then classify continuous applications according to their homotopy class. Each class is labelled with one or several numbers that characterize the homotopy property shared by all the members of this class. These numbers are called *homotopy invariants*, since they do not capture the difference between two homotopic applications, but only between two non-homotopic applications. This is an example of a topological invariant.

The simplest example illustrating an homotopy invariant appears when considering close curves (or loops). Obviously, in the plane, any loop can be continuously deformed into each other. Each curve representing the set of images of a periodic continuous application ( $A = S^1 \rightarrow B = \mathbb{R}^2$ ), it follows that all these applications are homotopic to each other. This is a pretty boring case, and all these maps have the same homotopic invariant. In particular, as they can all be continuously deformed to a point, this homotopy invariant is 0.

To get something interesting, one can modify the target space  $B$ , for instance by simply removing a point (e.g. the origin i.e.  $\mathbb{R}^2 \setminus \{0\}$ ) as illustrated in figure 4.1 (a). There any curve has to avoid the removed point, so that a loop that encircles it cannot be continuously deformed into a loop that does not. It can only be deformed into another loop that does encircle it as well. In the same way, this loop cannot be deformed neither into a loop that winds the origin twice, or more. The point appears as an *obstruction* that yields topological properties for the loops, such that they can be classified according to their winding number respectively to the removed point. This winding number is the homotopic invariant that classifies loops in the punctured plane, or equivalently, all the continuous applications  $S^1 \rightarrow S^1$ .

This set of all the homotopic classes, labelled by integer numbers corresponding to the winding numbers of the loops, consists in a group, called fundamental group or Poincaré group, and quoted  $\pi_1(S^1)$ . This  $S^1$  means that we are essentially classifying applications whose target space is  $S^1$ , since the distance of the curve from the point around which it winds does not play any role in the counting of winding numbers.

Note that the loops we are characterizing are oriented objects. They can be seen as trajectories. Quite naturally, a given close curve encircling once the origin, has a winding number  $W = +1$  if the loop is oriented counterclockwise and  $-1$  otherwise. The group  $\pi_1(S^1)$  owns an infinite number of elements, as the winding number can be an arbitrary positive or negative integer. This is written as  $\pi_1(S^1) \cong \mathbb{Z}$ .

An important application of winding numbers in physics is the characterization of *vortices*, that are topological defects of two-dimensional vector fields. They are points where the amplitude of the field vanishes and the phase becomes multi-valued and thus ill-defined. Vortices can be classified by a winding number : that is the winding of the phase around the singular point. Indeed, this number does not depend on the choice of loop one considers to evaluate the winding. Two examples are shown in figure 4.1 (b).

The fact that the homotopy group  $\pi_1(B) \neq \{0\}$  is *non trivial*, meaning that there exists different

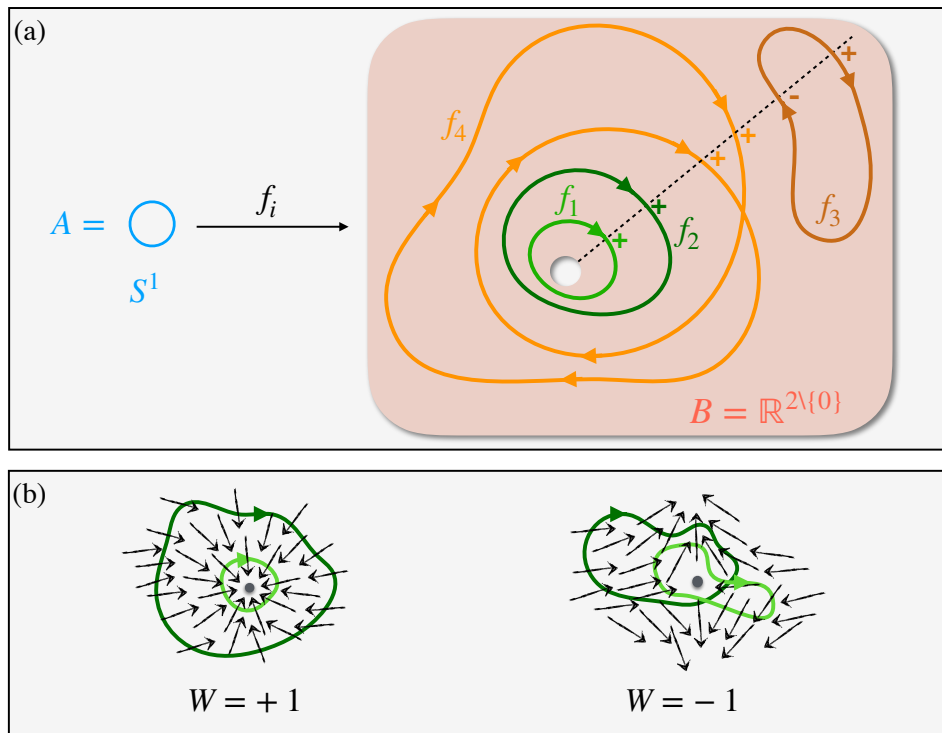


Figure 4.1 – (a) Geometric illustrations of elements of the homotopy group  $\pi_1(S^1)$ . The green loops represent homotopic applications  $f_1$  and  $f_2$  from  $S^1$  to  $\mathbb{R}^2 \setminus \{0\}$ , whose winding number with respect to the removed point is  $W = 1$ . These applications are not homotopic to  $f_3$  whose winding number is  $W = 0$  neither to  $f_4$  whose winding number is  $W = 2$ . (b) Examples of two vector fields that host topologically inequivalent defects (vortices).

classes of loops, is a probe of the *simply connectedness* of  $B$ . Roughly speaking, a space is not simply connected when it has "holes" in it, that make certain loops not contractible into a single point. The plane and the sphere are simply-connected spaces, while the punctured plane and the torus are not. In physics, the non-simply connectedness of the target space may have different origins. For instance, as it was pointed out, a defect like a phase singularity may play the role of the punctured point, leading to a classification of vector fields according to their homotopy properties. This is what is meant by *topological defect*. It may also happen that the non-simply connectedness of the target space is intrinsic to the physical object used to describe the physics. This is the case of the unitary group  $U(n)$  of  $n \times n$  unitary matrices that satisfies  $\pi_1(U(n)) \cong \mathbb{Z}$ .<sup>1</sup> This is of great importance in physics since evolution operators and scattering matrices are represented by unitary matrices. We shall come back to that point in more details in chapter 6.

So far, we have restricted ourselves to the base space  $A = S^1$ , but other spaces of higher dimension are also relevant in physics, for instance to classify the topological defects in ordered phases of matter. Along this line, the Kleman-Toulouse formula states that topological

<sup>1</sup>Note that for  $n = 1$ , the unitary matrix reduced to a complex number  $|z| = 1$  that lies on the unit circle in the complex plane, so that the homotopy group reduces to the Poincaré group.

defects of dimension  $d'$  may exist in a physical ordered phase in  $d$  dimensions provided that  $d - 1 = d' + c$  where  $c$  is the dimension of the "cage" that surround the defect. As an example, in a two dimensional system ( $d = 2$ ), a point-like defect ( $d' = 0$ ) is surrounded by a loop ( $c = 1$ ) and thus satisfies the Kleman-Toulouse formula. Such defects are the vortices already introduced above and are characterized by the homotopy group  $\pi_1(S^1) \cong \mathbb{Z}$ . Another famous example is the one of the ferromagnetic phase in  $d = 3$ , whose order parameter decomposes as  $\mathbf{M}(\mathbf{r}) = M_0 \hat{\mathbf{n}}$  where  $\hat{\mathbf{n}}$  is a unit vector in  $\mathbb{R}^3$  and thus belongs to  $S^2$ . Thus, at each point  $\mathbf{r} \in A$  that surrounds the hypothetic defect, one can assign a vector in  $S^2$ . If the defect is a point, then the cage is a sphere  $S^2$  and therefore the homotopy group classifying the distinct vector fields is  $\pi_2(S^2)$ , while if it is a line defect, the cage is a loop  $S^1$  surrounding it and the corresponding homotopy group is  $\pi_1(S^2)$ . Actually, it turns out that these two groups are drastically different : since  $\pi_2(S^2) \cong \mathbb{Z}$  while  $\pi_1(S^2) \cong 0$ , meaning that there is an infinite number of topologically distinct vector fields around the point defect but there is no line defect in a three-dimensional ferromagnetic. Here we have used examples of homotopy groups of spheres, whose most are still unknown, and that one can summarize as :

$$\pi_n(S^m) = \begin{cases} 0 & n < m \\ \mathbb{Z} & n = m \\ \text{big mess or unknown} & n > m \end{cases} \quad \text{e.g. } \pi_{10}(S^3) = \mathbb{Z}_{15} \quad (4.4)$$

where  $\mathbb{Z}_{15}$  means that there are 15 different homotopy classes for this group. We will not continue into that direction but rather come back to the fundamental group and make more precise the notion of winding number that will be useful for practical purposes.

#### 4.1.2 Winding and degree

The winding of a loop  $\gamma_f$  describes by a map  $S^1 \xrightarrow{f} \mathbb{R}^2 \setminus \{0\}$  is characterized by an integer number that counts the number of times the oriented loop winds around a singular point (e.g. the origin). This winding number of  $f$  is thus nothing but the total angle span by the parametrized curve  $\gamma_f(t)$  in units of  $2\pi$

$$W(f) = \frac{1}{2\pi} \int_{\gamma_f} dt \frac{d\theta(t)}{dt} . \quad (4.5)$$

This can be expressed geometrically by considering the trajectory  $\mathbf{r}(t)$  on the curve and seeing  $\mathbf{r}(t)$  as an in-plane vector whose origin is the singular point. The velocity is then the tangent vector to this curve at point  $\mathbf{r}(t)$ . Their vector product points toward the perpendicular direction to the plane with a positive or negative orientation according to the orientation of the loop. The integral of this quantity, once normalized, from one point on the curve to another, defines an angle. By integrating over the full trajectory one gets the total angle accumulated

along the trajectory, which is the winding number of the map  $f$  in unit of  $2\pi$  :

$$W(f) = \frac{1}{2\pi} \int_{\gamma_f} dt \frac{\mathbf{r}(t) \times \dot{\mathbf{r}}(t)}{\|\mathbf{r}(t)\|^2} \cdot \mathbf{e}_z. \quad (4.6)$$

As already mentioned, the distance  $\|\mathbf{r}(t)\|$  of the curve to the singular point does not play any role in the winding, as long as it does not vanish, as it is clear from Eq. (4.5). This justifies that we shall make no difference between the maps  $S^1 \rightarrow \mathbb{R}^2 \setminus \{0\}$  to the punctured plane and the maps  $S^1 \rightarrow S^1$  to the circle, since they are homotopic when they have the same winding number. We shall denote this equivalence by the relation  $\pi(S^1) \simeq \pi_1(\mathbb{R}^2 \setminus \{0\})$  and sometimes abusively write  $S^1 \simeq \mathbb{R}^2 \setminus \{0\}$ . Note that one can also see the punctured plane  $\mathbb{R}^2 \setminus \{0\}$  as the punctured complex plane  $\mathbb{C} \setminus \{0\}$ , and thus write  $\mathbb{R}^2 \setminus \{0\} \simeq \mathbb{C} \setminus \{0\}$ , as well as  $S^1 \simeq U(1)$  where  $U(1)$  denotes the complex numbers of modulus 1. This yields the following expression for the winding number of a complex map  $t \in S^1 \rightarrow z(t) \in \mathbb{C} \setminus \{0\}$  where  $z(t)/|z(t)| = e^{i\theta(t)} \equiv u \in U(1)$

$$W = \frac{1}{2\pi i} \int_{S^1} u^* \frac{du}{dt} dt = \frac{\theta(t=2\pi) - \theta(t=0)}{2\pi} \quad (4.7)$$

which coincides indeed with the definition of the winding number (4.5).

In practice, there is a more elegant and convenient way to compute the winding number : it is obtained by drawing a half infinite originating at the singular point, and counts algebraically the number of intersections of the loop with this line, as shown in figure 4.1. This information is actually encoded into the sign of the integrand of (4.6), but the advantage in this method is that one does not need to compute an integral. Noting  $\theta_0$  the angular direction of the line, an intersection of the line with the loop occurs for some images  $f(t_i^{(0)})$ , which we would abusively note  $f(t_i^{(0)}) = \theta_0$ . Reciprocally, this defined pre-images  $t_i^{(0)} = f^{-1}(\theta_0)$  so that one would like to write

$$W(f) = \sum_{t_i^{(0)} = f^{-1}(\theta_0)} \operatorname{sgn} \left[ \left( \mathbf{r}(t) \times \dot{\mathbf{r}}(t) \right) \Big|_{\theta_0} \cdot \mathbf{e}_z \right] \quad (4.8)$$

$$= \sum_{t_i^{(0)} = f^{-1}(\theta_0)} \operatorname{sgn} \left[ \left. \frac{d\theta}{dt} \right|_{\theta_0} \right]. \quad (4.9)$$

This expression of the winding number is called the *degree* of  $f$ . More generally, the degree of a map  $A \xrightarrow{f} B$  between two orientable spaces of same dimension reads

$$W(f) = \operatorname{deg}(f) \equiv \sum_{t_i^{(0)} = f^{-1}(y_0)} \operatorname{sgn} \left[ \det \left( \frac{\partial y^\alpha}{\partial t^\beta} \right)_{y_0} \right] \quad (4.10)$$

where  $t^\alpha$  and  $y^\beta$  denote the local coordinates of  $A$  and  $B$  respectively, and  $\frac{\partial y^\alpha}{\partial t^\beta}$  denotes the Jacobian matrix that encodes this change of coordinates. Importantly, as illustrated with the example of the loop, the degree does not depend on the choice of the image  $y_0$ . It is an homotopy invariant that generalizes the winding number of an application  $f : S^1 \rightarrow S^1$  to

higher dimensions manifolds.

### 4.1.3 Winding of an Eulerian graph

As an homotopy invariant, the winding number is so to speak "blind" to continuous deformations of the oriented loop it characterizes. In particular, the loop may self-intersect. In that case, it can be seen as an *oriented graph* whose nodes (or vertices in the language of graph theory) are the self-intersections and the links between nodes (or edges) are oriented. By construction, when following the entire parametrized curve  $\gamma(t)$  as a trajectory, each link can be span exactly once when completing a full cycle. Graphs satisfying this property are called *Eulerian*, as they were introduced by Euler in its famous solution of the seven Bridges of Königsberg problem<sup>2</sup>. Eulerian graphs have the *unique* remarkable property that each node is the intersection of an *even* number of links, which is obviously satisfied in this construction. This is a powerful result, as it is sufficient to check the parity of the nodes of any graph to certify that it can be seen as a loop. As a consequence, the winding number (with respect to a point  $O$ ) of an oriented Eulerian graph is well defined, and is obtained geometrically by counting algebraically the intersection number between any semi-infinite line originating at  $O$  and the oriented links of the graph that are crossed by that arbitrary line. This winding property will be used in chapter 6 to characterize topological properties of evolution operators.

## 4.2 Topological aspects of degeneracy points

### 4.2.1 Energy degeneracies as defects

As discussed in the previous section, winding numbers are defined with respect to a point, which can be a defect in a solid for instance. The analogs of such defects exists in parameter space  $\Lambda$  of coordinates  $\boldsymbol{\lambda} = (\dots \lambda_i \dots)$  and consist in degeneracy points i.e. points of coordinates  $\boldsymbol{\lambda}^{(0)}$  at which at least two energy levels of a physical system coincide  $E_n(\boldsymbol{\lambda}^{(0)}) = E_m(\boldsymbol{\lambda}^{(0)})$ .

Let us detail this point by considering the simple but generic case of a  $2 \times 2$  Hamiltonian

$$H(\boldsymbol{\lambda}) = h_0(\boldsymbol{\lambda})\mathbb{1} + \mathbf{h}(\boldsymbol{\lambda}) \cdot \boldsymbol{\sigma} \quad (4.11)$$

where  $\boldsymbol{\sigma} = (\sigma_x, \sigma_y, \sigma_z)$  is the vector of Pauli matrices. The eigenenergies are

$$E_{\pm}(\boldsymbol{\lambda}) = h_0(\boldsymbol{\lambda}) \pm \|\mathbf{h}(\boldsymbol{\lambda})\| \quad (4.12)$$

so that a degeneracy point at  $\boldsymbol{\lambda}^{(0)}$  satisfies

$$E_+(\boldsymbol{\lambda}^{(0)}) = E_-(\boldsymbol{\lambda}^{(0)}) \Leftrightarrow \|\mathbf{h}(\boldsymbol{\lambda}^{(0)})\| = 0. \quad (4.13)$$

---

<sup>2</sup>The problem was to know whether it was possible, during a walk, to cross the seven bridges of Königsberg exactly once. Graph theory shows that it is not possible, the corresponding graph being not Eulerian.

If one removes this degeneracy point, one can introduce the normalized vector  $\mathbf{n}(\boldsymbol{\lambda}) \equiv \frac{\mathbf{h}(\boldsymbol{\lambda})}{\|\mathbf{h}(\boldsymbol{\lambda})\|}$  that defines a map from parameter space to the unit sphere  $\lambda : A = \Lambda \setminus \{\boldsymbol{\lambda}^{(0)}\} \xrightarrow{n} S^2$ . We shall refer to  $\mathbf{n}$  as the *normalized Hamiltonian map* (and equivalently to  $\mathbf{h}$  as the *Hamiltonian map*). It is then tempting to classify such Hamiltonians according to the homotopy properties of such maps, which are given by the homotopy group  $\pi_A(S^2)$ . We saw that homotopy groups are complicated and mostly unknown. Yet, in the case of a three-dimensional parameter space  $A = \mathbb{R}^3 \setminus \{0\} \cong S^2$ , the homotopy group  $\pi_2(S^2) = \mathbb{Z}$  is non-trivial (see (4.4)). Even though this is a very particular case, it is also very common, if only because these three dimensions of the base space may simply coincide with the three spatial dimensions. We already pointed out the example of point-like defects in the three-dimensional ferromagnetic phase. Here are two other milestone examples illustrating this case.

The first one is a spin one-half coupled to an external magnetic field of arbitrary orientation  $\mathbf{n}$ , for which the Hamiltonian reads  $H = -\mu_B B \mathbf{n} \cdot \boldsymbol{\sigma}$  where  $\mu_B$  is the Bohr magneton. Note that in that case, the system is externally controlled by the magnetic field. This situation was considered by Mikael Berry in his seminal paper of 1984 to illustrate the geometrical phase accumulated by an eigenstate when the magnetic field is cyclically and adiabatically varied [10].

The second example is found in condensed matter, when two Bloch bands of a solid touch at some point in the Brillouin zone. In the neighbourhood of these degeneracy points, the Hamiltonian has the typical form  $H = \hbar v_g \mathbf{h}(\mathbf{k}) \cdot \boldsymbol{\sigma}$ , where  $v_g$  is the group velocity at the band touching (that equals the Fermi velocity when the Fermi energy lies at the band crossing points). Generically, unless some additional symmetry is present,  $\mathbf{h}(\mathbf{k})$  is linear in  $\mathbf{k}$ , so that  $H$  effectively describes Weyl fermions, whose dispersion relation is also linear with  $\mathbf{k}$ . Here  $\sigma$  does not designate an actual spin, but rather an effective *pseudo*-spin that originates from other degrees of freedom (e.g. orbitals or sublattices). Moreover, parameter space is the reciprocal space and  $\boldsymbol{\lambda} = \mathbf{k}$  is not an external tunable parameter as a magnetic field. Still, this model is formally equivalent to the previous one, and both are thus characterized by the same homotopy group  $\pi_2(S^2) = \mathbb{Z}$ , whose elements are characterized by the degree of the map  $\mathbf{n}$ . An expression of this degree will be derived in a next section.

### 4.2.2 Phase singularity of the eigenstates

The normalized eigenstates  $\Psi_{\pm}$  of the Hamiltonian (4.11) read

$$\Psi_+ = \frac{e^{i\chi_+}}{\sqrt{2h(h-h_z)}} \begin{pmatrix} h_x - ih_y \\ h - h_z \end{pmatrix} \quad \text{and} \quad \Psi_- = \frac{e^{i\chi_-}}{\sqrt{2h(h+h_z)}} \begin{pmatrix} h_x + ih_y \\ -h - h_z \end{pmatrix} \quad (4.14)$$

where  $h \equiv \|\mathbf{h}\|$  and  $\chi_{\pm}$  is an arbitrary phase that depends on  $\boldsymbol{\lambda}$ . For any value of  $\boldsymbol{\lambda}$ , we have a gauge freedom for the choice of  $\chi_{\pm}$ , like usually in quantum mechanics. This means that for a given  $\boldsymbol{\lambda}$ , there is not a single state that describes the system, but a family of them that all differ to each other by a phase factor. This is, in a sense, a multi-valuation of the solution.

## Chapter 4. Basic concepts

---

In contrast, the projectors  $P_{\pm} \equiv |\Psi_{\pm}\rangle\langle\Psi_{\pm}|$  do not depend on the gauge and are thus always single-valued. Once the gauge is chosen, the eigenstate should be single-valued as well. This is however not always the case, as one can suspect from (4.14) when  $h = \pm h_z$ .

To see it more clearly, let us use the spherical coordinates, and parametrize the spinor on the Bloch sphere, where it becomes explicit that the eigenstates only depend on  $\mathbf{n}$  (up to the gauge choice) :

$$\Psi_+ = e^{i\chi_+} \begin{pmatrix} \cos \frac{\theta}{2} e^{-i\phi} \\ \sin \frac{\theta}{2} \end{pmatrix} \quad \text{and} \quad \Psi_- = e^{i\chi_-} \begin{pmatrix} \sin \frac{\theta}{2} e^{-i\phi} \\ -\cos \frac{\theta}{2} \end{pmatrix}. \quad (4.15)$$

There, setting  $\mathbf{n} = n_z > 0$  or equivalently  $\theta = 0$  (north pole), the eigenstate  $\Psi_+$  becomes

$$\Psi_+ \stackrel{\theta=0}{=} e^{i\chi_+} \begin{pmatrix} e^{-i\phi} \\ 0 \end{pmatrix} \quad \text{at the north pole of the Bloch sphere} \quad (4.16)$$

which is multi-valued even after the gauge has been fixed, unless we make the particular gauge choice  $e^{i\chi_+} = e^{i\phi}$ . This fixes the multi-valued of the eigenstate, but only at the north pole. Indeed, in this gauge, the eigenstate becomes multivalued at the south pole  $\theta = \pi$

$$\Psi_+ \stackrel{\theta=\pi}{=} \begin{pmatrix} 0 \\ e^{i\phi} \end{pmatrix} \quad (\text{with } e^{i\chi_+} = e^{i\phi}) \quad \text{at the south pole of the Bloch sphere.} \quad (4.17)$$

Actually, the multi-valuedness of the eigenstates cannot be fixed by a *global* gauge choice. Or say otherwise, there does not exist a smooth function  $\chi$  that makes the eigenstate single-valued everywhere on the Bloch sphere. One can only choose *locally* a gauge that makes the eigenstate single-valued. Thus the eigenstates are only piece-wise single-valued. This reflects a topological property of the eigenstates, as their phase cannot be defined smoothly globally and has to have a singularity somewhere, similarly to a vortex. This topological property is inherently related to the gauge freedom, and is described by the theory of fiber-bundles that we need to briefly introduce now.

### 4.2.3 Some insights on fiber bundles

Fiber bundles constitute a rigorous construction of a product of spaces. Locally, the product of two spaces, say a segment  $[-1, 1]$  and a circle  $S^1$  is given by the usual cartesian product. But globally, this does not necessarily hold since a twist may occur. In that case, the fiber-bundle is said to be topological. This is the celebrated example of the Moebius strip that differs by a twist from the cylinder. These two structures both result from the product of the segment with the circle, but the Moebius strip can only be seen as the cartesian product  $[-1, 1] \times S^1$  locally. Fiber bundles are in particular useful to make meaningful the notion of parametrized vector space. The vector space (here the segment) is called the fiber, while the space that parametrizes the fiber (here the circle) is called the base space.

Another intuitive example of a fiber-bundle is the family of tangent vector spaces to the sphere  $S^2$ . In that case, the vector space is the tangent plane to the sphere and the base space is the sphere itself. The tangent vector bundle is thus the collection of all tangent vectors at any point of the sphere. This vector bundle is also topological, and its twist can be seen in the tangent vector field to the sphere, that necessarily has two vortices, which are precisely points where the phase (i.e. the angle of the tangent vectors with respect to an arbitrary direction) is multi-valued. The position of these singularities depends on the gauge choice, in the language of physicists, or of the section of the fiber bundle as mathematicians would say. But the total vorticity, equals to 2 in that example, cannot change. This is a topological invariant of this fiber bundle, and this result is known as the hairy ball theorem.

The fiber bundles we are interested in resemble this hairy ball : the base space is also the sphere  $S^2$  but the fibers (the hairs) are complex vector spaces made of all eigenstates  $\Psi$ , that only differ by a phase (or gauge choice), that is

$$F_{\pm}(\boldsymbol{\lambda}) = \{e^{i\chi_{\pm}(\boldsymbol{\lambda})}\Psi_{\pm}(\boldsymbol{\lambda}), e^{i\chi_{\pm}(\boldsymbol{\lambda})} \in U(1)\} . \quad (4.18)$$

A fiber  $F_{\pm}(\boldsymbol{\lambda})$  thus defines the equivalent class of the states  $\Psi_{\pm}(\boldsymbol{\lambda})$ . The fiber bundle is also associated to a family of projectors  $\boldsymbol{\lambda} \rightarrow P(\boldsymbol{\lambda})$ , which, as already mentioned, are single valued. States that belong to the same fiber have the same projector. The topological property of the fiber bundle is also encoded into  $P(\boldsymbol{\lambda})$ , and one can equivalently express the topological invariant of the fiber bundle with the eigenstates or with the projectors.

The fiber-bundle constructed from the fibers (4.18) are referred to as  $U(1)$ -complex vector bundles of rank 1. There are many others, of different dimensions, real or complex, with group structures different from  $U(1)$ , but this simple example already englobes many interesting physical situations.

To express the topological invariants of fiber bundles, one needs now to introduce some definitions of differential geometry.

### 4.2.4 Degree of the Hamiltonian map

#### Brief summary on differential calculus

There are many books that give detailed and consistent introductions to differential forms, such as [76, 29] that are dedicated to physicists. Here we present a digest summary that sketches a few basic definitions and results that are useful for the following.

Differential forms constitute a generalization of functions. A usual function  $\boldsymbol{\lambda} : \Lambda \rightarrow f(\boldsymbol{\lambda}) \equiv \omega_0$  is then a 0-form, while its differential (provided it is differentiable)  $df$  is an example of a 1-form. More generally, a 1-form is a kind of vector, called covector as it transforms as a covariant vector [29], and decomposes as  $\omega_1 = \omega_1^i d\lambda_i$  (where we use the implicit sum convention). If the dimension of parameter space  $\Lambda$ , that is our base space, is  $N$ , then the set of 1-forms

## Chapter 4. Basic concepts

$\Omega^1(\Lambda)$  is also of dimension  $N$ . A 2-form  $\omega_2$  is a anti-symmetric tensor that decomposes as  $\omega_2 = \omega_{jk} d\lambda_j \wedge d\lambda_k$  (with  $j < k$ ), where the wedge product  $\wedge$  generalizes the vector product defined in  $\mathbb{R}^3$  to any dimension, by satisfying

$$d\lambda_j \wedge d\lambda_k = -d\lambda_k \wedge d\lambda_j \quad (4.19)$$

and in particular  $d\lambda_j \wedge d\lambda_j = 0$ . By extension an  $r$ -form is a totally anti-symmetric tensor that decomposes as  $\omega_r = \omega_{j_1, j_2, \dots, j_r}^r d\lambda_{j_1} \wedge d\lambda_{j_2} \wedge \dots \wedge d\lambda_{j_r}$ , and in particular the set  $\Omega^N(\Lambda)$  of  $N$ -forms contains a single element  $\omega_N = \omega_{1, 2, \dots, N}^N d\lambda_1 \wedge d\lambda_2 \wedge \dots \wedge d\lambda_N$ .

As recalled at the beginning of this section, if  $f$  is a 0-form (a function) then  $df$  is a 1-form. This familiar result generalizes to any differential forms, with the *exterior derivative* on forms  $d$  that constitutes a map  $\Omega^r(\Lambda) \xrightarrow{d} \Omega^{r+1}(\Lambda)$ ; namely, the (exterior) derivative of an  $r$ -form is an  $(r+1)$ -form. In practice it is obtained as

$$d\omega_r \equiv \frac{\partial}{\partial \lambda_{r+1}} \left( \omega_{j_1, j_2, \dots, j_r}^r \right) d\lambda_{r+1} \wedge d\lambda_{j_1} \wedge d\lambda_{j_2} \wedge \dots \wedge d\lambda_{j_r}. \quad (4.20)$$

Such an  $(r+1)$ -form,  $\omega^{r+1} = d\omega^r$  is called an *exact* form, as it is derived from an  $r$ -form (such as  $df$ ). It may also happen that a form  $\omega$  satisfies  $d\omega = 0$ . This is called a *closed* form. Importantly, the anti-symmetric relation (4.19) imposes that  $d(d\omega_r) = 0$ , implying that any exact form is closed. The reciprocal is not true.

A differential form is an object that one can integrate over manifolds. In particular, if the dimension of a manifold  $M$  is  $r$ , then  $\int_M \omega_r$  is a number. Of particular importance is the volume form  $\Omega_{S^n}$ , that is an  $n$ -form whose integral over a sphere  $S^n$  embedded in  $\mathbb{R}^{n+1}$  is 1. In cartesian coordinates, it reads

$$\Omega_{S^n} \equiv \sum_{i=1}^{n+1} (-1)^{n+1} \frac{x_i dx_1 \wedge \dots \wedge dx_{i-1} \wedge dx_{i+1} \wedge \dots \wedge dx_{n+1}}{\gamma_n (x_1^2 + x_2^2 + \dots + x_{n+1}^2)^{(n+1)/2}} \quad (4.21)$$

where  $\gamma_n = 2\pi^{\frac{n+1}{2}} / \Gamma(\frac{n+1}{2})$  with  $\Gamma(x)$  the Euler function, is the surface of the unit sphere  $S^n$ . Of particular importance for the following are the two examples in  $\mathbb{R}^2$  and  $\mathbb{R}^3$

$$\Omega_{S^1} = \frac{xdy - ydx}{2\pi(x^2 + y^2)} \quad \text{and} \quad \Omega_{S^2} = \frac{xdy \wedge dz + ydz \wedge dy + zdx \wedge dy}{4\pi(x^2 + y^2 + z^2)^{3/2}}. \quad (4.22)$$

A key result in differential calculus is Stokes theorem, that relates the integral of a differential form  $\omega$  with that of its derivative  $d\omega$ , *when it exists everywhere over  $M$* , as

$$\text{Stokes theorem :} \quad \int_M d\omega = \int_{\partial M} \omega \quad (4.23)$$

where  $\partial M$  denotes the boundary of the manifold  $M$ .

### Expression of the degree

Finally, we will need a second theorem, known as Brouwer theorem, that relates the integrals of a differential form over two different manifolds  $A$  and  $B$  of same dimension  $n$ . Consider a differential form  $\omega$  defined over the manifold  $B$  of local coordinates  $\mathbf{y} = (y_1, \dots, y_n)$ , i.e.  $\omega = \omega_{j_1, \dots, j_n}(\mathbf{y}) dy_{j_1} \wedge \dots \wedge dy_{j_n}$ , and a map  $f$  between the two manifolds  $\mathbf{x}: A \rightarrow \mathbf{y} = f(\mathbf{x}) \in B$ . Then one can define a form on  $A$  from  $\omega$ , through the action of  $f$ . It is called the *pull-back* of  $\omega$  and reads

$$f^* \omega = \omega_{j_1, \dots, j_n}(f(\mathbf{y})) \det \left( \frac{\partial y^\alpha}{\partial x^\beta} \right) dx_{j_1} \wedge \dots \wedge dx_{j_n} \quad (4.24)$$

where the Jacobian matrix accounts for the change of local coordinates. Then one has the following

$$\text{Brouwer theorem:} \quad \int_A f^* \omega = \deg f \int_B \omega \quad (4.25)$$

where the degree of  $f$  was defined in (4.10). An important application of the Brouwer theorem is that it gives an integral formulation of the degree of a map, which one obtained when applying the formula (4.25) when  $B = S^n$  for the volume form  $\Omega_{S^n}$ .

For instance, in the case where of the punctured plane  $B = \mathbb{R}^2 \setminus \{0\} \cong S^1$ , one gets

$$\deg h = \int_{\lambda \in S^1} h^* \Omega_{S^1} \quad (4.26)$$

$$= \int_{\lambda \in S^1} \frac{1}{2\pi h^2} (h_x dh_y - h_y dh_x) . \quad (4.27)$$

Interpreting  $\mathbf{h} = (h_x, h_x) = (x(t), y(t))$  as a vector position that depends on a parameter  $t \in S^1$ , one recovers immediately the winding number  $W$  defined in (4.6).

We will be particularly interested in the case of Hamiltonian maps  $S^2 \xrightarrow{h} S^2$ . In that case the degree reads

$$\deg h = \int_{\lambda \in S^2} h^* \Omega_{S^2} \quad (4.28)$$

$$= \int_{\lambda \in S^2} \frac{1}{4\pi h^3} (h_x dh_y \wedge dh_z + h_y dh_z \wedge dh_x + h_z dh_x \wedge dh_y) \quad (4.29)$$

where the  $h_i$ 's are functions of  $\lambda_\alpha$  so that  $dh_i = \frac{\partial h_i}{\partial \lambda_\alpha} d\lambda_\alpha$ , and one gets

$$\deg h = \frac{1}{4\pi} \int_{\lambda \in S^2} \frac{\epsilon^{ijk}}{h^3} h_i \frac{\partial h_j}{\partial \lambda_\alpha} \frac{\partial h_k}{\partial \lambda_\beta} d\lambda_\alpha \wedge d\lambda_\beta \quad (4.30)$$

Finally, using the usual vectorial notation in  $\mathbb{R}^3$ , this expression takes the form

$$\deg h = \frac{1}{4\pi} \sum_{\alpha, \beta} \int_{S^2} \frac{\mathbf{h}}{h^3} \cdot \left( \frac{\partial \mathbf{h}}{\partial \lambda_\alpha} \times \frac{\partial \mathbf{h}}{\partial \lambda_\beta} \right) d\lambda_\alpha \wedge d\lambda_\beta \quad (4.31)$$

This formula has a direct meaningful geometrical interpretation : it tells that the degree of the maps  $S^2 \xrightarrow{h} S^2$  is a wrapping number, meaning that it counts the number of times the vector  $\mathbf{h}/h = \mathbf{n}$  wraps the target sphere  $S^2$  when  $\boldsymbol{\lambda}$  spans the entire base space  $S^2$ .

### 4.3 Berry curvature and first Chern number

#### 4.3.1 Topology from the eigenstates

The language of differential forms is particularly convenient to reveal the topological and geometrical structures of physical systems. Of main importance to characterize the eigenstates  $|\Psi_n(\boldsymbol{\lambda})\rangle$  of a quantum Hamiltonian that is smoothly parametrized over a base space  $\Lambda$ , or actually any eigenstates of a parametrized linear Hermitian eigenvalues problem

$$H(\boldsymbol{\lambda})|\Psi_n(\boldsymbol{\lambda})\rangle = E_n(\boldsymbol{\lambda})|\Psi_n(\boldsymbol{\lambda})\rangle \quad (4.32)$$

that one can encounter in particular in wave physics, are geometrical tools introduced by Berry and Simon, called *Berry connection* and *Berry curvature* [10, 95]. The Berry connection is a 1-form defined from each parametrized eigenstate as<sup>3</sup>

$$\begin{aligned} \mathcal{A}^{(n)}(\boldsymbol{\lambda}) &\equiv i \langle \Psi_n | d | \Psi_n \rangle \\ &= i \langle \Psi_n | \frac{\partial}{\partial \lambda_j} | \Psi_n \rangle d\lambda_j \\ &\equiv A_j^{(n)}(\boldsymbol{\lambda}) d\lambda_j \end{aligned} \quad (4.33)$$

and the Berry curvature is an exact 2-form obtained as the derivative of the connection as

$$\begin{aligned} \mathcal{F}^{(n)}(\boldsymbol{\lambda}) &\equiv d\mathcal{A}^{(n)}(\boldsymbol{\lambda}) \\ &= \sum_{j < k} \left( \frac{\partial A_k^{(n)}}{\partial \lambda_j} - \frac{\partial A_j^{(n)}}{\partial \lambda_k} \right) d\lambda_j \wedge d\lambda_k \\ &\equiv F_{jk} d\lambda_j \wedge d\lambda_k \end{aligned} \quad (4.34)$$

It is thus a closed form i.e.  $d\mathcal{F}^{(n)} = 0$ . Note that the Berry connection is not gauge invariant : when a gauge transformation is performed on a state  $|\Psi\rangle \rightarrow |\tilde{\Psi}\rangle = e^{i\chi(\boldsymbol{\lambda})} |\Psi\rangle$ , then the Berry

---

<sup>3</sup>This definition fits the one of Berry and Simon but differs by a minus sign from the one mostly encountered in solid states physics when dealing with Bloch bands.

connection transforms as

$$\mathcal{A}^{(n)} \rightarrow \tilde{\mathcal{A}}^{(n)} = i \langle \tilde{\Psi}_n | d | \tilde{\Psi}_n \rangle \quad (4.35)$$

$$= -d\chi + \mathcal{A}^{(n)}. \quad (4.36)$$

Since  $d\chi$  is an exact 1-form, then  $d(d\chi) = 0$  and therefore the Berry curvature  $\mathcal{F}^{(n)}$  is gauge invariant. It is actually an observable quantity.

For now, let us express the Berry curvature in a more physical form. By taking the derivative with respect to  $\lambda_j$  of the eigenvalue equation (4.32) one gets the relation

$$\langle \Psi_m | \partial_{\lambda_j} | \Psi_n \rangle = \frac{\langle \Psi_m | \partial_{\lambda_j} H | \Psi_n \rangle}{E_n - E_m} \quad (4.37)$$

that one can substitute in (4.34) after having injected a closure relation  $\sum_m | \Psi_m \rangle \langle \Psi_m | = \mathbb{1}$ , to end up with

$$\mathcal{F}^{(n)}(\boldsymbol{\lambda}) = i \sum_{j,k} \sum_{m \neq n} \frac{\langle \Psi_n | \partial_{\lambda_j} H | \Psi_m \rangle \langle \Psi_m | \partial_{\lambda_k} H | \Psi_n \rangle}{(E_n - E_m)^2} d\lambda_j \wedge d\lambda_k \quad (4.38)$$

The advantage of this formula is three-fold. First, it does not assume anymore that the eigenstates are smooth with respect to the parameters  $\boldsymbol{\lambda}$ . Second, using the anti-symmetry of the wedge product, it is straightforward to show from (4.38), the important relation

$$\sum_n \mathcal{F}^{(n)}(\boldsymbol{\lambda}) = 0 \quad (4.39)$$

which can somehow be seen as a conservation relation. It also implies that one necessarily needs at least two intern degrees of freedom (orbital, spin, classical fields...) in the eigenvalues problem (4.32) to have a non-zero Berry curvature. Finally, the denominator in the formula (4.38) reveals a divergence of the curvature at the degeneracy points  $E_n(\boldsymbol{\lambda}_0) = E_m(\boldsymbol{\lambda}_0)$ , meaning that  $\mathcal{F}^{(n)}(\boldsymbol{\lambda})$  is maximum for  $\boldsymbol{\lambda}$  where the gap is the smaller. These degeneracies, or level crossings can be interpreted as the sources of Berry curvature, and thus act as monopoles, that are referred to as *Berry monopoles*. Usually, a monopole has a charge, given by the flux of the field it generates, through a closed surface that surrounds it. Such a charge can be defined here and turns out to be an integer-valued topological number, called the *first Chern number*

$$\mathcal{C}_n = \frac{1}{2\pi} \int_{S^2} \mathcal{F}^{(n)} \in \mathbb{Z}. \quad (4.40)$$

The first Chern number  $\mathcal{C}_n$  characterizes the topological property of the fiber bundle defined as the collection of the parametrized eigenstates  $| \Psi_n(\boldsymbol{\lambda}) \rangle$  over the base space  $S^2$ , as sketched in figure 4.2. It encodes a global property, unlike the Berry curvature that is a local quantity.

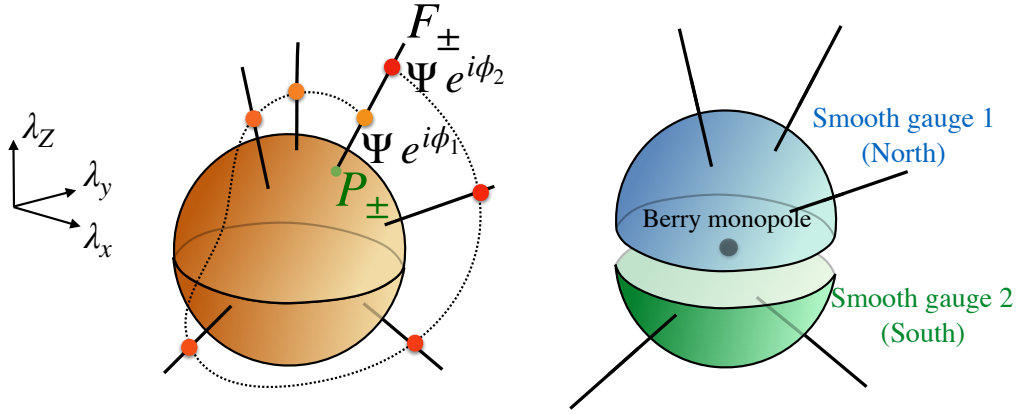


Figure 4.2 – (a)  $U(1)$  fiber-bundle as a continuous collection of fibers  $F$  over the sphere defined in parameter space  $\lambda$ . Two states in the same fiber only differ by a phase; they thus have the same projector onto the base space. The impossibility to define smoothly this phase over the base space is a manifestation of the topological property of the fiber bundle, encoded into the Chern number. (b) This Chern number is the quantized flux through the sphere of the Berry curvature generated by the degeneracy point, called Berry monopole. The existence of a non-zero Chern number imposes the 1-form Berry connection to be defined smoothly only piecewise.

Note that from (4.39) one immediately gets the *topological charge conservation*

$$\sum_n \mathcal{C}_n = 0. \quad (4.41)$$

For a two-fold degeneracy, the two collections of eigenstates parametrized on the surrounding sphere have opposite topological charges. This is the most standard situation, encountered for instance for Weyl fermions. More generally, for an  $n$ -fold degeneracy, the  $n$  different eigenstates define as many fiber bundles whose Chern numbers are a priori different in absolute value. The same degeneracy thus leads to different topological charges  $\mathcal{C}_n$  that depend on the fiber bundle. The fact that the Chern number is zero for a single level system is consistent with the fact that the monopole consists in a degeneracy, that necessarily implies at least two levels.

### 4.3.2 Topological charge of a two-fold degeneracy point

The simplest and also more common example of a physical model that exhibits topological properties from a degeneracy point is the generic  $2 \times 2$  Hamiltonian introduced in (4.11). We shall use this model to give more insight about the meaning of the first Chern number and show how to compute it by different ways.

### Chern number as an obstruction to Stokes theorem

We introduced the Berry curvature  $\mathcal{F}$  as the exterior derivative of the 1-form Berry connection  $\mathcal{A}$  i.e.  $\mathcal{F} \equiv d\mathcal{A}$ . Their integrals are thus related via Stokes theorem (4.23)

$$\int_{S^2} \mathcal{F} = \int_{\partial S^2} \mathcal{A}. \quad (4.42)$$

Since the sphere  $S^2$  is a closed surface, it does not have a boundary ( $\partial S^2 = 0$ ), and the right hand member of this equality always vanishes. This wrong result originates from a mistake one makes when stating that  $\mathcal{F} = d\mathcal{A}$  *everywhere*. However we saw that the Berry connection (like the eigenstates) is ill-defined at some points that depend on the gauge choice. Therefore the equality  $\mathcal{F} = d\mathcal{A}$  is only valid in a domain where these points have been excluded. Note that previously, we integrated the Berry curvature that was derived from the Berry connection in a specific gauge with the same equality. This is legitimate, since the Berry curvature is a gauge invariant quantity : the expression one obtains with a specific gauge that makes smooth the Berry connection in a certain domain, is the same as the one one gets with another gauge that is smooth where the previous one was not. In other words, one can always find a gauge where the equality  $\mathcal{F} = d\mathcal{A}$  holds, so that it is always safe to work with  $\mathcal{F}$ . But one cannot find a gauge that is smooth everywhere and would imply that  $\mathcal{F} = d\mathcal{A}$  is always valid, unless the fiber-bundle is topological trivial, as meant by (4.42). For this reason, the Chern number is often said to be an *obstruction* to Stokes theorem, which gives another insight about its topological meaning.

We must give up the Stokes theorem when considering the entire parameter space, that is  $S^2$  in our case. But one can still use it piecewise, on domains where  $\mathcal{F} = d\mathcal{A}$  is a valid equality. These are defined with different gauges. Let us make it explicit for the state  $\Psi_+$  of the two-level model :

$$\text{south gauge: } \chi = 0 \quad |\Psi_+^S\rangle = \begin{pmatrix} \cos \frac{\theta}{2} e^{-i\phi} \\ \sin \frac{\theta}{2} \end{pmatrix} \quad \text{valid for } \theta \neq 0 \quad (4.43)$$

$$\text{north gauge: } \chi = \phi \quad |\Psi_+^N\rangle = \begin{pmatrix} \cos \frac{\theta}{2} \\ \sin \frac{\theta}{2} e^{i\phi} \end{pmatrix} \quad \text{valid for } \theta \neq \pi \quad (4.44)$$

from which the Berry connection is computed in the local spherical coordinates

$$\mathcal{A} = i \langle \Psi | \partial_\theta | \Psi \rangle d\theta + i \langle \Psi | \partial_\phi | \Psi \rangle d\phi \quad (4.45)$$

leading to

$$\text{south gauge: } \chi = 0 \quad \mathcal{A}_+^S = \cos^2 \frac{\theta}{2} d\phi \quad \text{valid for } \theta \neq 0 \quad (4.46)$$

$$\text{north gauge: } \chi = \pi \quad \mathcal{A}_+^N = -\sin^2 \frac{\theta}{2} d\phi \quad \text{valid for } \theta \neq \pi \quad (4.47)$$

In passing, one can check that these two different expressions indeed yield the same Berry

## Chapter 4. Basic concepts

---

curvature  $\mathcal{F}^+ = -\frac{1}{2} \sin\theta d\theta \wedge d\phi$  whose expression is valid for any  $\theta$ . This is actually (and consistently) equal to  $2\pi\Omega_{S^2}$  in spherical coordinates.

The Chern number can now be computed via Stokes theorem by safely using  $\mathcal{F} = d\mathcal{A}$  on different patches when this equality make sense, and for instance over north hemisphere (NH) and south hemisphere (SH) respectively, as illustrated in figure 4.2 :

$$\mathcal{C}_+ = \frac{1}{2\pi} \int_{S^2} \mathcal{F}_+ \quad (4.48)$$

$$= \frac{1}{2\pi} \int_{\text{NH}} \mathcal{F}_+ + \frac{1}{2\pi} \int_{\text{SH}} \mathcal{F}_+ \quad (4.49)$$

$$= \frac{1}{2\pi} \int_{\text{NH}} d\mathcal{A}_+^N + \frac{1}{2\pi} \int_{\text{SH}} d\mathcal{A}_+^S \quad (4.50)$$

so that Stokes theorem can be safely used to get

$$\mathcal{C}_+ = \frac{1}{2\pi} \int_{\partial\text{NH}} \mathcal{A}_+^N + \frac{1}{2\pi} \int_{\partial\text{SH}} \mathcal{A}_+^S \quad (4.51)$$

where the boundary of an hemisphere is the equator, that is defined by  $\theta = \pi/2$ . The orientation of the surface, encoded into  $d\theta \wedge d\phi$  rather than  $-d\theta \wedge d\phi$  in the Berry curvature tells that the Chern number is the flux of  $\mathcal{F}$  through the sphere, emanating from the monopole toward the exterior. The line integral along the equator must keep track of this orientation, so that the boundary of the north and south hemispheres is the same equator line  $\gamma$  but oriented in opposite directions :

$$\mathcal{C}_+ = \frac{1}{2\pi} \int_{\gamma} \mathcal{A}_+^N|_{\theta=\pi/2} - \mathcal{A}_+^S|_{\theta=\pi/2} = -\frac{1}{2\pi} \int_0^{2\pi} d\phi = -1 \quad (4.52)$$

after substitution of the Berry connections by their expression in their corresponding gauges.

One important remark is that the two connections are related by the gauge transformation (4.36) that one can re-express as

$$|\Psi\rangle \rightarrow |\tilde{\Psi}\rangle = e^{i\chi(\lambda)} |\Psi\rangle \rightarrow \mathcal{A} \rightarrow \mathcal{A} + ie^{-i\chi} d e^{i\chi} \quad (4.53)$$

where  $e^{i\chi} \in U(1)$  is called the *transition function*. It tells how the two smooth pieces of the fiber bundle (i.e. where the eigenstates are single-valued once the gauge is fixed) can be glued together. A non-zero Chern number thus corresponds to a winding of this function

$$\mathcal{C} = \frac{1}{2\pi} \int_{\gamma} \mathcal{A} - \tilde{\mathcal{A}} = -\frac{1}{2\pi i} \int_{\gamma} e^{-i\chi} d e^{i\chi}, \quad (4.54)$$

highlighting the "twist" of the fiber bundle. So the value of  $\mathcal{C}_+ = -1$  of the example can be found directly without even specifying the explicit expression of the different connections, since we know the gauge transformation between the two hemispheres.

### Chern number as a degree

The 1-form Berry connection associated to the eigenstate  $\Psi_+$ , can be expressed with the local coordinates  $(h_x, h_y, h_z)$  of the target space  $S^2$  embedded in  $\mathbb{R}^3$  as

$$\mathcal{A}_+ = i \langle \Psi_+ | \partial_{h_x} | \Psi_+ \rangle dk_x + i \langle \Psi_+ | \partial_{h_y} | \Psi_+ \rangle dk_y + i \langle \Psi_+ | \partial_{h_z} | \Psi_+ \rangle dk_z. \quad (4.55)$$

Of course, a gauge must be specified to compute it explicitly. For instance, in the south gauge, one gets after a tedious calculation

$$\mathcal{A}_+^S = -\frac{1}{2} \frac{h_y dh_x - h_x dh_y}{h(h - h_z)} \quad (4.56)$$

which is indeed well defined everywhere but at the north pole ( $h_z = h$ ). The Berry curvature can then be calculated from its definition (4.34) and one finds

$$\mathcal{F}_+ = -\frac{1}{2h^3} (h_x dh_y \wedge dh_z + h_y dh_z \wedge dh_x + h_z dh_x \wedge dh_y) = -2\pi \Omega_{S^2} \quad (4.57)$$

which does not depend on the gauge anymore. Now we add the information that  $h$  is a map from the base space  $\mathbb{R}^{3 \setminus \{0\}} \cong S^2$  to the target space  $\mathbb{R}^{3 \setminus \{0\}} \cong S^2$ . The Chern number can thus be expressed as

$$\int_{S^2} \mathcal{F}_+ = -2\pi \int_{S^2} h^* \Omega_{S^2} = -2\pi \deg h \int_{S^2} \Omega_{S^2}. \quad (4.58)$$

The last integral being equals to 1 by definition, one gets the important result

$$\mathcal{C}_\pm = \mp \deg h \quad (4.59)$$

where the derivation for  $\mathcal{C}_-$  is similar. It is remarkable that for this basic model, the Chern numbers of the two families of eigenstates exactly coincide with the degree of the Hamiltonian map : the Chern numbers, that characterize the topology of the complex fiber-bundles, reduce to the homotopy invariant wrapping number of the sphere. In practice, it could be very convenient to compute the Chern numbers by using the definition of the degree (4.10) of the Hamiltonian map. The difficulty of computing an integral is replaced by the one of finding the pre-images as

$$\mathcal{C}_\pm = \sum_{\mathbf{q}^{(0)} = h^{-1}(y_0)} \operatorname{sgn} \det \begin{pmatrix} \partial_{\lambda_1} h_x & \partial_{\lambda_1} h_y & \partial_{\lambda_1} h_z \\ \partial_{\lambda_2} h_x & \partial_{\lambda_2} h_y & \partial_{\lambda_2} h_z \\ \partial_{\lambda_3} h_x & \partial_{\lambda_3} h_y & \partial_{\lambda_3} h_z \end{pmatrix} \Big|_{y_0 = \mathbf{h}(\lambda^{(0)})} \quad (4.60)$$

where  $y_0$  is any regular point such that the determinant is not singular.

### Calculation of the topological charge in a few examples

For the sake of concreteness, let us compute the Chern number assigned to a two-fold degeneracy point by using the degree formula. Consider the simplest possible example of the Weyl Hamiltonians  $H_{W_{\pm}} = \pm \hbar v_F \mathbf{q} \cdot \boldsymbol{\sigma}$  meaning that  $\mathbf{h}_{\pm}(\mathbf{q}) = \pm \mathbf{q}$ , and the dispersion relation is linear with  $\mathbf{q}$ . The Chern numbers  $\mathcal{C}_{-}^{(W_{\pm})}$  for the family of eigenstates  $\Psi_{-}$  that surrounds the two degeneracy points read

$$\mathcal{C}_{-}^{(W_{\pm})} = \sum_{\mathbf{q}^{(0)} = h^{-1}(y_0)} \text{sgn det} \begin{pmatrix} \pm 1 & 0 & 0 \\ 0 & \pm 1 & 0 \\ 0 & 0 & \pm 1 \end{pmatrix} \Big|_{y_0 = \mathbf{h}(\mathbf{q}^{(0)})}. \quad (4.61)$$

In that case there is no need to specify a pre-image and one directly gets  $\mathcal{C}_{-}^{(W_{\pm})} = \pm 1$ , which is often said to be *the* topological charge of the Weyl points, or its chirality or its helicity.

A less trivial example is provided by the following model, called "double Weyl node", for which  $\mathbf{h}(\mathbf{q}) = (q_y^2/2 - q_x^2/2, q_x q_y, q_z)$ . The quadratic terms in momentum yield a quadratic dispersion relation along  $q_x$  and  $q_y$  at the band touching point. The Jacobian matrix yields

$$\det \left( \frac{\partial h^i}{\partial q_j} \right) = -(q_x^2 + q_y^2) \quad (4.62)$$

whose value depends on the "direction"  $y_0 = \mathbf{h}(\mathbf{q}_i^{(0)})$ . Let us choose  $y_0 = h_x > 0$ . This implies  $q_x q_y = 0$  and  $q_z = 0$ . There are thus two pre-images  $\mathbf{q}_1^{(0)} = (0, q_y > 0, 0)$  and  $\mathbf{q}_2^{(0)} = (0, -q_y < 0, 0)$  of the point  $y_0 = (q_y^{(0)2}/2, 0, 0)$ . These two pre-images have the same negative contribution in the degree formula so that finally  $\mathcal{C}_{-} = -2$ .

These two examples show that the topological charge of a two-fold degeneracy could be  $|\mathcal{C}| \neq 1$  only when the dispersion relation is non-linear. Another physical example is found in gyro-electric media, as discussed in chapter 2. This non-linearity is however not sufficient in general. In contrast, for linear dispersion relations, the topological charge is fixed to  $|\mathcal{C}| = 1$ . Another way to obtain different Chern numbers is to consider an n-fold degeneracy point, as we shall see in a next section.

## 4.4 Berry monopoles

### The Berry model : a slowly rotating version of the Zeeman coupling

In its seminal paper of 1984, Berry introduced a simple model to illustrate the geometrical phase accumulated by a state adiabatically driven along a cycle in parameter space, and now days known as Berry phase [10].<sup>4</sup> We shall deviate from its original purpose and present this

---

<sup>4</sup>The concept of geometric phase, known as holonomy in mathematics, is relevant beyond the approximation of the adiabatic limit, and was generalized for instance by Aharonov and Anandan. For that reason, a distinction is sometimes made in some books between the Berry phase that assumed adiabaticity and the geometric phase that

model because it allows a simple and useful generalization of the topological charges  $\pm\mathcal{C}$  beyond two-fold degeneracy points.

The model consists in an arbitrary spin  $\hat{\mathbf{S}}$  coupled to an external magnetic field  $\mathbf{B}$  of orientation  $\mathbf{n}(\theta, \phi) = (\sin\theta \cos\phi, \sin\theta \sin\phi, \cos\theta)$  that can vary *adiabatically*. Here,  $\theta$  and  $\phi$  represent the polar and azimuthal angles in the laboratory frame respectively. This adiabatic prescription was originally made to guarantee that no transition occurs between the different energy levels and in particular that no level crossing may occur during the evolution. One can thus follow in time an instantaneous state of the following Hamiltonian

$$H(\theta, \phi) = \mathcal{E} \mathbf{n}(\theta, \phi) \cdot \hat{\mathbf{S}} \quad (4.63)$$

where  $\mathcal{E} = -\mu_B B$ . In the case of a spin 1/2, this model consists in the two-level system that was extensively presented in the previous sections, and for which the two-fold degeneracy point at  $\mathcal{E} = 0$  carries topological charges  $\mathcal{C}_{\pm} = \mp 1$ . For higher spins  $S = 1, 3/2, 2 \dots$ , the Hilbert space has dimension  $2S + 1$  and therefore the point  $\mathcal{E} = 0$  is  $2S + 1$ -fold degenerated. We shall see that such degeneracies yield higher Chern numbers.

One can compute the Berry curvature either by using the Stokes theorem in different regular patches or by using the formula (4.38), both technics being equally good. But in both cases, one needs an explicit dependence in the longitudinal and azimuthal angles  $\theta$  and  $\phi$  of the eigenstates and the Hamiltonian to differentiate them with respect to these variables. Let us fix the quantization axis to be along the  $z$  direction in the laboratory frame, so that

$$\hat{S}_z |m, \mathbf{e}_z\rangle = m |m, \mathbf{e}_z\rangle \quad (4.64)$$

where  $\hat{S}_z = \mathbf{e}_z \cdot \hat{\mathbf{S}}$ . The operator  $\hat{S}_z$  is related to the Hamiltonian  $\mathbf{n} \cdot \hat{\mathbf{S}}$  by a rotation, represented by a unitary operator that depends on the longitudinal and azimuthal angles  $U(\theta, \phi)$  as

$$\mathbf{n}(\theta, \phi) \cdot \hat{\mathbf{S}} \equiv U(\theta, \phi) \mathbf{e}_z \cdot \hat{\mathbf{S}} U^\dagger(\theta, \phi) = U(\theta, \phi) \hat{S}_z U^\dagger(\theta, \phi) \quad (4.65)$$

which relates the eigenstates of the "rotated" Hamiltonian  $H(\theta, \phi)$  to those of  $\hat{S}_z$

$$\begin{aligned} H(\theta, \phi) |m, \mathbf{n}\rangle &= \mathcal{E} m |m, \mathbf{n}\rangle \\ |m, \mathbf{n}\rangle &\equiv U(\theta, \phi) |m, \mathbf{e}_z\rangle . \end{aligned} \quad (4.66)$$

The rotation operator  $U(\theta, \phi)$  is not uniquely defined. For instance, one can choose for its representation

$$U(\theta, \phi) = e^{-i\phi \hat{S}_z} e^{-i\theta \hat{S}_y} . \quad (4.67)$$

Now that we have an explicit dependence in  $\theta$  and  $\phi$  of the Hamiltonian and its eigenstates, one can differentiate them and compute the Berry curvature, for instance with formula (4.38).

---

does not.

## Chapter 4. Basic concepts

---

Formula (4.38) implies terms of the form

$$\langle m, \mathbf{n} | \partial_\theta H(\theta, \phi) | p, \mathbf{n} \rangle \langle p, \mathbf{n} | \partial_\phi H(\theta, \phi) | p, \mathbf{n} \rangle \quad (4.68)$$

that can be computed from (4.66) and (4.67), and recalling the expression of a rotation of  $\hat{S}_z$  by an angle  $\theta$  around the  $y$  axis

$$e^{-i\theta \hat{S}_y} \hat{S}_z e^{i\theta \hat{S}_y} = \cos \theta \hat{S}_z + \sin \theta \hat{S}_x \quad (4.69)$$

one finds

$$\langle m, \mathbf{n} | \partial_\theta H(\theta, \phi) | p, \mathbf{n} \rangle = \mathcal{E} \langle m, \mathbf{e}_z | \hat{S}_x | p, \mathbf{e}_z \rangle \quad (4.70)$$

$$\langle p, \mathbf{n} | \partial_\phi H(\theta, \phi) | m, \mathbf{n} \rangle = \mathcal{E} \sin \theta \langle p, \mathbf{e}_z | \hat{S}_y | m, \mathbf{e}_z \rangle \quad (4.71)$$

These quantities can be computed with the spin ladder operators  $\hat{S}_+ = \hat{S}_x + i\hat{S}_y$  and  $\hat{S}_- = \hat{S}_x - i\hat{S}_y$ , and one ends up with the important result

$$\mathcal{F}_m = -m \sin \theta d\theta \wedge d\phi \quad (4.72)$$

that was first found by Berry. One recognizes the volume form  $4\pi\Omega_{S^2} = \sin \theta d\theta \wedge d\phi$  of the sphere  $S^2$  in spherical coordinates. It follows that its integral over  $S^2$  straightforwardly gives the useful result

$$\mathcal{C}_m = -2m . \quad (4.73)$$

This result was originally derived in a different way by Avron, Sadun, Segert and Simon [5]. In the case of a spin  $1/2$ , where  $m = \pm 1/2$ , one recovers the result  $\mathcal{C}_\pm = \mp 1$  of the previous section. For higher spins, the Chern numbers becomes higher and increase with the labelling of the eigenstates, that is with the eigen-energies. In particular, the shallow water model discussed in Part I, chapter 2 corresponds to a spin 1 problem, and its Chern numbers are directly inferred as  $(\mathcal{C}_-, \mathcal{C}_0, \mathcal{C}_+) = (2, 0, -2)$ .

### Generalized Berry model

One can conclude this section by doing a step further, and noticing that this standard result was derived for identity Hamiltonian maps whose degree is 1. This leads us to consider the more general model

$$H = \mathbf{h}(\boldsymbol{\lambda}) \cdot \hat{\mathbf{S}} \quad (4.74)$$

that defines the Hamiltonian map

$$\boldsymbol{\lambda} = \mathbf{B} : \mathbb{R}^3 \setminus \{0\} \cong S^2 \xrightarrow{h} \mathbf{h}(\boldsymbol{\lambda}) \in \mathbb{R}^3 \setminus \{0\} \cong S^2 . \quad (4.75)$$

that may wrap the target sphere several times, and thus change the value of the Chern number. Such a map is well defined for any spin value, and not only for spin 1/2, since the basis of the spin algebra  $[\hat{S}_\alpha; \hat{S}_\beta] = ie^{\alpha\beta\gamma} \hat{S}_\gamma$  contains exactly three elements, and therefore  $\mathbf{h} \in \mathbb{R}^{3 \setminus \{0\}}$  for each eigenstate  $|m, \mathbf{n}\rangle$  as long as the gap does not close.

Starting by recognizing the volume form  $\sin\theta d\theta \wedge d\phi = 4\pi\Omega_{S^2}$  of the sphere  $S^2$  in spherical coordinates in the expression (4.72) of the Berry curvature, one can use the Brouwer theorem (4.25) that leads to

$$C_m = \frac{1}{2\pi} \int_{S^2} \mathcal{F}_m = -2m \int_{S^2} h^* \Omega_{S^2} = -2m \deg h \int_{S^2} \Omega_{S^2} \quad (4.76)$$

which gives the final result for the topological charges of the generalized Berry model (4.74)

$$\mathcal{C}_m = -2m \deg h. \quad (4.77)$$

This formula generalizes the formula (4.59) obtained for  $2 \times 2$  Hamiltonians ( $m = \pm 1/2$ ), as well as (4.73)  $\mathcal{C}_m = -2m$  obtained for Berry monopoles ( $\deg h = 1$ ). It shows that the value of a topological charge originating from degeneracy points in parameter space  $\mathbf{R}^3$  has may have two distinct origins : the order of the degeneracy (property of  $\hat{\mathbf{S}}$ ) and the wrapping of the Hamiltonian map (homotopy property of  $\mathbf{h}(\boldsymbol{\lambda})$ ).



## 5 Spectral Flow and degeneracy points

Mais pour le principe, et pour l'exemple aussi,  
Je trouve qu'il est bon d'exagérer ainsi.

---

Edmond Rostand,  
*Cyrano de Bergerac*

As shown in chapter 4, band degeneracies are sources of geometrical Berry curvature. It follows that, in three dimensional parameter space  $(\lambda_1, \lambda_2, \lambda_3)$ ,  $U(1)$ -fiber bundles constructed on the unit sphere enclosing the degeneracy point for each continuous family of eigenstate  $\Psi_n(\lambda_1, \lambda_2, \lambda_3)$  concerned with the band touching, have a non-trivial topology captured by the first Chern number  $\mathcal{C}_n$ . This topological property has a direct physical consequence on the existence of chiral modes that emerge when a certain anisotropy (e.g. in space) is considered for one of the parameters  $\lambda_i$ .

### 5.1 An anisotropic 2D Dirac Hamiltonian

A canonical example exhibiting a degeneracy point in condensed matter is given by the Dirac Hamiltonian in two dimensions

$$H_{\text{Dirac}}(k_x, k_y, m) = k_x \sigma_x + k_y \sigma_y + m \sigma_z = \begin{pmatrix} m & k_x - i k_y \\ k_x + i k_y & m \end{pmatrix} \quad (5.1)$$

whose spectrum  $E_{\pm} = \pm \sqrt{k_x^2 + k_y^2 + m^2}$  has a two-fold degeneracy at  $(k_x, k_y, m) = (0, 0, 0)$ . Such Hamiltonian generically describes a linear two-band crossing in two dimensions when  $m = 0$ . It is a particular  $2 \times 2$  Hamiltonian discussed in chapter 4 for which we shown that  $\mathcal{C}_{\pm} = \mp 1$ .

The physical manifestation of this Chern number appears when considering a "dual" anisotropic problem, where the mass term  $m$  is a smooth function of space, say along the  $x$  direction, that changes sign somewhere. The system being not invariant by translation along  $x$  anymore, the

Hamiltonian becomes

$$\mathcal{H}_{\text{Dirac}}(i\partial_x, k_y, x) = \begin{pmatrix} m(x) & i\partial_x - ik_y \\ i\partial_x + ik_y & -m(x) \end{pmatrix}. \quad (5.2)$$

Note that we have kept the same order for the entries (scalars or operators) of the matrix, that corresponds to the ordered sequence of the three Pauli matrices. While  $H_{\text{Dirac}}(k_x, k_y, m)$  is simply a matrix of numbers,  $\mathcal{H}_{\text{Dirac}}(i\partial_x, k_y, x)$  is a matrix of objects that do not commute in general, and is therefore more involved to diagonalize. However, the Chern numbers computed for  $H_{\text{Dirac}}(k_x, k_y, m)$  already gives an important information on the spectrum of  $\mathcal{H}_{\text{Dirac}}(i\partial_x, k_y, x)$ .

The full spectrum of  $\mathcal{H}_{\text{Dirac}}(i\partial_x, k_y, x)$  can be computed quite easily in the simple case of a linear spatial dependence of the mass  $m(x) \sim x$ .<sup>1</sup> The problem to be solved becomes a set of two coupled differential equations where the only non-constant coefficients are linear with  $x$ . This suggests solutions given by Hermite functions. A direct brute force diagonalisation indeed leads to an Hermite equation for each of the components  $(\varphi^A, \varphi^B)$  of an eigenvector. Instead, one can perform a unitary transformation that preserves the cyclic ordering of the entries  $(i\partial_x, k_y, x)$  such that

$$\tilde{\mathcal{H}}_{\text{Dirac}}(x, i\partial_x, k_y) = R \mathcal{H}_{\text{Dirac}}(i\partial_x, k_y, x) R^\dagger = \begin{pmatrix} k_y & x + \partial_x \\ x - \partial_x & -k_y \end{pmatrix} \quad (5.3)$$

that is obtained for  $R = e^{-i\frac{\pi}{2\sqrt{2}}(\sigma_x + \sigma_z)} e^{i\frac{\pi}{4}\sigma_z}$ . One recognizes the annihilation and creation operators  $a = \frac{1}{\sqrt{2}}(y + \partial_y)$  and  $a^\dagger = \frac{1}{\sqrt{2}}(y - \partial_y)$ , that satisfy  $[a, a^\dagger] = 1$  and act on the Hermite functions  $\langle x|n\rangle = \varphi_n(x) = \frac{1}{(2^n n! \sqrt{\pi})^{1/2}} e^{-\frac{x^2}{2}} H_n(x)$  as  $a|n\rangle = \sqrt{n}|n-1\rangle$ ,  $a^\dagger|n\rangle = \sqrt{n+1}|n+1\rangle$  and  $a^\dagger a|n\rangle = n|n\rangle$ . The mode  $n \in \mathbb{N}$  corresponds to the number of zeros of  $\varphi_n(x)$ . As recalled in figure 5.1, the functions  $\varphi_n(x)$  are centered around  $x = 0$  (i.e.  $\langle x \rangle_n = 0$ ) that is where the mass term  $m$  changes sign, but their spreading increases with  $n$  as  $\langle x^2 \rangle_n = \frac{1}{2} + n$ .

The rotated Hamiltonian (5.3) suggests solutions of the form

$$\begin{pmatrix} k_y & \sqrt{2}a \\ \sqrt{2}a^\dagger & -k_y \end{pmatrix} \begin{pmatrix} \alpha_n |n\rangle \\ \alpha_{n+1} |n+1\rangle \end{pmatrix} = E_n \begin{pmatrix} \alpha_n |n\rangle \\ \alpha_{n+1} |n+1\rangle \end{pmatrix} \quad (5.4)$$

where the  $\alpha_i$  are coefficients. This ansatz yields the discrete spectrum

$$E_n^\pm = \pm \sqrt{k_y^2 + 2(n+1)} \quad n \in \mathbb{N} \quad (5.5)$$

that is shown in black in figure 5.2. As for the bulk Dirac Hamiltonian, this spectrum is still made of two branches of opposite energies that behave as  $E_n^\pm \sim \pm |k_y|$  for large  $k_y$ , but they are now constituted of an infinite number of discrete energy levels, that correspond to localized

<sup>1</sup>Such a choice corresponds for instance to a first order linearization of  $m(x) \sim x(\partial_x m)|_0 + O(x^2)$  of the mass term function that would change sign in  $x = 0$  with a derivative equals to unity.

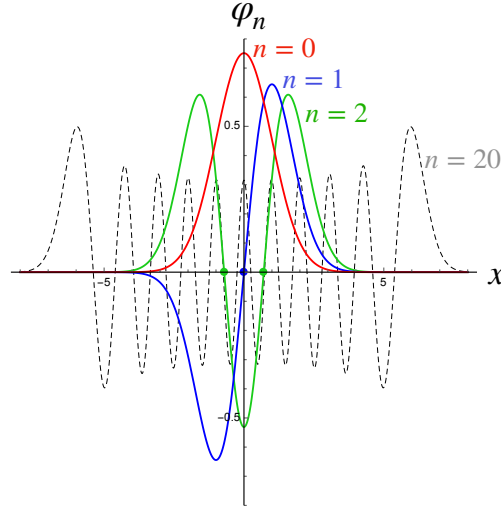


Figure 5.1 – Illustration of the spatial dependence of a few Hermite functions.

modes around  $m = 0$ . In particular, since  $n \in \mathbb{N}$ , the lower energy solution consists in two branches  $E_0^\pm = \pm \sqrt{k_y^2 + 1}$  and an associated eigenstate is

$$\Psi_0(x) = \begin{pmatrix} \langle x|0\rangle \\ \langle x|1\rangle \end{pmatrix} = \begin{pmatrix} 1 \\ \sqrt{2}x \end{pmatrix} e^{-\frac{x^2}{2}}. \quad (5.6)$$

The ansatz above does not account for all the solutions. Actually, an additional solution is suggested by the remarkable structure of  $\Psi_n$ , whose components  $\varphi_n^A$  and  $\varphi_n^B$  correspond to successive shifted modes  $n$  and  $n + 1$ . Then, by extrapolating this structure, one can easily check that there exists another lower energy solution  $\Psi_n$  that one may somehow abusively call " $n = -1$ ". This solution reads

$$\Psi_{-1}(x) = \begin{pmatrix} 0 \\ \langle x|0\rangle \end{pmatrix} = \begin{pmatrix} 0 \\ 1 \end{pmatrix} e^{-\frac{x^2}{2}} \quad (5.7)$$

and satisfies

$$\begin{pmatrix} k_y & \sqrt{2}a \\ \sqrt{2}a^\dagger & -k_y \end{pmatrix} \begin{pmatrix} 0 \\ |0\rangle \end{pmatrix} = E_{-1} \begin{pmatrix} 0 \\ |0\rangle \end{pmatrix} \quad (5.8)$$

which yields the single branch

$$E_{-1} = -k_y. \quad (5.9)$$

Unlike the other modes  $n \in \mathbb{N}$ , the dispersion relation of this extra mode cannot be inferred, even qualitatively, from the bulk dispersion. It has several remarkable properties: It is (1) non-dispersive, (2) localized and (3) minimally spread around where  $m(x)$  changes sign, (4) fully polarized onto one component only (e.g. spin in Dirac equation, pseudo-spin in graphene,

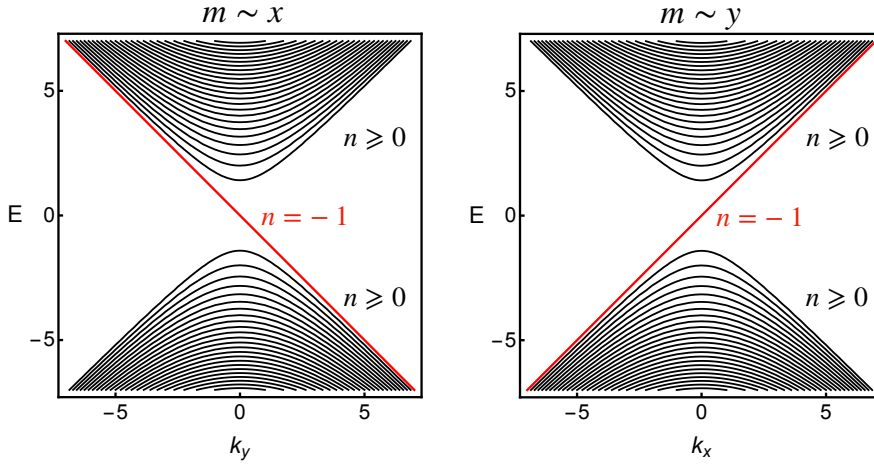


Figure 5.2 – Spectral flow for the Dirac Hamiltonian for  $m = x$  and  $m = y$ .

etc...), (5) the only accessible mode in the bulk gap and (6) it propagates with a negative group velocity for any  $k_y$ , i.e. it is a leftward *chiral* mode. Some of these properties, such as (1) and (4), are specific to this model, while others such as (5) and (6) are the consequence of (I) the existence of a bulk gap and (II) a more general property of this  $n = -1$  mode, called *spectral flow*, and that one could formulate as : *Its dispersion relation continuously connects the two energy branches  $E^+$  and  $E^-$  when varying  $k_y$ .* As a result, the branch  $E^+$  "looses" 1 mode while the branch  $E^-$  "gains" 1 mode when varying  $k_y$ . At this stage, one remarks that this gain/loss of modes is captured by the first Chern numbers  $\mathcal{C}_\pm$  of the bulk states whose energies  $\mathcal{E}^+ = \mathcal{E}^-$  match at some point in parameter space  $(k_x, k_y, m) = (0, 0, 0)$ . Denoting by  $\mathcal{N}_\pm$  the algebraic number of modes gained by the branch  $\pm$ , one gets the

$$\text{topological spectral flow} \quad \mathcal{C}_\pm = \mathcal{N}_\pm \quad (5.10)$$

that relates a topological property of the bulk eigenstates degeneracy to the algebraic number of modes  $\mathcal{N}$  that is *gained* by the branch  $\pm$  of the anisotropic physical system where the mass term changes sign in space. A variation of the number of modes in a branch is necessarily given by an integer number, but it is less obvious that this integer has a meaningful topological interpretation. Besides, note that the vanishing of the sum of Chern numbers  $\mathcal{C}_+ + \mathcal{C}_- = 0$  guarantees the balance between gained and lost modes when varying  $k_y$ , in consistence with the conservation of the number of modes. For that reason, the "flowing" chiral mode  $n = -1$  is said to be topological.

Equation (5.10) is a simple version of the Atiyah-Singer index formula that relates the rank of the projectors of  $\hat{\mathcal{H}}$  to the Chern numbers of the fiber bundles defined from the projectors of the parametrized  $H$ . This  $H$  can be seen as a semi-classical limit of  $\hat{\mathcal{H}}$ , and inversely  $\hat{\mathcal{H}}$  can be built from  $H$  by a quantization procedure, such as the Weyl quantization. Such quantization procedure gives a rigorous framework to the substitution  $k_x \rightarrow i\partial_x$ . The existence of a spectral

gap of  $H$  away from  $(k_x, k_y, m) = (0, 0, 0)$  then guaranties that  $\hat{\mathcal{H}}$  has discrete spectrum in the vicinity of  $k_y = 0$ , via the Weyl law. Much more details can be found in the notes of Frédéric Faure [27].

It worth finishing this section by discussing some subtleties regarding the relative sign between  $\mathcal{C}$  and  $\mathcal{N}$  in (5.10). First note that this sign depends on  $\text{sign}(\partial_x m)|_0$  that was positive in the example. The spectral flow would be reversed if  $m(x)$  was a decreasing function of  $x$  when it changes sign. Second, this sign also depends on the relative cyclic ordering between  $(k_x, k_y, m)$  and  $(i\partial_x, k_y, x)$ . The latest follows, up to a cyclic permutation, the sequence : *spectral flow parameter* ( $k_y$ )  $\rightarrow$  *position operator*  $\rightarrow$  *derivative operator*, meaning that each of these elements multiplies alternatively the Pauli matrices  $\sigma_x$ ,  $\sigma_y$  and  $\sigma_z$  in this cyclic order. For the opposite sequence *spectral flow parameter*  $\rightarrow$  *derivative operator*  $\rightarrow$  *position operator*, the topological spectral flow reads  $\mathcal{C}_\pm = -\mathcal{N}_\pm$ . This is what happens when considering for instance an anisotropic mass in the  $y$  direction, where the Hamiltonian now reads

$$\mathcal{H}_{\text{Dirac}}(k_x, i\partial_y, y) = \begin{pmatrix} y & k_x + \partial_y \\ k_x - \partial_y & -y \end{pmatrix} \xrightarrow{\text{rotation}} \tilde{\mathcal{H}}_{\text{Dirac}}(i\partial_y, y, k_x) = \begin{pmatrix} k_x & i\sqrt{2}a^\dagger \\ i\sqrt{2}a & -k_x \end{pmatrix} \quad (5.11)$$

and whose full energy spectrum, displayed in figure 5.2, shows a *rightward* chiral mode connecting the two energy branches.

## 5.2 A generalized "spin-oscillator" model

Highlighting the different key ingredients to generate a topological spectral flow in the anisotropic Dirac Hamiltonian allows us to propose a richer model whose both Chern numbers and spectral flows can still be completely solved analytically. In particular, this generalization includes the shallow water model introduced in part I. Indeed, the simplicity of the anisotropic Dirac Hamiltonian lies mainly on its decomposition in terms of (tensorial) products of Pauli matrices with (bosonic) ladder operators  $\hat{a}$  and  $\hat{a}^\dagger$ , and of a spectral flow parameter ( $\lambda = k_x$  or  $k_y$ ) that multiplies the diagonal ( $\sigma_z$ ) Pauli matrix. This structure can be generalized to arbitrary spins as

$$\text{operator Hamiltonian : } \quad \hat{\mathcal{H}} = \tau_1 x \hat{S}_x + \tau_2 i \partial_x \hat{S}_y + \lambda \hat{S}_z \quad (5.12a)$$

$$\text{"parameter" Hamiltonian : } \quad H_{\text{Cl}} = \lambda_1 \hat{S}_x + \lambda_2 \hat{S}_y + \lambda \hat{S}_z \quad (5.12b)$$

where  $\lambda \in \mathbb{R}$  and where the spin operators  $\hat{S}_i$  satisfy the usual Lie algebra  $[\hat{S}_\alpha, \hat{S}_\beta] = i\epsilon_{\alpha\beta\gamma} \hat{S}_\gamma$ . Note that for  $S = 1/2$ , one recovers the Dirac Hamiltonian (5.3) discussed in section 5.1 when  $\tau_1 = \tau_2 = 1$ , as  $\hat{\mathcal{H}} = S\mathcal{H}_{\text{Dirac}}$ .

The parameter Hamiltonian (5.12b) defines a Hamiltonian map from  $\mathbb{R}^3$  to  $S^2$  of degree 1. Its eigenvalue spectrum owns a  $2S + 1$ -fold degeneracy point at  $(\lambda = 0)$ . According to the formula (4.77), the parametrized families of eigenstates  $m$  are thus characterized by the Chern numbers  $\mathcal{C}_m = -2m$ . One thus expects this topological property to appear as a spectral flow



where we have defined the shorthand

$$\beta_m = \sqrt{(S(S+1) - m(m+1)(n+S-m))}. \quad (5.21)$$

Denoting by  $H_n^{(2S+1)}$  the matrix in (5.20), the associated characteristic polynomial  $P_n^{(2S+1)} = \det(H_n^{(2S+1)} - E_n \text{Id})$  is of order  $2S+1$  in  $E_n$  with real coefficients. For each  $n \in \mathbb{N}$ , the secular equation  $P_n^{(2S+1)} = 0$  yields  $2S+1$  real solutions, corresponding to  $2S+1$  energy branches  $E_n$ . Examples for  $S = 1, 3/2$  and  $2$  are listed in figure 5.3. None of these solutions manifest a spectral

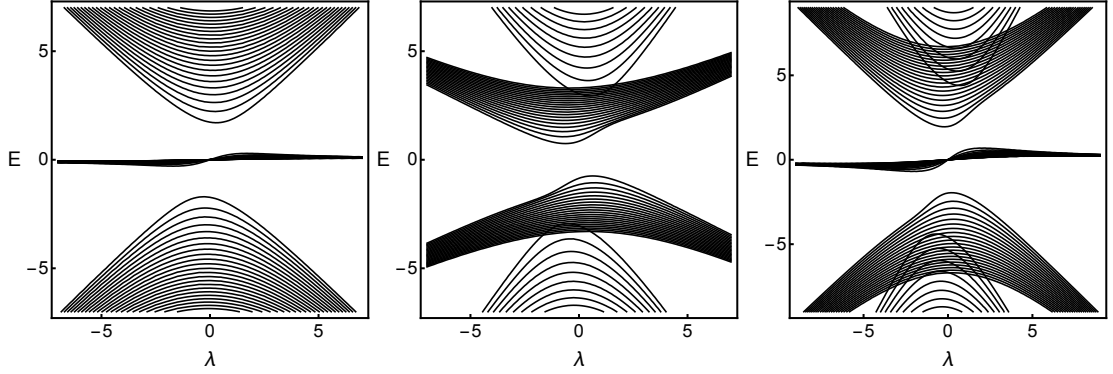


Figure 5.3 – Eigenvalue spectrum of the  $\hat{\mathcal{H}}$  obtained with the ansatz 0 in (5.19) for  $S = 1, S = 3/2$  and  $S = 2$ .

flow. Those that do develop a spectral flow can be constructed separately one by one. The procedure is similar to that we followed for the Dirac Hamiltonian. These additional modes are generated from a different ansatz. Indeed, the Hilbert space has not been full explored with the ansatz 0 (5.19) used above. In particular, note that the lowest allowed mode  $|0, \# \rangle$  is reached when  $n = 0$  and  $m = S$ , that is for  $\alpha_S |0, S \rangle$ . Therefore, this decomposition does not allow the other basis states  $|n + S - m, m \rangle$  to reach the fundamental mode  $|0, \# \rangle$ , unless  $n$  is negative. One can thus construct the missing solutions by removing  $|0, S \rangle$  in the decomposition and by replacing  $n = -1$  in the other remaining basis states  $|n + S - m, m \rangle$ , that leads to

$$\text{Ansatz -1: } |\Psi_{-1}\rangle = \sum_{m=-S}^{S-1} \alpha_m^{(-1)} |S-1-m, m\rangle. \quad (5.22)$$

The index  $-1$  indicates that the decomposition now runs over  $2S$  base states instead of  $2S+1$ . This ansatz gives a new eigenvalues problem whose matrix form  $H_{-1}^{2S}$  is obtained from  $H_n^{(2S+1)}$  by removing the last ligne and the last column in (5.20) and by substituting  $n = -1$ . The associated characteristic polynomial  $P_{-1}^{(2S)} = \det(H_{-1}^{(2S)} - E \text{Id})$  is of order  $2S$  in  $E$  and yields  $2S$  energy branches that connect the energy branches obtained previously with ansatz 0.

If  $S > 1/2$ , there are still base states that have not been considered. One thus has to apply  $2S$  times the procedure by setting  $n = -p$  and then retrieve  $p$  base states, which gives

$$\text{Ansatz -p: } |\Psi_{-p}\rangle = \sum_{m=-S}^{S-p} \alpha_m^{(-p)} |S-p-m, m\rangle. \quad (5.23)$$

until the Hilbert space has been fully considered. Each of these Ansatz yields a characteristic

## Chapter 5. Spectral Flow and degeneracy points

polynomial  $P_{-p}^{2S+1-p}$  of degree  $2S+1-p$  in  $E$  and thus as many energy branches that participate to the spectral flow. The procedure ends up with the solution

$$\text{Ansatz } -2S: \quad |\Psi_{-2S}\rangle = |0, -S\rangle \quad (5.24)$$

whose egenenergy consists in the single non-dispersive branch  $E = -S\lambda$ .

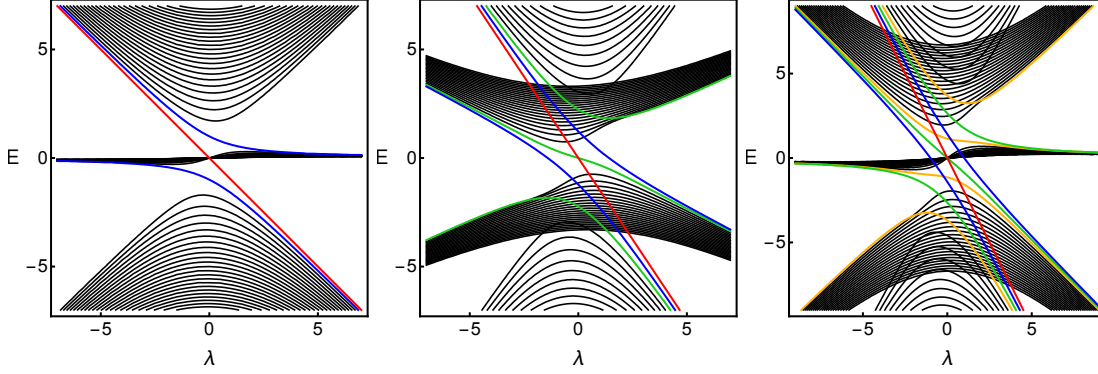


Figure 5.4 – Eigenvalue spectrum of the  $\hat{\mathcal{H}}$  for  $S = 1$ ,  $S = 3/2$  and  $S = 2$ . The black branches are obtained with the ansatz 0 and the colored spectral flows are obtained by applying the successive ansatz  $-p$  (5.23) : (red)  $p = 2S$ , (blue)  $p = 2S - 1$ , (green)  $p = 2S - 2$  and (yellow)  $p = 2S - 3$ .

The complete spectra are shown in figure 5.4. The spectral flows satisfy the relation  $\mathcal{N}_m = \mathcal{C}_m = -2m$  where  $\mathcal{N}_m$  is the number of modes that are gained by the band  $m$  when sweeping  $\lambda$ . It is instructive to see that some flowing modes do not cross the gap, and are thus completely superposed to "bulk" modes. These modes are not chiral neither, since their group velocity changes sign when bridging two bands.

Finally, it is worth noticing that the eigenvalue spectrum obtained in the spin 1 case coincides with that of the shallow water model, and more generally with many low frequency effective descriptions of wave spectra, like for instance for the transverse magnetic (TM) modes of a two-dimensional gyro-electric media, as discussed in chapter 2 in part I. The mapping between  $\hat{\mathcal{H}}$  for  $S = 1$  and  $\hat{\mathcal{H}}_{SW}$  that is the Hermitian matrix representing the linearized shallow water model in the Matsuno problem (see equation 2.7 with a linear dependence of  $f$  in  $y$ ) can be made explicitly by using the following unitary transformation

$$\hat{\mathcal{H}}_{SW} = U_{sw}^\dagger \hat{\mathcal{H}} U_{sw} \quad \text{with} \quad U_{sw} = \frac{1}{\sqrt{2}} \begin{pmatrix} 1 & 0 & 1 \\ 0 & \sqrt{2} & 0 \\ -1 & 0 & 1 \end{pmatrix} \quad (5.25)$$

and the substitutions  $\lambda \rightarrow k_x$ ,  $x \rightarrow i\partial_y$  and  $i\partial_x \rightarrow y$  that reverse the spectral, as discussed in the previous section, and in agreement with the spectrum found by Matsuno. Also, the Kelvin

wave is obtained as

$$U_{sw}^\dagger |\Psi_{-2}\rangle = U_{sw}^\dagger \begin{pmatrix} |0\rangle \\ 0 \\ 0 \end{pmatrix} = \frac{1}{\sqrt{2}} \begin{pmatrix} |0\rangle \\ 0 \\ |0\rangle \end{pmatrix} \quad (5.26)$$

which indeed describes a shallow water wave of fluid's thickness and of azimuthal velocity that are symmetric with respect to the equator, while the longitudinal velocity vanishes, as expected. The Yanai wave, that constitutes the second contribution to the spectral flow, is obtained similarly from  $|\Psi_{-1}\rangle$ .



# 6 Winding numbers in unitary dynamics : from Floquet systems to scattering networks

J'fais des trous, des p'tits trous, encore des p'tits trous.  
Des p'tits trous, des p'tits trous, toujours des p'tits trous.  
Des trous de seconde classe.  
Des trous d'première classe.

---

Serge Gainsbourg,  
*Le Poinçonneur Des Lilas*

## 6.1 Winding numbers in the unitary dynamics

A Floquet system is referred to a physical system described by a time periodic Hamiltonian  $H(t + T) = H(t)$ . It drives a time evolution encoded into the unitary operator  $U(t, t_0)$  that satisfies

$$i\partial_t U(t, t_0) = H(t)U(t, t_0) \tag{6.1}$$

where  $t_0$  is an arbitrary initial time. This evolution operator is represented by a  $N \times N$  unitary matrix  $U(\lambda)$ , where the parameter(s)  $\lambda$  could denote time  $t$  or other parameters such as the quasi-momentum  $k$ . These unitary matrices belong to the unitary group  $U(N)$  that is not simply-connected, i.e.  $\pi_1(U(N)) = \mathbb{Z}$ . This quick inspection already tells us that topological properties are expected to emerge in *periodic* dynamical systems, that is when the base space  $\lambda \in A \simeq S^1$ .

### 6.1.1 Winding of the Floquet operator

In periodically-driven systems, it is instructive to consider the Floquet operator  $U_F \equiv U(T, 0)$ . In one-dimensional crystals, the Bloch-Floquet operator  $U_F(k)$  depends on the quasi-momentum  $k$  that lives in the one-dimensional Brillouin zone  $BZ_{1D}$ . This provides us maps  $\lambda = k \in BZ_{1D} \simeq S^1 \xrightarrow{U_F} U(N)$  where  $N$  is the number of degrees of freedom (basically the number of orbitals

## Chapter 6. Winding numbers in unitary dynamics : from Floquet systems to scattering networks

---

in the unit cell for a spinless model) that fixes the number of bands. Homotopy properties of these maps are classified according to the group  $\pi_1(U(N)) = \mathbb{Z}$ , whose elements are the invariants

$$W[U_F] = \frac{1}{2\pi i} \int_{S^1} \text{tr} \left( U_F^{-1} \frac{\partial U_F}{\partial k} \right) dk \quad (6.2)$$

where the trace runs over Floquet states  $|\Psi_n\rangle(k)$  that are eigenstates of  $U_F(k)$  with eigen-energies  $e^{-i\epsilon_n T}$ , where  $\epsilon_n$  is called the quasi-energy. This winding number can thus be expressed as the sum of the windings of the (dimensionless) quasi-energies  $\epsilon_n = \epsilon_n T$

$$W[U_F] = - \sum_{n=1}^N \frac{1}{2\pi} \int_{S^1} \frac{\partial \epsilon_n(k)}{\partial k} dk. \quad (6.3)$$

Adding a hypothesis of adiabaticity, i.e. that an instantaneous state  $|\psi_n(t, k)\rangle$  remains an eigenstate during the time evolution, up to a phase, then the reduced winding number

$$\tilde{W}[U_F] = - \sum_{n=1}^{N_{occ}} \frac{1}{2\pi} \int_{S^1} \frac{\partial \epsilon_n(k)}{\partial k} dk \quad (6.4)$$

is directly related to the Chern numbers  $C_n$  of the fiber bundles built from the parametrized eigenstates  $|\psi_n(t, k)\rangle$  over the torus  $(t, k) \in S^1 \times S^1 = T^2 = \text{as}$

$$\tilde{W}[U_F] = \sum_{n=1}^{N_{occ}} C_n \equiv C \quad (6.5)$$

This Chern number  $C$  is itself directly related to the averaged current

$$J \equiv \int_0^T \frac{dt}{T} \langle j(t) \rangle = e \sum_{n=1}^{N_{occ}} \int_0^T \frac{dt}{T} \int_{\text{BZ}_{1D}} \frac{dk}{2\pi} \langle \psi_n | \frac{\partial x(t)}{\partial t} | \psi_n \rangle \quad (6.6)$$

as

$$J = \frac{e}{T} C. \quad (6.7)$$

This is the quantized current predicted by Thouless in 1993 [100], revisited by Kitagawa, Berg, Rudner and Demler in 2010 as the winding of the quasi-energies [58], and observed in cold atoms in 2015 [69, 77], that describes a charge pumping through an insulator that is adiabatically periodically driven in time.

### 6.1.2 Winding of the time-evolution operator and anomalous chiral states

Consider now the time-evolution operator  $U(t)$  of a Floquet system. They define maps  $\lambda = t \in S^1 \rightarrow U(N)$  whose homotopy group  $\pi_1(U(N)) \in \mathbb{Z}$  is non-trivial, suggesting that topological properties may arise from the dynamics. Of course, to define a "loop" in  $U(N)$ , one needs a map that is periodic. This is in general not the case for time-evolution operators. Indeed,

## 6.1. Winding numbers in the unitary dynamics

after a time  $T$ , the system has evolved through  $U(t = T)$  which is generically different from  $U(t = 0) = \mathbb{1}$ .

The trick to get a "periodized" evolution operator consists in "extracting" the periodic part of the evolution operator. This is possible thanks to Floquet theorem: since  $U(t)$  is solution of the Schrödinger-like equation with periodic coefficient (Hamiltonian)  $H(t + T) = H(t)$  it admits the decomposition

$$\begin{aligned} \text{Floquet theorem: } \quad V(t) &= U(t)e^{iH_{\text{eff}}t} \\ e^{-iH_{\text{eff}}T} &\equiv U(T) \end{aligned} \tag{6.8}$$

that automatically satisfies  $V(t) = V(t + T)$ .

As illustrated in figure 6.1 (a), the unitary operator  $V(t)$  somehow compares two paths in the unitaries, that start from  $\mathbb{1}$  and end at  $U(T)$ : Path 1 is drawn by the evolution operator  $U(t)$  given by a time-ordering exponential of the time dependent Hamiltonian  $H(t)$ ; Path 2 is given by a "stroboscopic evolution"  $e^{-iH_{\text{eff}}t}$  that is driven by a time-independent effective Hamiltonian  $H_{\text{eff}}$ . The first one describes the actual dynamics of the system, and thus encodes the full "movie" of the evolution, while the second one is just a shortcut that *a priori* only reproduces faithfully a snapshot of the final scene. Following these two paths one after the other, one ends up with a loop in the unitaries that is described by  $V(t)$ . Is this loop contractible? I.e. can path 1 be continuously deformed into path 2? Or say it more formally, are the unitary operators  $U(t)$  and  $e^{-iH_{\text{eff}}t}$  homotop?

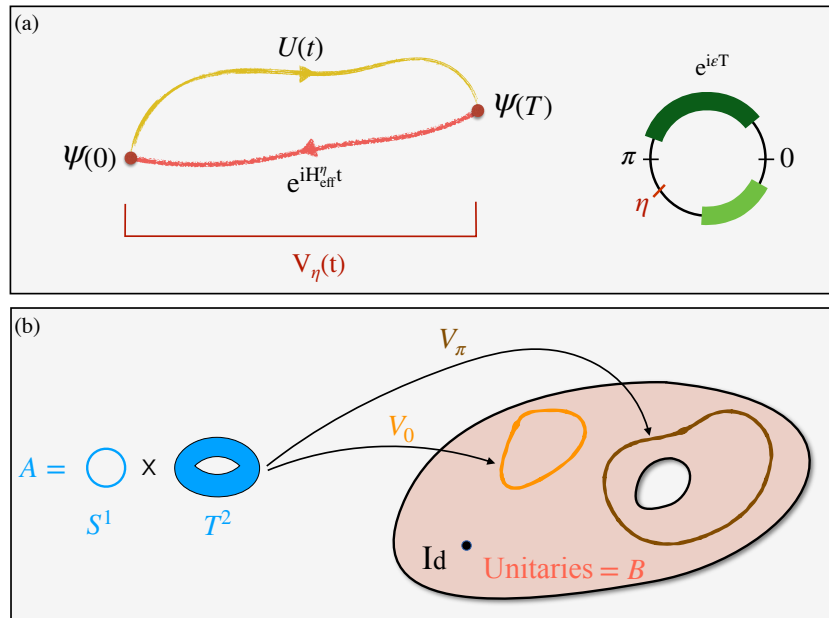


Figure 6.1 – Sketches of the construction of the periodized evolution operator  $V_\eta(t)$  and of its homotopy properties that depend on the spectral gap  $\eta$  of the Floquet operator.

## Chapter 6. Winding numbers in unitary dynamics : from Floquet systems to scattering networks

---

The answer to this question is given by the winding number of this operator, defined as the winding of its determinant

$$W[U] = \frac{1}{2\pi i} \int_0^T dt \frac{\partial}{\partial t} \log \det V \quad (6.9)$$

$$= \frac{1}{2\pi i} \int_0^T \text{tr} \left( V^{-1} \frac{\partial V}{\partial t} \right) dt \quad (6.10)$$

$$= \frac{1}{2\pi i} \int_{S^1} \text{tr} (V^{-1} dV) \quad (6.11)$$

that generalizes the definition (4.7) of the winding number to  $N \times N$  unitary matrices. The last line, written as the integral of a 1-form on the group  $U(N)$ , gives some insight about its generalization for larger parameter spaces.

Indeed, it may happen that the evolution operator also depends periodically of other parameters. Of particular importance is the Bloch evolution operator  $U(\mathbf{k}, t)$  that also depends on the quasi-momenta  $\mathbf{k}$ . Thus the relevant "winding numbers" must actually classify maps  $(\mathbf{k}, t) \in S^1 \times S^1 \times \dots \times S^1 \xrightarrow{V} U(N)$ , with homotopy groups  $\pi_n(U(N))$ . Are these groups trivial for  $n > 1$ ? Bott periodicity theorem answers that question by stating that

$$\pi_n(U(N)) = \begin{cases} \{0\} & n \text{ even} \\ \mathbb{Z} & n \text{ odd} . \end{cases} \quad (6.12)$$

So when  $n$  is odd, one can expect a topological property of the evolution operator. The expression of the associated topological invariants generalizes that of the winding number (6.11) obtained for  $n = 1$ . The case  $n = 3$  is particularly physically relevant since it includes the situation where the parameter space is made of the product of a two-dimensional Brillouin zone  $BZ_{2D}$  and a time-periodicity,<sup>1</sup> namely periodically driven 2D lattices, a situation that is encountered in many areas of physics such as condensed matter, cold atoms and photonics, among others. This is the particular case we shall focus on.

The invariants that describe such periodic dynamics can be expressed with the periodized evolution operator  $V(t)$  as [13]

$$W[U] = \frac{1}{24\pi^2} \int_{BZ_{2D}} \int_{S^1} \text{tr} (V^{-1} dV)^3 \in \mathbb{Z} \quad (6.13)$$

where the power 3 means the application of the  $\wedge$  product three times as

$$V^{-1} dV \wedge V^{-1} dV \wedge V^{-1} dV \quad (6.14)$$

between the 1-forms

$$dV = \frac{\partial V}{\partial \lambda_1} d\lambda_1 + \frac{\partial V}{\partial \lambda_2} d\lambda_2 + \frac{\partial V}{\partial \lambda_3} d\lambda_3 \quad (6.15)$$

---

<sup>1</sup>Here we admit that taking  $S^3$  or  $T^3$  as the parameter space does not change the homotopy invariant.

with  $\{\lambda_i\} = \{k_x, k_y, t\}$  and where we recall the rule  $d\lambda_1 \wedge d\lambda_2 = -d\lambda_2 \wedge d\lambda_1$ .

### 6.1.3 Gap invariants *v.s.* band invariants

A situation particularly interesting is the one where the spectrum of the Floquet operator  $U_F = U(T)$  is gapped. In that case, the system stroboscopically mimics an insulator, called *Floquet insulator*. Its quasi-energy spectrum can equivalently be seen as the one of the gapped effective Hamiltonian  $H_{\text{eff}}(\mathbf{k})$ , following the spectral decomposition

$$U_F = \sum_n e^{-i\varepsilon_n(\mathbf{k})} P_n(\mathbf{k}) \quad (6.16)$$

$$H_{\text{eff}}(\mathbf{k}) = \sum_n \varepsilon_n(\mathbf{k}) P_n(\mathbf{k}) \quad (6.17)$$

with the spectral projectors  $P_n(\mathbf{k}) = |\Psi_n(\mathbf{k})\rangle \langle \Psi_n(\mathbf{k})|$ . Since the quasi-energy bands  $\varepsilon_n(\mathbf{k})$  are assumed to be well separated here, each projector  $P_n(\mathbf{k})$  defines the usual U(1)-fiber-bundle over the two-dimensional Brillouin zone  $\text{BZ}_{2\text{D}}$  characterized by the first Chern number  $C_n$ .

Notice that (6.17) was obtained by applying "i ln" to (6.16). This is only sketchy since the logarithm must be specified with a branch cut. To avoid any unwanted discontinuity in the eigenstates, a reasonable choice is to fix the branch cut at a quasi-energy  $\eta$  that lies in one of the spectral gaps. Doing so defines different effective Hamiltonians

$$H_{\text{eff}}^\eta(\mathbf{k}) = i \sum_n \ln_{-\eta} \left( e^{-i\varepsilon_n(\mathbf{k})} \right) P_n(\mathbf{k}) \quad (6.18)$$

whose some of eigenvalues may be shifted by  $2\pi$  according to the choice of the branch cut. It follows that these Hamiltonian differ from each others by a projector on the bands that are contained in between their branch cuts. To make it clearer, two effective Hamiltonians with different branch cuts read

$$H_{\text{eff}}^{\eta=0} = \sum_{n=1}^N \varepsilon_n P_n \quad (6.19)$$

$$H_{\text{eff}}^\eta = \sum_{n=2}^N \varepsilon_n P_n + (\varepsilon_1 + 2\pi) P_1 \quad (6.20)$$

where we used  $\ln_0 e^{i\varphi} = i\varphi$  for  $0 < \varphi < 2\pi$ , and therefore  $H_{\text{eff}}^\eta - H_{\text{eff}}^0 = 2\pi P_1$ . More generally if a set of  $m$  quasi-energy bands is confined between two gaps  $\eta$  and  $\eta'$ , such that  $\eta < \varepsilon_j \cdots \varepsilon_{j+m} < \eta' < 2\pi$  then

$$H_{\text{eff}}^\eta(\mathbf{k}) - H_{\text{eff}}^{\eta'}(\mathbf{k}) = 2\pi P_{\eta,\eta'}(\mathbf{k}) . \quad (6.21)$$

where  $P_{\eta,\eta'}(\mathbf{k})$  is the projector on the  $m$  states  $\Psi_j(\mathbf{k})$ . As a consequence their corresponding

periodized evolution operators differ as

$$V_{\eta}^{-1}(\mathbf{k}, t) V_{\eta'}(\mathbf{k}, t) = e^{2i\pi t P_{\eta, \eta'}(\mathbf{k})} \quad (6.22)$$

which yields the key relation between the different invariants

$$W_{\eta'}[U] - W_{\eta}[U] = C_{\eta, \eta'} \quad (6.23)$$

as found by Rudner, Lindner, Berg and Levin in 2013 [91]. This equation relates the **gap** homotopy invariants  $W_{\eta}[U]$  of the full dynamics to the **band** (fiber-bundle) topological invariants  $C_n$  of the Floquet operator  $U(t = T)$ . One immediately sees that the former has more information than the latter, as expected since the information content of the entire evolution over a period is greater than that of the last snapshot. This means that there are topological properties in the dynamics that are not captured by the effective Hamiltonian, and more generally not captured by any static Hamiltonian. In particular, when all the  $W$  invariants are equal, the first Chern numbers of all the bands vanish. This is referred to as an *anomalous topological Floquet* regime. Actually, it was shown that the number  $n_{\eta}$  of chiral edge states in a spectral gap  $\eta$  of the Floquet operator is [91]

$$n_{\eta} = W_{\eta}[U]. \quad (6.24)$$

In the anomalous Floquet regime, the edge states are thus said to be *chiral anomalous*. Formulas (6.23) and (6.24) describe the bulk-edge correspondence in Floquet systems [91].

#### 6.1.4 Phase rotation symmetry

The anomalous Floquet regime shows topological properties with no counterpart in static systems, such as the chiral anomalous edge states. It would be thus interesting to find a way to engineer them on purpose. What are the ingredients? First, one needs the Chern numbers to vanish. This is not a sufficient condition, but it is necessary. Then one needs a way to distinguish – say by homotopy – two dynamics. If two dynamical systems cannot be smoothly deformed one into the other, *and* if their Chern numbers are zero, thus anomalous edge states are expected to arise at their interface.

The vanishing of the Chern numbers can be seen as resulting from some constrain. Since one wants the possibility to have chiral edge states at the same time, which is not possible in static systems, this constrain must operate at the level of the evolution operator rather than that of the Hamiltonian. A specificity of Floquet systems (and more generally unitary systems) is that their spectrum, as a phase spectrum, is periodic. This periodicity allows the existence of a possible *phase-rotation symmetry* that shifts all the eigenvalues on the unit circle in the complex plane as  $e^{-i\varepsilon_1} \rightarrow e^{-i\varepsilon_2} \rightarrow \dots \rightarrow e^{-i\varepsilon_N} \rightarrow e^{-i\varepsilon_1}$  as well as their corresponding eigenstates. A Floquet operator  $\tilde{U}_F \in U(N)$  (and more generally any unitary operator) is said to be phase rotation symmetric when it exists a unitary operator  $\mathcal{Z}$ , called phase rotation

## 6.1. Winding numbers in the unitary dynamics

symmetry operator, such that [22]

$$\mathcal{Z}\tilde{U}_F\mathcal{Z}^{-1} = e^{i2\pi/N}\tilde{U}_F. \quad (6.25)$$

Note that it leaves the evolution operator over  $N$  periods invariant since

$$\mathcal{Z}\tilde{U}_F^N\mathcal{Z}^{-1} = \tilde{U}_F^N. \quad (6.26)$$

This symmetry is extremely demanding : it is satisfied only when all the eigenvalues  $e^{-i\varepsilon}$  are equally spaced by an angle  $2\pi/N$  on the unit circle, which is in general not the case for an arbitrary gapped operator  $U_F$ , hence the  $\sim$  notation in (6.25).

Assume this symmetry is satisfied, then an eigenstate of  $\tilde{U}_F$  is transformed as  $|\psi_n\rangle \rightarrow \mathcal{Z}|\psi_n\rangle = |\psi_{n+1[N]}\rangle$  which is also an eigenstate of  $\tilde{U}_F$ , so that the projectors  $P_n(\mathbf{k}) = |\psi_n(\mathbf{k})\rangle\langle\psi_n(\mathbf{k})|$  are related through the symmetry as

$$P_n(\mathbf{k}) = \mathcal{Z}^{n-1}P_1(\mathbf{k})\mathcal{Z}^{-(n-1)} \quad (6.27)$$

Let us recall that the Chern number  $C_n$  can be expressed from the family of projectors  $\mathbf{k} \rightarrow P_n(\mathbf{k})$  on the band  $n$  as

$$C_n \equiv \text{Ch}(P_n) = \frac{1}{2i\pi} \int \text{tr} P_n dP_n \wedge dP_n \quad (6.28)$$

which is invariant under a ( $\mathbf{k}$  independent) unitary transformation. In particular

$$\text{Ch}(P_n) = \text{Ch}(\mathcal{Z}P_n\mathcal{Z}^{-1}) \quad (6.29)$$

implying that the Chern numbers of each bands are equal for a phase rotation symmetric evolution

$$C_1 = \text{Ch}(P_1) = \text{Ch}(\mathcal{Z}^n P_1 \mathcal{Z}^{-n}) = \text{Ch}(P_{1+n}) = C_{1+n}. \quad (6.30)$$

Since, in addition, the sum of the Chern numbers over each band vanishes

$$\sum_{n=1}^N C_n = 0 \quad (6.31)$$

it follows that the Chern number of each band vanishes. To summarize, the phase rotation symmetry is a constrain that is specific to unitary systems and that imposes the vanishing of the Chern numbers. This result may however seem to be useless since (6.25) is a very strong condition to be fulfilled. The phase rotation symmetry is a fragile property that is only critically satisfied for very specific evolution operators. In contrast, as a topological invariant, the Chern numbers cannot change value unless one of the gaps closes. One is thus free to continuously deform the bands, e.g. flatten them and organize them such that they are equally spaced on

the unit circle, without changing the topological properties. In other words, it may exist a homotopy that continuously connects  $U_F(\mathbf{k})$  to  $\tilde{U}_F(\mathbf{k})$  without closing the gaps. In that case, the Chern numbers of  $U_F$  all vanish.

In the next section, we will present a class of models for which these conditions are met.

## 6.2 Discrete-time dynamics as scattering networks

### 6.2.1 Graph representation of a periodically driven model

Discrete-time dependent tight-binding models were proposed on the honeycomb lattice [58] and the square lattice [91] to realize Floquet "topological insulators". In these models, the hopping energy terms  $J$  that couple nearest neighbors are successively switched on and off around each plaquette in a clockwise or counter-clockwise way, therefore breaking time-reversal symmetry during a period of drive. Each time period  $T$  is decomposed in a finite time-ordered sequence of constant-in-time tight-binding Hamiltonians that describe arrays of uncoupled dimers whose sites are coupled by  $J_i$  during a time  $\tau_i$ , as depicted in figure 6.2 (a) for the square lattice.

The bulk (Bloch) Hamiltonian for this tight-binding model reads

$$H(t, \mathbf{k}) = \begin{cases} J_1 h_1(\mathbf{k}) & 0 < t < \tau_1 \\ J_2 h_2(\mathbf{k}) & \tau_1 < t < \tau_2 \\ J_3 h_3(\mathbf{k}) & \tau_2 < t < \tau_3 \\ J_4 h_4(\mathbf{k}) & \tau_3 < t < T \end{cases} \quad (6.32)$$

where  $\mathbf{k}$  is the quasi-momentum and  $h_j$  is an hermitian matrix that reads

$$\begin{aligned} h_1(\mathbf{k}) &= \begin{pmatrix} 0 & e^{ik_+} \\ e^{-ik_+} & 0 \end{pmatrix}, & h_2(\mathbf{k}) &= \begin{pmatrix} 0 & e^{ik_-} \\ e^{-ik_-} & 0 \end{pmatrix} \\ h_3(\mathbf{k}) &= \begin{pmatrix} 0 & e^{-ik_+} \\ e^{ik_+} & 0 \end{pmatrix}, & h_4(\mathbf{k}) &= \begin{pmatrix} 0 & e^{-ik_-} \\ e^{ik_-} & 0 \end{pmatrix} \end{aligned} \quad (6.33)$$

with  $k_{\pm} = \mathbf{k} \cdot \frac{\mathbf{e}_1 \pm \mathbf{e}_2}{2}$  where  $\mathbf{e}_1$  and  $\mathbf{e}_2$  are the vector basis of the Bravais lattice.

Setting the dimensionless *phase coupling parameters*  $\theta_j \equiv \hbar J_j \tau_j$ , an evolution operator  $U_j(\mathbf{k}) = e^{-i\theta_j h_j(\mathbf{k})}$  can be assigned to each time step, and can be factorized as

$$\begin{aligned} U_1(\mathbf{k}) &= B(k_+)S(\theta_1)B(k_+) & U_2(\mathbf{k}) &= B(k_-)S(\theta_2)B(k_-) \\ U_3(\mathbf{k}) &= B(-k_+)S(\theta_3)B(-k_+) & U_4(\mathbf{k}) &= B(-k_-)S(\theta_4)B(-k_-) \end{aligned} \quad (6.34)$$

## 6.2. Discrete-time dynamics as scattering networks

where

$$B(\mathbf{k}) = \begin{pmatrix} 0 & e^{i\frac{k}{2}} \\ e^{-i\frac{k}{2}} & 0 \end{pmatrix}, \quad S_j = \begin{pmatrix} \cos\theta_j & -i\sin\theta_j \\ -i\sin\theta_j & \cos\theta_j \end{pmatrix}. \quad (6.35)$$

Thus, each part of the evolution can be split into elementary steps that encode either a displacement through  $B(\mathbf{k})$  or a coupling through the scattering matrix  $S_j$ .

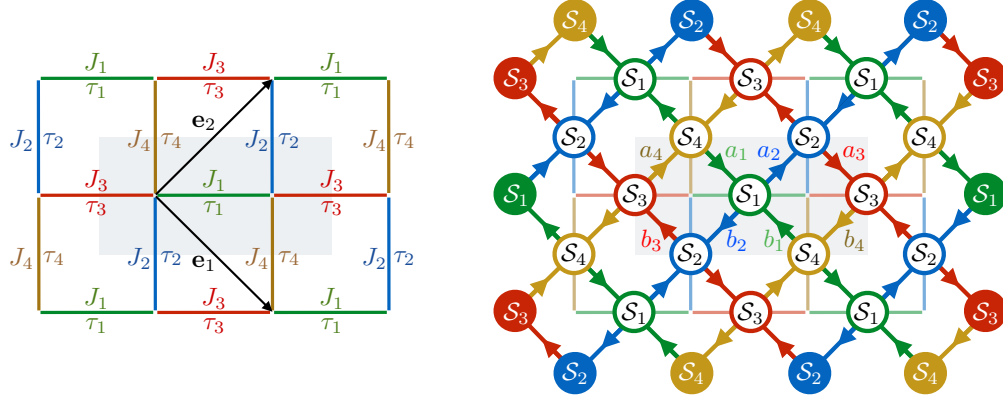


**Figure 6.2** – (left) Discrete-time dependent tight-binding model for the square lattice and (right) its scattering network representation (L-lattice). The successive time steps of duration  $\tau_i$  with couplings of amplitude  $J_i$  are represented in the same color than the scattering matrices they generate. A unit cell of the two lattices is represented by a grey rectangle, and a basis of the Bravais lattice is given by  $\vec{e}_1$  and  $\vec{e}_2$ . Note that while the tight-binding model has two inequivalent sites per unit cell, the L-lattice has eight inequivalent oriented links (and four scattering matrices).

The (Floquet) evolution operator after a time period from  $t = 0$  to  $t = T$ , reads

$$U_F(\mathbf{k}) = U_4(\mathbf{k})U_3(\mathbf{k})U_2(\mathbf{k})U_1(\mathbf{k}). \quad (6.36)$$

Substituting the  $U_j$ 's by their decomposition (6.34) yields

$$U_F(\mathbf{k}) = B(-k_-)S_4 \cdot T_{\mathbf{e}_1} S_3 T_{-\mathbf{e}_2} S_2 T_{-\mathbf{e}_1} S_1 B(k_+) \quad (6.37)$$

where  $T_{\mathbf{e}_j}$  is a "sublattice dependent" translation operator in the directions  $\pm\mathbf{e}_j/2$  that reads

$$T_{\mathbf{e}_j} \equiv \begin{pmatrix} e^{i\frac{\mathbf{k}\cdot\mathbf{e}_j}{2}} & 0 \\ 0 & e^{-i\frac{\mathbf{k}\cdot\mathbf{e}_j}{2}} \end{pmatrix}. \quad (6.38)$$

The definition of the Floquet evolution operator is not unique, as it depends on the choice of origin of time. One can thus choose a different origin by a cyclic permutation of the unitary steps in (6.36). Starting the evolution by the translation operation  $T_{\mathbf{e}_2}$ , one thus equivalently describes the periodic dynamics by the Floquet operator

$$\tilde{U}_F(\mathbf{k}) = S_4 T_{\mathbf{e}_1} S_3 T_{-\mathbf{e}_2} S_2 T_{-\mathbf{e}_1} S_1 T_{\mathbf{e}_2}. \quad (6.39)$$

The expression (6.39) has a straightforward interpretation in real space : it shows that the evolution can be seen as a staggered succession of local scattering processes  $S_j$  followed by a free propagation in the directions  $\pm\mathbf{e}_1$  or  $\pm\mathbf{e}_2$ . Representing the scattering processes by circles, and the free propagations by straight arrows in directions  $\pm\mathbf{e}_j$ , one gets a version of the celebrated scattering matrix network called *L-lattice* that was introduced by Chalker and Coddington in the context of the quantum percolation transition between plateaus of the quantized Hall effect (see figure 6.2 (b)) [17, 45]. The corresponding Floquet tight-binding model is superimposed to this network in figure 6.2 (b) to emphasize the connection between the two models. The construction of the oriented scattering network from the discrete-time dependent tight-binding model becomes intuitive: the pairs of sites that are coupled during a time-step in the tight-binding model are replaced by scattering matrices. These matrices are then connected by oriented links whose orientation satisfies the time-ordering of the dynamics. The oriented scattering lattice then obtained thus represents a periodic (Floquet) dynamics. This periodicity is visible directly on the network since any path along the oriented links encounters an ordered periodic sequence of scattering events. For this reason, such networks can be qualified as *cyclic*. Note that a unit cell of this oriented lattice contains 4 scattering nodes and 8 oriented links, while the original tight-binding model only contains 2 inequivalent sublattices.

Finally, alternatively to the Floquet evolution operator and following Chalker, Coddington and Ho, [17, 45], one can write down a "one-step" evolution operator on the network as

$$\mathcal{U}(\mathbf{k}) \equiv \begin{pmatrix} 0 & 0 & 0 & S_4.T_{\mathbf{e}_1} \\ S_1.T_{\mathbf{e}_2} & 0 & 0 & 0 \\ 0 & S_2.T_{-\mathbf{e}_1} & 0 & 0 \\ 0 & 0 & S_3.T_{-\mathbf{e}_2} & 0 \end{pmatrix}. \quad (6.40)$$

in the basis of the 8 oriented links  $(a_1, b_1, \dots, a_4, b_4)$  where the pair  $(a_j, b_j)$  enters the scattering matrix  $S_j$ . The form of the one-step evolution operator  $\mathcal{U}$  is reminiscent of the *cyclic* structure of the oriented network. The different Floquet evolution operators (i.e. defined with different origins of time) are then simply inferred by taking  $\mathcal{U}^4(\mathbf{k})$ . A correspondence between the Floquet (or discrete-time quantum walk) point of view given by (6.39) and the network point of view given by (6.40), in particular for the characterization of their topological properties through the winding number  $W_\eta[U]$  is detailed in [22].

This writing of the evolution operator is natural for networks, and turns out to be useful to reveal a phase rotation symmetry of this system.

### 6.2.2 Phase rotation symmetry of a cyclic graph

The L-lattice is an example of a cyclic oriented lattice. By definition, a cyclic oriented lattice is a periodic (i.e. Bravais lattice) oriented network in which the oriented links that constitute the unit cell can be followed in a cyclic sequence to form a closed loop. Since the nodes

of the network represent scattering processes, one can choose the scattering parameters  $\theta_j$  such that states (or wave packets transmitted along a link) are trapped along the loops without being partially transferred to the next unit cell. In such a *loops configuration* the lattice simply consists in an array of disconnected and identical loops, as illustrated in figure 6.3. Physically, it is clear that the system is in an insulating state, which guarantees that the phase (or quasi-energy) bands are well separated by gaps, so that their Chern numbers are well defined. Importantly, one can show that a loops configuration precisely corresponds to a phase rotation symmetric point!

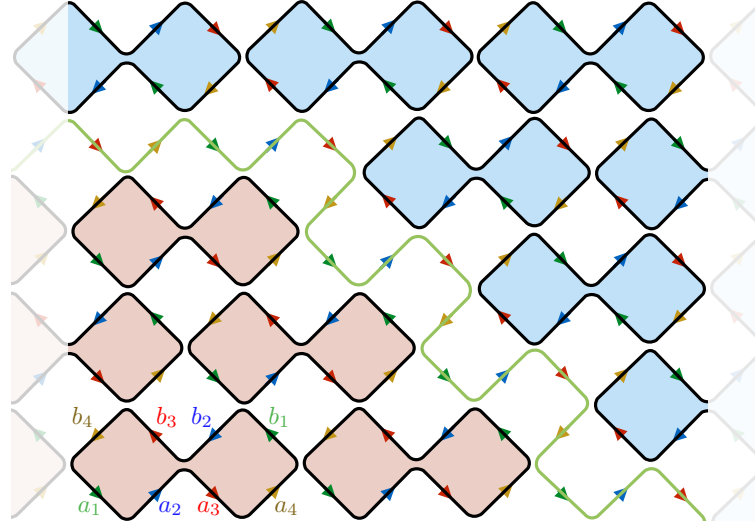


Figure 6.3 – Two domains of close loops with clockwise (red) and anti-clockwise (blue) circulation. These two domains satisfy a phase rotation symmetry. As a consequence, their evolution operator have vanishing Chern numbers. At the interface a chiral mode (green) of the Floquet anomalous regime appears.

Indeed, for such a configuration, the bulk evolution operator can always factorize as

$$\mathcal{U}(\mathbf{k}) = B(\mathbf{k}) \Pi \quad (6.41)$$

where  $B(\mathbf{k})$  is a diagonal unitary matrix encoding the phases (including the Bloch phases) accumulated from one link to another, and where  $\Pi$  is a unitary matrix that owns one and only one coefficient 1 on each of its rows and each of its columns. The matrices  $\Pi$  represent the elements of the permutation group (or symmetric group  $S_N \in SU(N)$ ), which indeed captures the loop structure. One can always re-order the successive links of the loops by a change of basis  $\Pi_0 = M\Pi M^{-1}$  so that

$$\Pi_0 = \begin{pmatrix} 0 & \cdots & \cdots & 0 & 1 \\ 1 & 0 & \cdots & & 0 \\ & 1 & & & \vdots \\ & & \ddots & & 0 \\ 0 & \cdots & 0 & 1 & 0 \end{pmatrix}. \quad (6.42)$$

## Chapter 6. Winding numbers in unitary dynamics : from Floquet systems to scattering networks

---

We notice that the eigenvalues of  $\Pi_0$  are the  $N$  roots of unity  $\{\tau, \tau^2, \dots, \tau^N\}$  with  $\tau = e^{i2\pi/N}$ . From there, one defines the diagonal matrix  $\mathcal{Z}_0$  that lists these eigenvalues as

$$\mathcal{Z}_0 = \text{diag}(\tau, \tau^2, \dots, \tau^N). \quad (6.43)$$

It follows directly that

$$\mathcal{Z}_0 \Pi_0 = \begin{pmatrix} 0 & \dots & \dots & 0 & \tau \\ \tau^2 & 0 & \dots & & 0 \\ \vdots & \tau^3 & & & \vdots \\ & & \ddots & & 0 \\ 0 & \dots & 0 & \tau^N & 0 \end{pmatrix} \quad (\Pi_0 \mathcal{Z}_0)^{-1} = \begin{pmatrix} 0 & \tau^{-1} & \dots & & 0 \\ \vdots & 0 & \tau^{-2} & \dots & 0 \\ & & \ddots & \ddots & \\ & & & 0 & \tau^{1-N} \\ \tau^{-N} & 0 & \dots & 0 & 0 \end{pmatrix} \quad (6.44)$$

and thus

$$\mathcal{Z} \Pi (\Pi \mathcal{Z})^{-1} = \tau \text{Id} \quad (6.45)$$

after the change of basis  $\mathcal{Z} \equiv M^{-1} \mathcal{Z}_0 M$ . The matrices  $B(\mathbf{k})$  and  $\mathcal{Z}$  being diagonal, they commute, so that one infers from (6.45) that the evolution operator of the network in a loops configuration satisfies

$$\mathcal{Z} \mathcal{U}(\mathbf{k}) \mathcal{Z}^{-1} = e^{i2\pi/N} \mathcal{U}(\mathbf{k}). \quad (6.46)$$

This is precisely the phase rotation symmetry defined in equation (6.25). As a consequence, the  $N$  bands of  $\mathcal{U}(\mathbf{k})$  carry a vanishing first Chern number, as long as the bands do not cross when varying the parameters  $\theta_j$ 's away from the critical value for which the loops configuration is obtained.

The reasoning above not only relates the loops configuration to the phase rotation symmetry, but also shows how to obtain the expression of the phase-rotation symmetry operator. For concreteness, consider the two domains of disconnected loops represented in 6.3 in the L-lattice. They are defined by blue clockwise cycles  $c_1 : a_1 \rightarrow a_2 \rightarrow a_3 \rightarrow b_4 \rightarrow b_1 \rightarrow b_2 \rightarrow b_3 \rightarrow a_4$  and red counter-clockwise cycles  $c_2 : a_1 \rightarrow a_2 \rightarrow a_3 \rightarrow a_4 \rightarrow b_1 \rightarrow b_2 \rightarrow b_3 \rightarrow b_4$  respectively. The factorization (6.41) of the bulk evolution operator (6.40) in each domain defines the

permutation matrices

$$\Pi_{c_1} = \begin{pmatrix} 0 & 0 & 0 & 0 & 0 & 0 & 1 & 0 \\ 0 & 0 & 0 & 0 & 0 & 0 & 0 & 1 \\ 1 & 0 & 0 & 0 & 0 & 0 & 0 & 0 \\ 0 & 1 & 0 & 0 & 0 & 0 & 0 & 0 \\ 0 & 0 & 1 & 0 & 0 & 0 & 0 & 0 \\ 0 & 0 & 0 & 1 & 0 & 0 & 0 & 0 \\ 0 & 0 & 0 & 0 & 0 & 1 & 0 & 0 \\ 0 & 0 & 0 & 0 & 1 & 0 & 0 & 0 \end{pmatrix} \quad \Pi_{c_2} = \begin{pmatrix} 0 & 0 & 0 & 0 & 0 & 0 & 0 & 1 \\ 0 & 0 & 0 & 0 & 0 & 0 & 1 & 0 \\ 1 & 0 & 0 & 0 & 0 & 0 & 0 & 0 \\ 0 & 1 & 0 & 0 & 0 & 0 & 0 & 0 \\ 0 & 0 & 1 & 0 & 0 & 0 & 0 & 0 \\ 0 & 0 & 0 & 1 & 0 & 0 & 0 & 0 \\ 0 & 0 & 0 & 0 & 1 & 0 & 0 & 0 \\ 0 & 0 & 0 & 0 & 0 & 1 & 0 & 0 \end{pmatrix}. \quad (6.47)$$

The matrix  $M$  can then be obtained as  $M = BA^{-1}$  where  $A$  and  $B$  satisfy  $\Pi = AZ_0A^{-1}$  and  $\Pi_0 = BZ_0B^{-1}$ . These matrices are easily found explicitly

$$B = \begin{pmatrix} \tau^8 & \tau^8 \\ \tau^7 & \tau^6 & \tau^5 & \tau^4 & \tau^3 & \tau^2 & \tau & \tau^8 \\ \tau^6 & \tau^4 & \tau^2 & \tau^8 & \tau^6 & \tau^4 & \tau^2 & \tau^8 \\ \tau^5 & \tau^2 & \tau^7 & \tau^4 & \tau & \tau^6 & \tau^3 & \tau^8 \\ \tau^4 & \tau^8 & \tau^4 & \tau^8 & \tau^4 & \tau^8 & \tau^4 & \tau^8 \\ \tau^3 & \tau^6 & \tau & \tau^4 & \tau^7 & \tau^2 & \tau^5 & \tau^8 \\ \tau^2 & \tau^4 & \tau^6 & \tau^8 & \tau^2 & \tau^4 & \tau^6 & \tau^8 \\ \tau & \tau^2 & \tau^3 & \tau^4 & \tau^5 & \tau^6 & \tau^7 & \tau^8 \end{pmatrix}$$

$$A_{c_1} = \begin{pmatrix} \tau^8 & \tau^8 \\ \tau^4 & \tau^8 & \tau^4 & \tau^8 & \tau^4 & \tau^8 & \tau^4 & \tau^8 \\ \tau^7 & \tau^6 & \tau^5 & \tau^4 & \tau^3 & \tau^2 & \tau & \tau^8 \\ \tau^3 & \tau^6 & \tau & \tau^4 & \tau^7 & \tau^2 & \tau^5 & \tau^8 \\ \tau^6 & \tau^4 & \tau^2 & \tau^8 & \tau^6 & \tau^4 & \tau^2 & \tau^8 \\ \tau^2 & \tau^4 & \tau^6 & \tau^8 & \tau^2 & \tau^4 & \tau^6 & \tau^8 \\ \tau & \tau^2 & \tau^3 & \tau^4 & \tau^5 & \tau^6 & \tau^7 & \tau^8 \\ \tau^5 & \tau^2 & \tau^7 & \tau^4 & \tau & \tau^6 & \tau^3 & \tau^8 \end{pmatrix} \quad A_{c_2} = \begin{pmatrix} \tau^8 & \tau^8 \\ \tau^4 & \tau^8 & \tau^4 & \tau^8 & \tau^4 & \tau^8 & \tau^4 & \tau^8 \\ \tau^7 & \tau^6 & \tau^5 & \tau^4 & \tau^3 & \tau^2 & \tau & \tau^8 \\ \tau^3 & \tau^6 & \tau & \tau^4 & \tau^7 & \tau^2 & \tau^5 & \tau^8 \\ \tau^6 & \tau^4 & \tau^2 & \tau^8 & \tau^6 & \tau^4 & \tau^2 & \tau^8 \\ \tau^2 & \tau^4 & \tau^6 & \tau^8 & \tau^2 & \tau^4 & \tau^6 & \tau^8 \\ \tau^5 & \tau^2 & \tau^7 & \tau^4 & \lambda & \tau^6 & \tau^3 & \tau^8 \\ \tau & \tau^2 & \tau^3 & \tau^4 & \tau^5 & \tau^6 & \tau^7 & \tau^8 \end{pmatrix} \quad (6.48)$$

leading to the phase rotation symmetry operators

$$\mathcal{Z}_{c_1} = \text{diag}(\tau, \tau^5, \tau^2, \tau^6, \tau^3, \tau^7, \tau^8, \tau^4) \quad \mathcal{Z}_{c_2} = \text{diag}(\tau, \tau^5, \tau^2, \tau^6, \tau^3, \tau^7, \tau^4, \tau^8) \quad (6.49)$$

for the two disjoint domains. Therefore, they both carry vanishing Chern numbers, and this remains true away from the special phase rotation symmetry point when the two domains do not simply consist in disconnected loops. On this example, the two domains differ by the orientation of their loops, so that, at the interface, it *necessarily* exists an oriented path that belongs to neither domain. This is an *anomalous* chiral interface state. This analysis is in agreement with a direct calculation of the gap invariants  $W_{c_1}$  and  $W_{c_2}$  whose difference is 1,

thus signaling the existence of an interface state.

The example above reveals that the existence of interface anomalous chiral states essentially lies on the existence of the possible existence of domains of loops of opposite circulations in the associated graph. This property is not specific to this model, and can actually be generalized to *arbitrary random* oriented scattering networks as we shall see.

### 6.2.3 Topological chiral states in random scattering networks

It is unlikely that any oriented network can be mapped onto a periodically driven tight-binding model, such as the L-lattice. A random network is in general *not* cyclic, and thus does not reproduce the intrinsic periodic driving of a Floquet system. However, it turns out that a chiral mode *always* exists at the interface between two domains of arbitrary oriented scattering networks that can be continuously deformed (by changing the coupling parameters without closing the gap) into domains of loops of opposite circulations, and that these two opposite domains can always exist in any planar scattering network. This provides a natural generalization of anomalous chiral states *beyond Floquet systems*.

Instead of extending the definition of the bulk invariants of the evolution operators (namely the first Chern numbers and the  $W$  invariants) to random networks, we shall prove this statement by means of elementary graph theory [110]. An oriented scattering network is represented by an oriented graph, that is a set of nodes (or vertices) connected by oriented links (or edges). The only physical constrain one imposes is that the nodes represent unitary scattering processes. Therefore, for a given node, the number of incoming and outgoing oriented links must be the same. This yields very peculiar graphs, called Eulerian graphs, that have been defined in section 4.1.3.

Eulerian graphs have many nice properties. One of them is known as the *two-colors theorem*; this theorem states that the faces of the graph can always be colored with two distinct colors so that two adjacent faces are always colored differently.<sup>2</sup> In a less artistic fashion, an orientation of the links surrounding each face of the graph can be assigned bijectively with its color.

A second key theorem is due to Veblen [105]. Veblen theorem states that it is always possible to decompose an Eulerian graph as a union of disjoint simple *cycles*.<sup>3</sup> This is the generalization of the domains of loops depicted in figure 6.3 where the loops are not identical anymore and may differ from each other in size and shape. When the network is a periodic lattice, the Veblen decomposition corresponds to a phase rotation symmetry point as discussed in the previous section. Because of the two-colors theorem, there are two distinct Veblen decompositions, according to the orientation of the loops.

---

<sup>2</sup>Or in other words, the dual graph of an Eulerian graphs (whose vertices coincide with the centers of the faces of the original graph) is bipartite.

<sup>3</sup>This decomposition is not unique. Here we implicitly consider the "minimal" decompositions i.e. where the cycles simply coincide with the faces of the graph.

Let us now consider an arbitrary scattering network i.e. Eulerian graph, as the one depicted in figure 6.4 (a). Its faces can be colored according to the two-colors theorem, consistently with the orientation of every links. Consider now two domains,  $D_1$  and  $D_2$  such that  $D_2$  surrounds  $D_1$ . They are separated by the graph  $I$  that constitutes the interface between  $D_1$  and  $D_2$ . In general,  $I$  has a finite width; it is not necessarily a single oriented path as in figure 6.3. Let us consider two cases, shown in figure 6.4 (b) and (c), where  $D_1$  is fixed, but the interior boundary of  $D_2$  is changed so that the two boundaries that delimit  $I$  have either the same circulations (6.4 (b)) or opposite circulations (6.4 (c)), as emphasized by thick lines. As a consequence, the domains  $D_1$  and  $D_2$  allow different Veblen decompositions in the first case, but the same decomposition in the second case. This situation is a random version of the interface between the two distinct loops configurations in the L-lattice in figure 6.3.

The statement is then the following : when the Veblen decompositions of the two domains have opposite circulations, the flow entailed by the coherent discrete-time dynamics in the interface graph is quantized while it is zero if the circulations are identical [19]. For instance it is equals to  $+1$  in the case shown in figure 6.4 (d), indicating the existence of a counter-clockwise chiral mode. This flow can be defined formally and the statement above can be derived mathematically. However it can also be justified in a more geometrical way by inspecting the interface graph.

We already noticed that the relative orientations of the loops configurations in  $D_1$  and  $D_2$  is fixed by the relative circulation of their common boundaries with  $I$ , as indicated by thick lines in figures 6.4 (b) and (c). This, in turn, fixes the parity of the width of  $I$ . This can be seen from the colors of the faces of the interface graph that are adjacent to the inner and outer frontier: they have the same color for  $I_2$  and different colors for  $I_1$ . Again, this is simply because the color of a face indicates the circulation of its links that surround it. Then, since by construction the interface graphs are also Eulerian, it follows that the interface graphs  $I_1$  and  $I_2$  have different winding numbers, as we defined in section 4.1.3. This is explicitly shown in figure 6.5 (a) and (b).

Since the interface graphs are Eulerian, they can be span by visiting successively each link (following their orientation). Examples of such Eulerian *circuits* are shown for  $I_1$  and  $I_2$  in figures 6.5 (c) and (d). This existence of such circuit is not unique, but the winding number  $W$  imposes that any of them must wind  $W$  times. A non zero winding number of the interface graph also implies that the Veblen decomposition necessarily leaves a winding circuit, as shown for  $I_1$  in figure 6.5 (e). In contrast, the Veblen decomposition of  $I_2$  consists only in disconnected loops that cannot allow any flow circulating around the graph. The quantization of the flow mentioned above, that equals the winding number, indicates that the flow is conserved in the interface graph whatever the value of the scattering parameters at its nodes, and is thus the same for these different decompositions or any disordered configuration where these parameters would have been taken randomly.

To conclude this part, one should stress that it is remarkable that topological properties of a

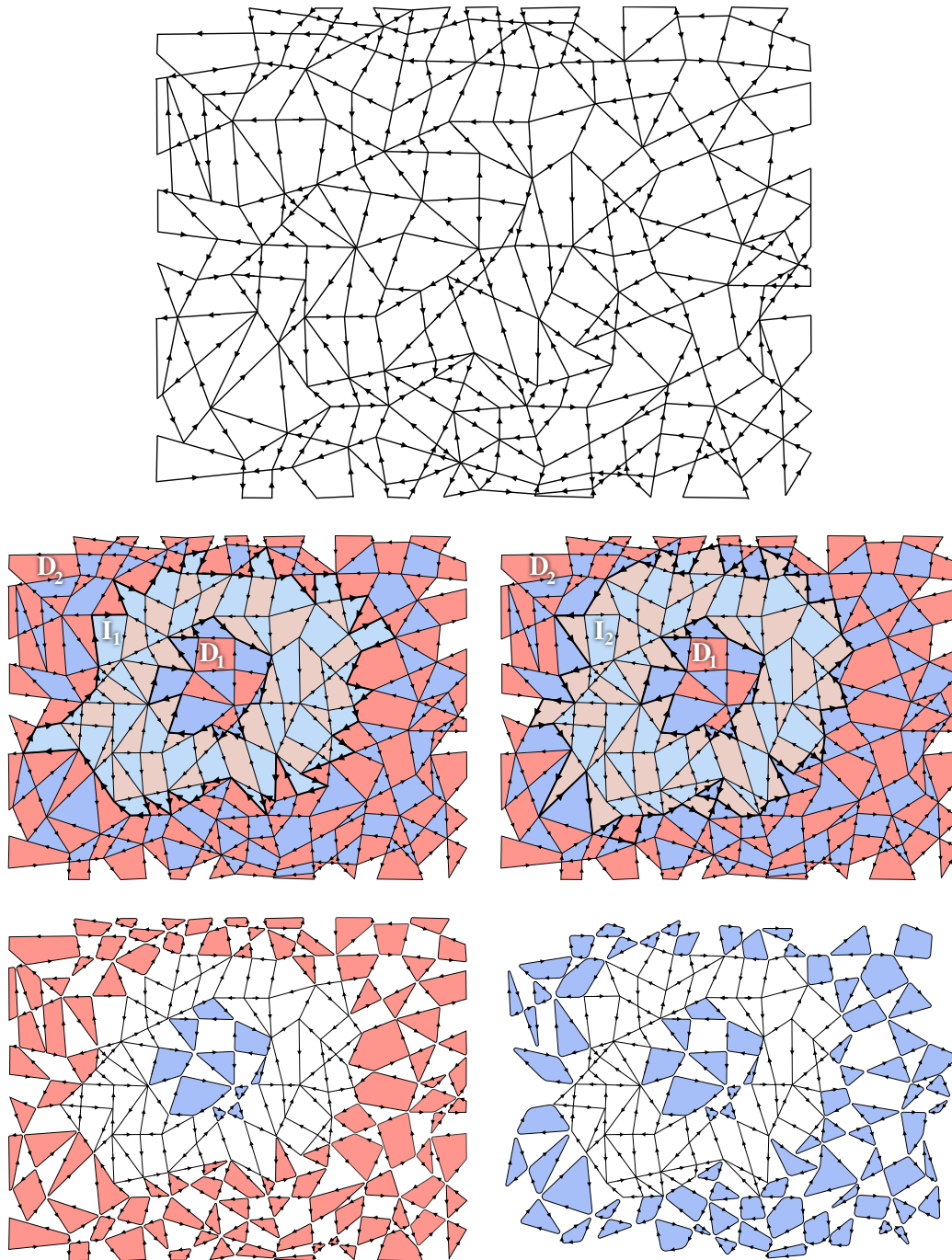


Figure 6.4 – Random oriented scattering network. Consider two domains  $D_1$  and  $D_2$  and their finite size interface  $I$ . The scattering parameters of the nodes of  $D_1$  can be continuously tuned to reach a clockwise Veblen decomposition, while those of  $D_2$  are tuned to either a counterclockwise (left) or clockwise decomposition (right). In the first case, the flow circulating around  $I$  is quantized and the winding number of  $I$  is 1. In the second case the flow is zero, as well as the winding number of  $I$ .

dynamical system (Floquet or not) can be simply inferred geometrically from the properties of the graphs, even in a disordered case.

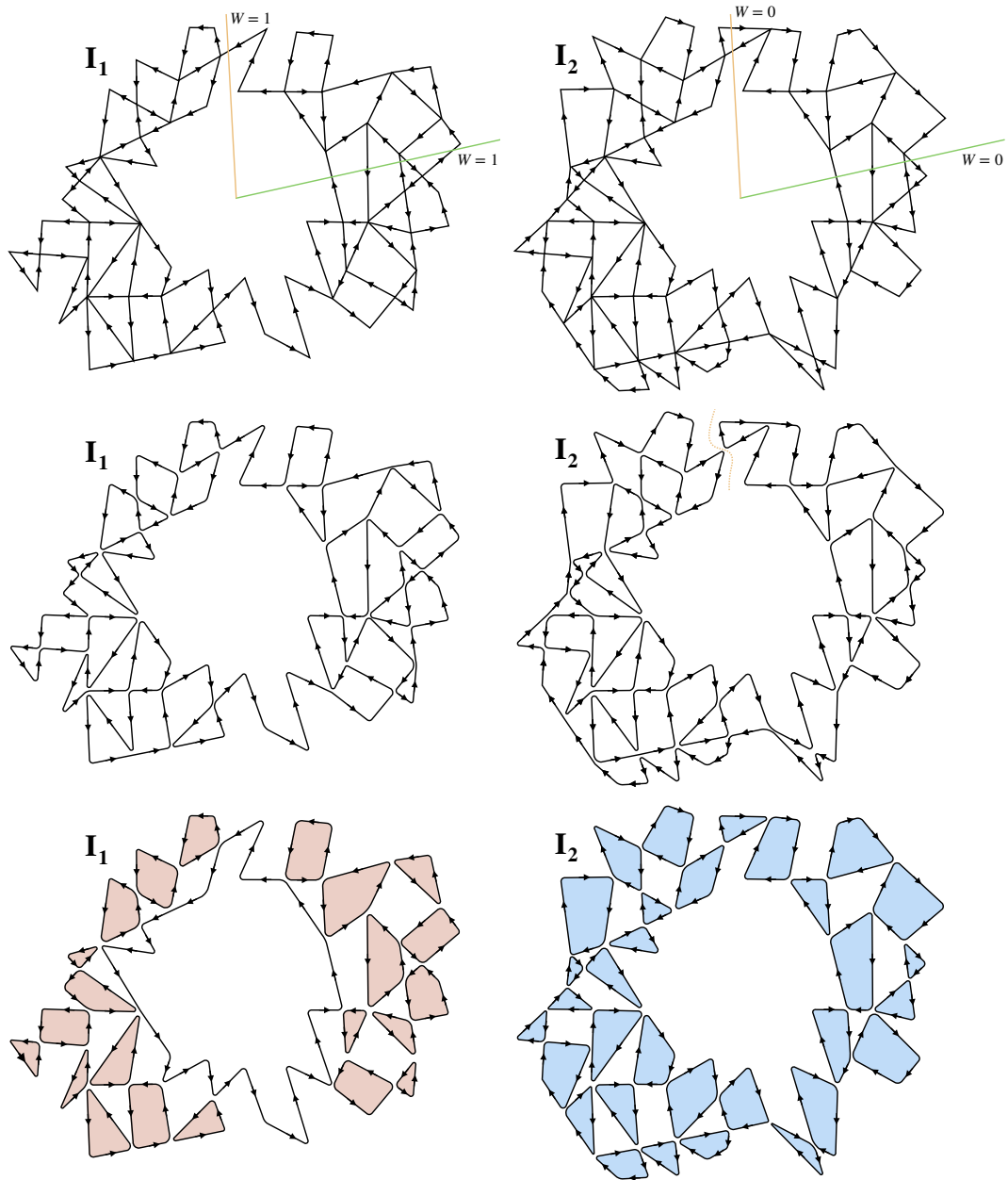


Figure 6.5 – Interface graphs  $I_1$  and  $I_2$  of the figure 6.4. (First line) Geometrical evaluation of their winding number. (Second line) Decomposition of  $I_1$  into a close loop that winds once. Such decomposition is not possible for  $I_2$ . (Third line)  $I_2$  allows a Veblen decomposition in minimal cycles, while a close loop of winding equals to 1 necessarily survives the decomposition of  $I_1$





## Bibliography

- [1] Y. Aharonov and D. Bohm. Significance of electromagnetic potentials in the quantum theory. *Phys. Rev.*, 115:485–491, Aug 1959. doi: 10.1103/PhysRev.115.485. URL <https://link.aps.org/doi/10.1103/PhysRev.115.485>.
- [2] Monika Aidelsburger, Sylvain Nascimbene, and Nathan Goldman. Artificial gauge fields in materials and engineered systems. *Comptes Rendus Physique*, 19, 2018.
- [3] J. K. Asbóth, B. Tarasinski, and P. Delplace. Chiral symmetry and bulk-boundary correspondence in periodically driven one-dimensional systems. *Phys. Rev. B*, 90:125143, Sep 2014. doi: 10.1103/PhysRevB.90.125143. URL <https://link.aps.org/doi/10.1103/PhysRevB.90.125143>.
- [4] János K. Asbóth and Jonathan M. Edge. Edge-state-enhanced transport in a two-dimensional quantum walk. *Phys. Rev. A*, 91(2), feb 2015. doi: 10.1103/physreva.91.022324.
- [5] J. E. Avron, L. Sadun, J. Segert, and B. Simon. Chern numbers, quaternions, and berry's phases in fermi systems. *Commun. Math. Phys.*, 124:595–627, 1989.
- [6] Florent Baboux, Eli Levy, Aristide Lemaître, Carmen Gómez, Elisabeth Galopin, Luc Le Gratiet, Isabelle Sagnes, Alberto Amo, Jacqueline Bloch, and Eric Akkermans. Measuring topological invariants from generalized edge states in polaritonic quasicrystals. *Phys. Rev. B*, 95:161114, Apr 2017. doi: 10.1103/PhysRevB.95.161114. URL <https://link.aps.org/doi/10.1103/PhysRevB.95.161114>.
- [7] L. Balents. Viewpoint: Weyl electron kiss. *Physics*, 4:36, 2011.
- [8] M. Bellec, C. Michel, H. Zhang, S. Tzortzakis, and P. Delplace. Non-diffracting states in one-dimensional floquet photonic topological insulators. *EPL (Europhysics Letters)*, 119(1):14003, jul 2017. doi: 10.1209/0295-5075/119/14003. URL <https://doi.org/10.1209/0295-5075%2F119%2F14003>.
- [9] B. Andrei Bernevig, Taylor L. Hughes, and Shou-Cheng Zhang. Quantum spin hall effect and topological phase transition in hgte quantum wells. *Science*, 314(5806):1757–1761, 2006. ISSN 0036-8075. doi: 10.1126/science.1133734. URL <https://science.sciencemag.org/content/314/5806/1757>.

## Bibliography

---

- [10] M. V. Berry. Quantal phase factors accompanying adiabatic changes. *Proceedings of the Royal Society of London. Series A, Mathematical and Physical Sciences*, 392, 1984.
- [11] M. V. Berry, R. G. Chambers, M. D. Large, C. Upstill, and J. C. Walmsley. Wavefront dislocations in the aharonov-bohm effect and its water wave analogue. *Eur. J. Phys.*, 1: 154, 1980.
- [12] Michael Berry. Making waves in physics. *Nature*, 403:21, January 2000.
- [13] R. Bott and R. Seeley. Some remarks on the paper of callias: “axial anomalies and index theorems on open spaces”. *Comm. Math. Phys.*, 62(3):235–245, 1978. URL <https://projecteuclid.org/443/euclid.cmp/1103904396>.
- [14] M. Büttiker. Absence of backscattering in the quantum hall effect in multiprobe conductors. *Phys. Rev. B*, 38:9375–9389, Nov 1988. doi: 10.1103/PhysRevB.38.9375. URL <https://link.aps.org/doi/10.1103/PhysRevB.38.9375>.
- [15] Edited by I. M. James. *History of Topology*. Elsevier, second edition edition, 2006.
- [16] David Carpentier, Pierre Delplace, Michel Fruchart, and Krzysztof Gawędzki. Topological index for periodically driven time-reversal invariant 2d systems. *Phys. Rev. Lett.*, 114: 106806, Mar 2015. doi: 10.1103/PhysRevLett.114.106806. URL <https://link.aps.org/doi/10.1103/PhysRevLett.114.106806>.
- [17] J T Chalker and P D Coddington. Percolation, quantum tunnelling and the integer hall effect. *J. Phys. C: Solid State Phys.*, 21(14):2665–2679, may 1988. doi: 10.1088/0022-3719/21/14/008.
- [18] S.-S. Chern. On the curvatura integra in a riemannian manifold. *Annals of Mathematics*, 46:674, 1945.
- [19] P. Delplace. Topological chiral modes in random scattering networks. *arXiv*, page 1905.11194, 2019.
- [20] P. Delplace, D. Ullmo, and G. Montambaux. Zak phase and the existence of edge states in graphene. *Phys. Rev. B*, 84:195452, Nov 2011. doi: 10.1103/PhysRevB.84.195452. URL <https://link.aps.org/doi/10.1103/PhysRevB.84.195452>.
- [21] Pierre Delplace, Álvaro Gómez-León, and Gloria Platero. Merging of dirac points and floquet topological transitions in ac-driven graphene. *Phys. Rev. B*, 88:245422, Dec 2013. doi: 10.1103/PhysRevB.88.245422. URL <https://link.aps.org/doi/10.1103/PhysRevB.88.245422>.
- [22] Pierre Delplace, Michel Fruchart, and Clément Tauber. Phase rotation symmetry and the topology of oriented scattering networks. *Phys. Rev. B*, 95:205413, May 2017. doi: 10.1103/PhysRevB.95.205413. URL <https://link.aps.org/doi/10.1103/PhysRevB.95.205413>.

- [23] P. A. M. Dirac. Quantised singularities in the electromagnetic field. *Proc. Roy. Soc. (London)*, A 133:487, 1931.
- [24] B.A. Dubrovin, A.T. Fomenko, and S.P. Novikov. *Modern Geometry— Methods and Applications: Part II: The Geometry and Topology of Manifolds*. Springer Science and Business Media, 1985.
- [25] C. Dutreix and P. Delplace. Geometrical phase shift in friedel oscillations. *Phys. Rev. B*, 96:195207, Nov 2017. doi: 10.1103/PhysRevB.96.195207. URL <https://link.aps.org/doi/10.1103/PhysRevB.96.195207>.
- [26] U. Fano. Atomic theory of electromagnetic interactions in dense materials. *Phys. Rev.*, 103:1202–1218, Sep 1956. doi: 10.1103/PhysRev.103.1202. URL <https://link.aps.org/doi/10.1103/PhysRev.103.1202>.
- [27] F Faure. Manifestation of the topological index formula in quantum waves and geophysical waves. *arXiv:1901.10592*, 2019.
- [28] Richard Feynman and Ralph Leighton. *Surely You're Joking, Mr. Feynman!* W. W. Norton, 1985.
- [29] T. Frankel. *The Geometry of Physics*. Cambridge University Press, third edition, 2012.
- [30] Michel Fruchart. Complex classes of periodically driven topological lattice systems. *Phys. Rev. B*, 93(11), mar 2016. doi: 10.1103/physrevb.93.115429.
- [31] George Gamow. *Biography of physics*. New York : Harper, 1961.
- [32] M. O. Goerbig. Electronic properties of graphene in a strong magnetic field. *Rev. Mod. Phys.*, 83:1193–1243, Nov 2011. doi: 10.1103/RevModPhys.83.1193. URL <https://link.aps.org/doi/10.1103/RevModPhys.83.1193>.
- [33] N. Goldman and J. Dalibard. Periodically driven quantum systems: Effective hamiltonians and engineered gauge fields. *Phys. Rev. X*, 4:031027, Aug 2014. doi: 10.1103/PhysRevX.4.031027. URL <https://link.aps.org/doi/10.1103/PhysRevX.4.031027>.
- [34] N Goldman, G Juzeliūnas, P Öhberg, and I B Spielman. Light-induced gauge fields for ultracold atoms. *Reports on Progress in Physics*, 77(12):126401, nov 2014. doi: 10.1088/0034-4885/77/12/126401. URL <https://doi.org/10.1088%2F0034-4885%2F77%2F12%2F126401>.
- [35] N. Goldman, J. C. Budich, and P. Zoller. Topological quantum matter with ultracold gases in optical lattices. *Nature Physics*, 12:639 EP –, 06 2016. URL <https://doi.org/10.1038/nphys3803>.
- [36] Álvaro Gómez-León, Pierre Delplace, and Gloria Platero. Engineering anomalous quantum hall plateaus and antichiral states with ac fields. *Phys. Rev. B*, 89:205408, May 2014. doi: 10.1103/PhysRevB.89.205408. URL <https://link.aps.org/doi/10.1103/PhysRevB.89.205408>.

## Bibliography

---

- [37] G.M. Graf and M Porta. Bulk–edge correspondence for two-dimensional topological insulators. *Commun. Math. Phys.*, 324:851, 2013.
- [38] G.M. Graf and C Tauber. Bulk–edge correspondence for two-dimensional floquet topological insulators. *Ann. Henri Poincaré*, 19(709), 2018.
- [39] Jonathan Guglielmon, Sheng Huang, Kevin P. Chen, and Mikael C. Rechtsman. Photonic realization of a transition to a strongly driven floquet topological phase. *Phys. Rev. A*, 97: 031801, Mar 2018. doi: 10.1103/PhysRevA.97.031801. URL <https://link.aps.org/doi/10.1103/PhysRevA.97.031801>.
- [40] F. D. M. Haldane. Model for a quantum hall effect without landau levels: Condensed-matter realization of the "parity anomaly". *Phys. Rev. Lett.*, 61:2015–2018, Oct 1988. doi: 10.1103/PhysRevLett.61.2015. URL <https://link.aps.org/doi/10.1103/PhysRevLett.61.2015>.
- [41] B. I. Halperin. Quantized hall conductance, current-carrying edge states, and the existence of extended states in a two-dimensional disordered potential. *Phys. Rev. B*, 25: 2185–2190, Feb 1982. doi: 10.1103/PhysRevB.25.2185. URL <https://link.aps.org/doi/10.1103/PhysRevB.25.2185>.
- [42] M. Z. Hasan and C. L. Kane. Colloquium: Topological insulators. *Rev. Mod. Phys.*, 82: 3045–3067, Nov 2010. doi: 10.1103/RevModPhys.82.3045. URL <https://link.aps.org/doi/10.1103/RevModPhys.82.3045>.
- [43] Yasuhiro Hatsugai. Edge states in the integer quantum hall effect and the riemann surface of the bloch function. *Phys. Rev. B*, 48:11851–11862, Oct 1993. doi: 10.1103/PhysRevB.48.11851. URL <https://link.aps.org/doi/10.1103/PhysRevB.48.11851>.
- [44] Yasuhiro Hatsugai. Chern number and edge states in the integer quantum hall effect. *Phys. Rev. Lett.*, 71:3697–3700, Nov 1993. doi: 10.1103/PhysRevLett.71.3697. URL <https://link.aps.org/doi/10.1103/PhysRevLett.71.3697>.
- [45] C.-M. Ho and J. T. Chalker. Models for the integer quantum hall effect: The network model, the dirac equation, and a tight-binding hamiltonian. *Phys. Rev. B*, 54(12):8708–8713, sep 1996. doi: 10.1103/physrevb.54.8708.
- [46] J. J. Hopfield. Theory of the contribution of excitons to the complex dielectric constant of crystals. *Phys. Rev.*, 112:1555–1567, Dec 1958. doi: 10.1103/PhysRev.112.1555. URL <https://link.aps.org/doi/10.1103/PhysRev.112.1555>.
- [47] Wenchao Hu, Jason C. Pillay, Kan Wu, Michael Pasek, Perry Ping Shum, and Y. D. Chong. Measurement of a topological edge invariant in a microwave network. *Phys. Rev. X*, 5: 011012, Feb 2015. doi: 10.1103/PhysRevX.5.011012. URL <https://link.aps.org/doi/10.1103/PhysRevX.5.011012>.

- [48] K. Iga. Transition modes of rotating shallow water waves in a channel. *Journal of Fluid Mechanics*, 294:367–390, 1995.
- [49] Keita Iga. Transition modes in stratified compressible fluids. *Fluid Dynamics Research*, 28(6):465, 2001.
- [50] Jun-ichi Inoue and Akihiro Tanaka. Photoinduced transition between conventional and topological insulators in two-dimensional electronic systems. *Phys. Rev. Lett.*, 105: 017401, Jun 2010. doi: 10.1103/PhysRevLett.105.017401. URL <https://link.aps.org/doi/10.1103/PhysRevLett.105.017401>.
- [51] R. Jackiw and C. Rebbi. Solitons with fermion number  $\frac{1}{2}$ . *Phys. Rev. D*, 13:3398–3409, Jun 1976. doi: 10.1103/PhysRevD.13.3398. URL <https://link.aps.org/doi/10.1103/PhysRevD.13.3398>.
- [52] J. D. Jackson. *Classical Electrodynamics*. New York: Wiley, third edition, 1999.
- [53] Gregor Jotzu, Michael Messer, Rémi Desbuquois, Martin Lebrat, Thomas Uehlinger, Daniel Greif, and Tilman Esslinger. Experimental realization of the topological haldane model with ultracold fermions. *Nature*, 515:237 EP –, 11 2014. URL <https://doi.org/10.1038/nature13915>.
- [54] C. L. Kane and E. J. Mele. Quantum spin hall effect in graphene. *Phys. Rev. Lett.*, 95: 226801, Nov 2005. doi: 10.1103/PhysRevLett.95.226801. URL <https://link.aps.org/doi/10.1103/PhysRevLett.95.226801>.
- [55] C. L. Kane and E. J. Mele.  $Z_2$  topological order and the quantum spin hall effect. *Phys. Rev. Lett.*, 95:146802, Sep 2005. doi: 10.1103/PhysRevLett.95.146802. URL <https://link.aps.org/doi/10.1103/PhysRevLett.95.146802>.
- [56] Yaroslav V. Kartashov and Dmitry V. Skryabin. Two-dimensional topological polariton laser. *Phys. Rev. Lett.*, 122:083902, Feb 2019. doi: 10.1103/PhysRevLett.122.083902. URL <https://link.aps.org/doi/10.1103/PhysRevLett.122.083902>.
- [57] George N. Kiladis, Matthew C. Wheeler, Patrick T. Haertel, Katherine H. Straub, and Paul E. Roundy. Convectively coupled equatorial waves. *Reviews of Geophysics*, 47(2): RG2003, 2009.
- [58] Takuya Kitagawa, Erez Berg, Mark Rudner, and Eugene Demler. Topological characterization of periodically driven quantum systems. *Phys. Rev. B*, 82:235114, Dec 2010. doi: 10.1103/PhysRevB.82.235114. URL <http://link.aps.org/doi/10.1103/PhysRevB.82.235114>.
- [59] Takuya Kitagawa, Mark S. Rudner, Erez Berg, and Eugene Demler. Exploring topological phases with quantum walks. *Phys. Rev. A*, 82:033429, Sep 2010. doi: 10.1103/PhysRevA.82.033429.

## Bibliography

---

- [60] Takuya Kitagawa, Matthew A. Broome, Alessandro Fedrizzi, Mark S. Rudner, Erez Berg, Ivan Kassal, Alán Aspuru-Guzik, Eugene Demler, and Andrew G. White. Observation of topologically protected bound states in photonic quantum walks. *Nature Communications*, 3:882, 2012.
- [61] K. v. Klitzing, G. Dorda, and M. Pepper. New method for high-accuracy determination of the fine-structure constant based on quantized hall resistance. *Phys. Rev. Lett.*, 45: 494–497, Aug 1980. doi: 10.1103/PhysRevLett.45.494. URL <https://link.aps.org/doi/10.1103/PhysRevLett.45.494>.
- [62] Mahito Kohmoto. Topological invariant and the quantization of the hall conductance. *Annals of Physics*, 160(2):343 – 354, 1985. ISSN 0003-4916. doi: [https://doi.org/10.1016/0003-4916\(85\)90148-4](https://doi.org/10.1016/0003-4916(85)90148-4). URL <http://www.sciencedirect.com/science/article/pii/0003491685901484>.
- [63] Markus König, Steffen Wiedmann, Christoph Brüne, Andreas Roth, Hartmut Buhmann, Laurens W. Molenkamp, Xiao-Liang Qi, and Shou-Cheng Zhang. Quantum spin hall insulator state in hgte quantum wells. *Science*, 318(5851):766–770, 2007. ISSN 0036-8075. doi: 10.1126/science.1148047. URL <https://science.sciencemag.org/content/318/5851/766>.
- [64] Horace Lamb. On atmospheric oscillations. *Proceedings of the Royal Society of London. Series A, Containing Papers of a Mathematical and Physical Character*, 84(574):551–572, 1911.
- [65] R. B. Laughlin. Quantized hall conductivity in two dimensions. *Phys. Rev. B*, 23:5632–5633, May 1981. doi: 10.1103/PhysRevB.23.5632. URL <https://link.aps.org/doi/10.1103/PhysRevB.23.5632>.
- [66] F Lemoult, N. Kaina, M. Fink, and G Lerosey. Soda cans metamaterial: A subwavelength-scaled phononic crystal. *Crystals*, 6:82, 2016. doi: 0.3390/cryst6070082. URL <https://doi.org/10.3390/cryst6070082>.
- [67] G. Q. Liang and Y. D. Chong. Optical resonator analog of a two-dimensional topological insulator. *Phys. Rev. Lett.*, 110(20), may 2013. doi: 10.1103/physrevlett.110.203904.
- [68] Netanel H. Lindner, Gil Refael, and Victor Galitski. Floquet topological insulator in semiconductor quantum wells. *Nature Physics*, 7:490 EP –, 03 2011. URL <https://doi.org/10.1038/nphys1926>.
- [69] M. Lohse, C. Schweizer, O. Zilberberg, M. Aidelsburger, and I. Bloch. A thouless quantum pump with ultracold bosonic atoms in an optical superlattice. *Nature Physics*, 12:350 EP –, 12 2015. URL <https://doi.org/10.1038/nphys3584>.
- [70] Veronica Ahufinger Bogdan Damski Aditi Sen Maciej Lewenstein, Anna Sanpera and Ujjwal Sen. Ultracold atomic gases in optical lattices: mimicking condensed matter physics and beyond. *Advances in Physics*, 56:243, 2006.

- [71] Lukas J. Maczewsky, Julia M. Zeuner, Stefan Nolte, and Alexander Szameit. Observation of photonic anomalous floquet topological insulators. *Nature Communications*, 8:13756 EP –, 01 2017. URL <https://doi.org/10.1038/ncomms13756>.
- [72] Lukas J. Maczewsky, Bastian Höckendorf, Mark Kremer, Matthias Heinrich Tobias Biesenthal, Andreas Alvermann, Holger Fehske, and Alexander Szameit. Fermionic time-reversal symmetry in a photonic topological insulator. *arXiv*, page 1812.07930, 2018.
- [73] Taroh Matsuno. Quasi-geostrophic motions in the equatorial area. *Journal of the Meteorological Society of Japan. Ser. II*, 44(1):25–43, 1966. doi: 10.2151/jmsj1965.44.1\_25.
- [74] Seababrat Mukherjee, Alexander Spracklen, Manuel Valiente, Erika Andersson, Patrik Öhberg, Nathan Goldman, and Robert R. Thomson. Experimental observation of anomalous topological edge modes in a slowly driven photonic lattice. *Nature Communications*, 8:13918 EP –, 01 2017. URL <https://doi.org/10.1038/ncomms13918>.
- [75] Shuichi Murakami. Phase transition between the quantum spin hall and insulator phases in 3d: emergence of a topological gapless phase. *New Journal of Physics*, 9(9): 356–356, sep 2007. doi: 10.1088/1367-2630/9/9/356. URL <https://doi.org/10.1088%2F1367-2630%2F9%2F9%2F356>.
- [76] M Nakahara. *Geometry, Topology and Physics*. CRC Press 2003, 2003.
- [77] Shuta Nakajima, Takafumi Tomita, Shintaro Taie, Tomohiro Ichinose, Hideki Ozawa, Lei Wang, Matthias Troyer, and Yoshiro Takahashi. Topological Thouless pumping of ultracold fermions. *Nature Physics*, 12:296 EP –, 01 2016. URL <https://doi.org/10.1038/nphys3622>.
- [78] Qian Niu and D. J. Thouless. Quantum hall effect with realistic boundary conditions. *Phys. Rev. B*, 35:2188–2197, Feb 1987. doi: 10.1103/PhysRevB.35.2188. URL <https://link.aps.org/doi/10.1103/PhysRevB.35.2188>.
- [79] Qian Niu, D. J. Thouless, and Yong-Shi Wu. Quantized hall conductance as a topological invariant. *Phys. Rev. B*, 31:3372–3377, Mar 1985. doi: 10.1103/PhysRevB.31.3372. URL <https://link.aps.org/doi/10.1103/PhysRevB.31.3372>.
- [80] J. F. Nye and M. V. Berry. Dislocations in wave trains. *Proc. Roy. Soc. (London)*, 336:165, 1974.
- [81] Takashi Oka and Hideo Aoki. Photovoltaic hall effect in graphene. *Phys. Rev. B*, 79: 081406, Feb 2009. doi: 10.1103/PhysRevB.79.081406. URL <https://link.aps.org/doi/10.1103/PhysRevB.79.081406>.
- [82] Tomoki Ozawa, Hannah M. Price, Alberto Amo, Nathan Goldman, Mohammad Hafezi, Ling Lu, Mikael C. Rechtsman, David Schuster, Jonathan Simon, Oded Zilberberg, and Iacopo Carusotto. Topological photonics. *Rev. Mod. Phys.*, 91:015006, Mar 2019. doi:

## Bibliography

---

- 10.1103/RevModPhys.91.015006. URL <https://link.aps.org/doi/10.1103/RevModPhys.91.015006>.
- [83] Michael Pasek and Y. D. Chong. Network models of photonic floquet topological insulators. *Phys. Rev. B*, 89(7), feb 2014. doi: 10.1103/physrevb.89.075113.
- [84] V. Peano, C. Brendel, M. Schmidt, and F. Marquardt. Topological phases of sound and light. *Phys. Rev. X*, 5:031011, Jul 2015. doi: 10.1103/PhysRevX.5.031011. URL <https://link.aps.org/doi/10.1103/PhysRevX.5.031011>.
- [85] J. B. Pendry, L. Martín-Moreno, and F. J. Garcia-Vidal. Mimicking surface plasmons with structured surfaces. *Science*, 305(5685):847–848, 2004. ISSN 0036-8075. doi: 10.1126/science.1098999. URL <https://science.sciencemag.org/content/305/5685/847>.
- [86] Yu-Gui Peng, Cheng-Zhi Qin, De-Gang Zhao, Ya-Xi Shen, Xiang-Yuan Xu, Ming Bao, Han Jia, and Xue-Feng Zhu. Experimental demonstration of anomalous floquet topological insulator for sound. *Nature Communications*, 7:13368 EP –, 11 2016. URL <https://doi.org/10.1038/ncomms13368>.
- [87] E. Prodan and H. Schulz-Baldes. *Bulk and Boundary Invariants for Complex Topological Insulators*. Springer International Publishing, 2016.
- [88] S. Raghu and F. D. M. Haldane. Analogs of quantum-hall-effect edge states in photonic crystals. *Phys. Rev. A*, 78:033834, Sep 2008. doi: 10.1103/PhysRevA.78.033834. URL <https://link.aps.org/doi/10.1103/PhysRevA.78.033834>.
- [89] Mikael C. Rechtsman, Julia M. Zeuner, Yonatan Plotnik, Yaakov Lumer, Daniel Podolsky, Felix Dreisow, Stefan Nolte, Mordechai Segev, and Alexander Szameit. Photonic floquet topological insulators. *Nature*, 496(7444):196–200, apr 2013. doi: 10.1038/nature12066.
- [90] N. Regnault and B. Andrei Bernevig. Fractional chern insulator. *Phys. Rev. X*, 1:021014, Dec 2011. doi: 10.1103/PhysRevX.1.021014. URL <https://link.aps.org/doi/10.1103/PhysRevX.1.021014>.
- [91] Mark S. Rudner, Netanel H. Lindner, Erez Berg, and Michael Levin. Anomalous edge states and the bulk-edge correspondence for periodically driven two-dimensional systems. *Phys. Rev. X*, 3(3), jul 2013. doi: 10.1103/physrevx.3.031005. URL <http://dx.doi.org/10.1103/physrevx.3.031005>.
- [92] Shinsei Ryu and Yasuhiro Hatsugai. Topological origin of zero-energy edge states in particle-hole symmetric systems. *Phys. Rev. Lett.*, 89:077002, Jul 2002. doi: 10.1103/PhysRevLett.89.077002. URL <https://link.aps.org/doi/10.1103/PhysRevLett.89.077002>.
- [93] Muhammad Sajid, Janos K. Asboth, Dieter Meschede, Reinhard Werner, and Andrea Alberti. Creating floquet chern insulators with magnetic quantum walks. *arXiv:1808.08923*, 2018.

- 
- [94] Andreas P. Schnyder, Shinsei Ryu, Akira Furusaki, and Andreas W. W. Ludwig. Classification of topological insulators and superconductors. *AIP Conference Proceedings*, page 1134, 2009.
- [95] Barry Simon. Holonomy, the quantum adiabatic theorem, and berry's phase. *Phys. Rev. Lett.*, 51:2167–2170, Dec 1983. doi: 10.1103/PhysRevLett.51.2167. URL <https://link.aps.org/doi/10.1103/PhysRevLett.51.2167>.
- [96] Anton Souslov, Benjamin C. van Zuiden, Denis Bartolo, and Vincenzo Vitelli. Topological sound in active-liquid metamaterials. *Nature Physics*, 13:1091 EP –, 07 2017. URL <https://doi.org/10.1038/nphys4193>.
- [97] Eric M. Spanton, Alexander A. Zibrov, Haoxin Zhou, Takashi Taniguchi, Kenji Watanabe, Michael P. Zaletel, and Andrea F. Young. Observation of fractional chern insulators in a van der waals heterostructure. *Science*, 360(6384):62–66, 2018. ISSN 0036-8075. doi: 10.1126/science.aan8458. URL <https://science.sciencemag.org/content/360/6384/62>.
- [98] I. B. Spielman. Raman processes and effective gauge potentials. *Phys. Rev. A*, 79:063613, Jun 2009. doi: 10.1103/PhysRevA.79.063613. URL <https://link.aps.org/doi/10.1103/PhysRevA.79.063613>.
- [99] Clément Tauber and Pierre Delplace. Topological edge states in two-gap unitary systems: a transfer matrix approach. *New Journal of Physics*, 17(11):115008, nov 2015. doi: 10.1088/1367-2630/17/11/115008. URL <https://doi.org/10.1088%2F1367-2630%2F17%2F11%2F115008>.
- [100] D. J. Thouless. Quantization of particle transport. *Phys. Rev. B*, 27:6083–6087, May 1983. doi: 10.1103/PhysRevB.27.6083. URL <https://link.aps.org/doi/10.1103/PhysRevB.27.6083>.
- [101] D. J. Thouless, M. Kohmoto, M. P. Nightingale, and M. den Nijs. Quantized hall conductance in a two-dimensional periodic potential. *Phys. Rev. Lett.*, 49:405–408, Aug 1982. doi: 10.1103/PhysRevLett.49.405. URL <https://link.aps.org/doi/10.1103/PhysRevLett.49.405>.
- [102] D. C. Tsui, H. L. Stormer, and A. C. Gossard. Two-dimensional magnetotransport in the extreme quantum limit. *Phys. Rev. Lett.*, 48:1559–1562, May 1982. doi: 10.1103/PhysRevLett.48.1559. URL <https://link.aps.org/doi/10.1103/PhysRevLett.48.1559>.
- [103] L. K. Upreti, C Evain, S. Randoux, P. Suret, A. Amo, and P. Delplace. Floquet winding metals. *arXiv*, page 1907.09914, 2019.
- [104] G. K. Vallis. *Atmospheric and Oceanic Fluid Dynamics : Fundamentals and Large-Scale Circulation*. Cambridge University Press, Cambridge, U. K., 2nd edition edition, 2017.
- [105] O Veblen. An application of modular equations in analysis situs. *Annals of Mathematics*, 14:86, 1912.

## Bibliography

---

- [106] G. E. Volovik. *The Universe in a Helium Droplet*. OUP Oxford, 2009.
- [107] Xiangang Wan, Ari M. Turner, Ashvin Vishwanath, and Sergey Y. Savrasov. Topological semimetal and fermi-arc surface states in the electronic structure of pyrochlore iridates. *Phys. Rev. B*, 83:205101, May 2011. doi: 10.1103/PhysRevB.83.205101. URL <https://link.aps.org/doi/10.1103/PhysRevB.83.205101>.
- [108] C. Wang and J. Picaut. Understanding ENSO physics - a review. *Earth's Climate: The Ocean-Atmosphere Interaction, Geophysical Monograph Series*, 147:21, 2004.
- [109] Z. Wang, Y. Chong, J. D. Joannopoulos, and M. Soljacic. Observation of unidirectional backscattering-immune topological electromagnetic states. *Physical review letters*, 461:772, 2009.
- [110] Douglas B. West. *Introduction to Graph Theory*. Pearson, second edition, 2000.
- [111] Martin Wimmer, Hannah M Price, Iacopo Carusotto, and Ulf Peschel. Experimental measurement of the berry curvature from anomalous transport. *Nature Physics*, 13(6):545, 2017.
- [112] Di Xiao, Wang Yao, and Qian Niu. Valley-contrasting physics in graphene: Magnetic moment and topological transport. *Phys. Rev. Lett.*, 99:236809, Dec 2007. doi: 10.1103/PhysRevLett.99.236809. URL <https://link.aps.org/doi/10.1103/PhysRevLett.99.236809>.
- [113] Su-Yang Xu, Ilya Belopolski, Nasser Alidoust, Madhab Neupane, Guang Bian, Chenglong Zhang, Raman Sankar, Guoqing Chang, Zhujun Yuan, Chi-Cheng Lee, Shin-Ming Huang, Hao Zheng, Jie Ma, Daniel S. Sanchez, BaoKai Wang, Arun Bansil, Fangcheng Chou, Pavel P. Shibayev, Hsin Lin, Shuang Jia, and M. Zahid Hasan. Discovery of a weyl fermion semimetal and topological fermi arcs. *Science*, 349(6248):613–617, 2015. ISSN 0036-8075. doi: 10.1126/science.aaa9297. URL <https://science.sciencemag.org/content/349/6248/613>.
- [114] S. Yves, R. Fleury, F. Lemoult, M. Fink, and G. Lerosey. Topological acoustic polaritons: robust sound manipulation at the subwavelength scale. *New J. Phys.*, 19:075003, 2017. doi: 10.1088/1367-2630/aa66f8. URL <https://doi.org/10.1088/1367-2630/aa66f8>.
- [115] S. E. Zebiak and M. A. Cane. A model el niño-southern oscillation. *Monthly Weather Review*, 115:2262, March 1987.
- [116] Xiujian Zhang, Meng Xiao, Ying Cheng, Ming-Hui Lu, and Johan Christensen. Topological sound. *Communications Physics*, 1(1):97, 2018. doi: 10.1038/s42005-018-0094-4. URL <https://doi.org/10.1038/s42005-018-0094-4>.
- [117] Martin R. Zirnbauer. Toward a theory of the integer quantum hall transition: Continuum limit of the chalker–coddington model. *Journal of Mathematical Physics*, 38(4):2007–2036, 1997. doi: 10.1063/1.531921. URL <https://doi.org/10.1063/1.531921>.